Doklady Physics, Vol. 46, No. 5, 2001, pp. 299–303. Translated from Doklady Akademii Nauk, Vol. 378, No. 1, 2001, pp. 33–37.

PHYSICS

Symmetric Regimes for Gas-Free Spin Combustion of a Hollow Cylinder

T. P. Ivleva

Presented by Academician A.G. Merzhanov November 1, 2000

Received November 24, 2000

Spin-combustion regimes were discovered while burning cylindrical samples pressed from hafnium powder in a nitrogen–argon mixture [1]. The authors of [1] observed the appearance and spiral motion of a bright spot (combustion center) over the lateral surface of a sample. Analysis of experiments has shown that the interaction between hafnium and nitrogen predominantly occurs in near-surface sample layers. In the case of gas-free combustion, surface layers can also often be distinguished because of their interaction with atmospheric oxygen, cooling, or special heating ("thermal cylinder" [2]). These facts make it possible to reduce solving the problem to considering combustion of a thin cylindrical shell. In [3], typical spin regimes were investigated numerically. However, later on, other regimes of spin propagation of the combustion front were experimentally obtained. In addition, counter motion of the combustion centers was observed in the experiments [4, 5]. As was shown in [3], in the case of classic spin burning, the motion of a combustion center can occur in both clockwise and counterclockwise directions. In addition, in the same region of parameters, there exists also a possibility of counter combustion-center motion, although such a regime is unstable.

In this study, we demonstrate that there exist regions of parameters wherein the counter motion of combustion centers is stable and the mechanism of possible counter propagation of the combustion front can be explained.

We consider the combustion of a sample having the shape of a thin-walled tube pressed from a mixture of solid reagents. We assume that initial reagents, as well reaction products, being in the solid phase, are characterized by the thermal homogeneity. The ignition is performed on the upper end of a sample, and the combustion front moves from the top to the bottom. We employ a simplified model of the process, which takes into account only the heat-transfer in the sample, the macrokinetics of interaction between reagents, and the heat dissipation to the environment of the cylinder.

The mathematical model can be written out in the following dimensionless form:

$$\frac{\partial\theta}{\partial\tau} = \frac{1}{R_0^2}\frac{\partial^2\theta}{\partial\varphi^2} + \frac{\partial^2\theta}{\partial z^2} + \frac{1}{\mathrm{Td}}\frac{\partial\eta}{\partial\tau} - \alpha_T(\theta-\theta_0),$$

$$\frac{\partial\eta}{\partial\tau} = \begin{cases} \mathrm{Td}(1-\eta)\exp\left(\dfrac{\theta}{1+\mathrm{Ar}\,\theta}\right) & \text{for } \eta < 1 \\ 0 \text{ for } \eta \geq 1, \end{cases}$$

$$\tau = 0, \quad 0 \leq \varphi \leq 2\pi, \quad 0 \leq z \leq z_0: \quad \theta = \theta_0, \quad \eta = 0,$$

$$\tau > 0, \quad 0 \leq \varphi \leq 2\pi, \quad z = 0: \quad \frac{\partial\theta}{\partial z} = 0,$$

$$\tau > 0, \quad 0 \leq \varphi \leq 2\pi,$$

$$z = z_0: \begin{cases} \theta = 0 \text{ for } \tau \leq \tau_{\mathrm{ign}} \\ \dfrac{\partial\theta}{\partial z} = 0 \text{ for } \tau > \tau_{\mathrm{ign}}, \end{cases}$$

$$\tau > 0, \quad 0 \leq z \leq z_0, \quad \theta(0, z) = \theta(2\pi, z),$$

$$\frac{\partial\theta(0, z)}{\partial\varphi} = \frac{\partial\theta(2\pi, z)}{\partial\varphi}.$$

We use the following notation:

$$\theta = \frac{(T-T_*)E}{RT_*^2}, \quad t_* = \frac{cRT_*^2}{k_0EQ}\exp\left(\frac{E}{RT_*}\right),$$

$$\tau = \frac{t}{t_*}, \quad \tau_{\mathrm{ign}} = \frac{t_{\mathrm{ign}}}{t_*},$$

$$h_*^2 = \frac{\lambda t_*}{c\rho_0}, \quad z = \frac{h}{h_*}, \quad R_0 = \frac{r_0}{h_*}, \quad z_0 = \frac{h_0}{h_*},$$

$$\mathrm{Ar} = \frac{RT_*}{E}, \quad \mathrm{Td} = \frac{cRT_*^2}{EQ}, \quad \theta_0 = -\frac{1}{\mathrm{Td}}, \quad \alpha_T = \frac{\alpha_t h_*}{\lambda}.$$

Institute of Structural Macrokinetics and Problems of Materials Technology, Russian Academy of Sciences, Chernogolovka, Moscow oblast, 142432 Russia

1028-3358/01/4605-0299$21.00

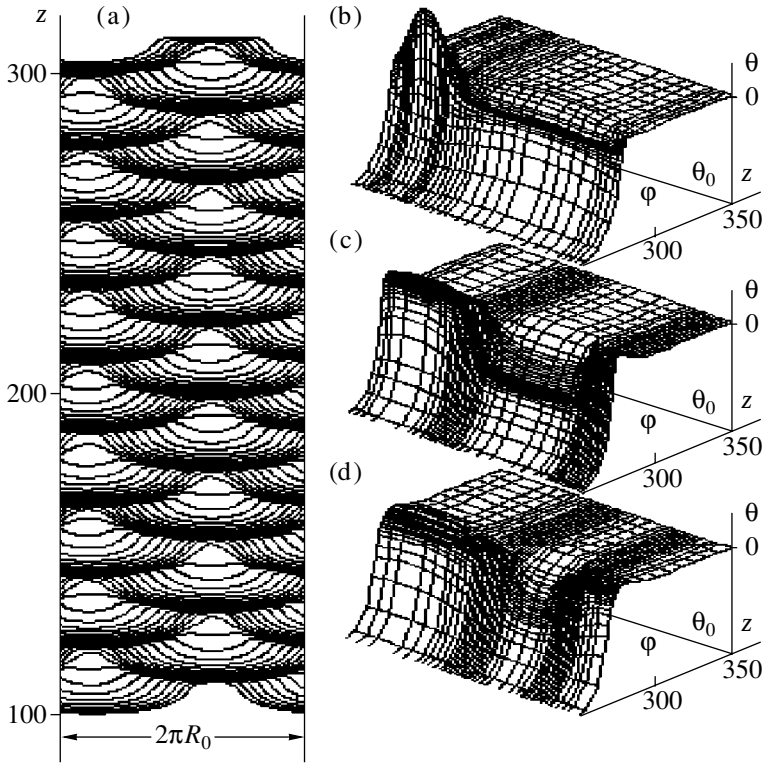

Fig. 1. (a) Positions of the combustion front at successive ($\Delta\tau = 10$) time moments ($\alpha_{st} \approx 0.75$, $R_0 \approx 13$) and the temperature distribution in the combustion front (only the near-front domain is shown); (b) formation of a high-temperature zone at a point of merging combustion centers; (c) and (d) propagation of the front from the merging point upon decreasing the temperature in the reaction zone.

Here, T is temperature; $T_* = T_0 + \frac{Q}{c}$ is the characteristic temperature (we take it as equal to the adiabatic-combustion temperature); T_0 is the ambient temperature and the initial temperature of the sample; c is the specific heat; Q is the thermal effect of the reaction; η is the conversion level for a limiting component; ρ_0 is the mass of the condense phase per unit volume; t is time; φ and h are the spatial coordinates (angular and along the cylindrical axis, respectively); λ is the heat conductivity; k_0 is the preexponential factor; E is the activation energy; R is the gas universal constant; α_t is the factor determining the heat-transfer from the sample surface to the environment (in this study, $\alpha_t = 0$); r_0 and h_0 are the radius and the height of the cylinder, respectively; t_{ign} is the time of action of the ignition pulse; and Td and Ar are the Thodes and Arrhenius criteria, respectively (similar to [6]).

This mathematical model of the combustion process was numerically investigated using the finite-difference method. We employed a nonuniform spatial calculation mesh with a nonfixed number of nodes, which was adapted to the desired solution. To do this, the mesh nodes were concentrated in the domain of the combustion front. As the sample burns, sample buildup occurred from the reagent side and reaction products far from the front were cut off. These properties of the calculation mesh made it possible to reduce the time of attaining the steady-state regime and, on the other hand, to accelerate the calculation procedure. As defining parameters, α_{st} and R_0 were used. The parameter $\alpha_{st} = 9.1\text{Td} - 2.5\text{Ar}$ defined in [7] (at $\alpha_{st} < 1$) characterizes the depth of penetration into the domain in which the plane steady front is unstable. The boundary separating the stable and unstable one-dimensional regimes is determined by the condition $\alpha_{st} = 1$. The parameter R_0 corresponds to the ratio of the cylinder radius and the characteristic value of the reaction zone. It was conditionally supposed that the front is a set of points on the cylindrical surface where half the limiting reagent has reacted.

Figure 1 shows a regime that can be observed for small-diameter samples. This regime was obtained for single-center spin combustion after reducing the sample diameter. The mechanism of the front propagation is the following. After merging combustion centers, a zone arises in which, owing to the cumulative effect, the temperature is considerably higher than that in each combustion center. However, because of the smallness of the sample radius, a well heated zone does not yet form at this time instant in the domain of fresh reagents. Therefore, the combustion of materials occurs as unreacted reagents are heated owing to a high-temperature zone arising in the area of combustion-center merging.

The front line takes the form of an arc with its center at the point of merging. With removing the reaction front from this point, the front velocity decreases as long as the front sections approach each other on the opposite side of the cylinder. There, the combustion centers merge again and the process is repeated.[1] Figures 1b–1d show the temperature distribution on the evolvent of the cylinder surface for the time elapsed from the combustion-center merging to the subsequent merging on the opposite side. The question naturally arises as to whether this mode can be considered a steady-state regime. In the plot, nine periods are shown. While performing the calculations, the periodicity of the system behavior remained unchanged for 40 periods. This fact implies that, furthermore, the combustion type also does not change. The region of existence of this regime is rather narrow. An insignificant decrease in the sample diameter may result in transformation of the combustion into pulsatory propagation of the reaction front. Conversely, with increasing the sample diameter, the regime can be transformed into the classic spin regime with a single combustion center. For the stability criterion used in Fig. 1, i.e., for $\alpha_{st} \approx 0.76$, this regime exists in the interval $10.5 < R_0 < 15.9$. It is worth noting that, due to the nonuniqueness in the case of $12.2 < R_0 < 15.9$, the sample combustion may proceed in both the regime presented in Fig. 1 and the classic spin regime.

In study [5], the regime referred to as circular combustion is described. This regime was reproduced in the process of the numerical simulation of the initial system of equations. In essence, this regime is intermediate between the plane pulsatory one and the counter spin regime described above. Therefore, this type of combustion front propagation can be more adequately termed pulsatory-spin waves. In this regime, as before, "depression" zones and rapid-combustion zones of well-heated layers change each other. However, the combustion front is curved and the combustion of the well-heated layer occurs as a result of the motion of front sections moving toward each other. After merging the combustion centers, i.e., after complete burning of a layer heated during the preceding period, a depression appears again. Due to the front curvature, the next ignition occurs (after the heating of the subsequent layer has been completed) in the zone with the maximum front delay. This is explained by the summation of heat flows from neighboring domains advancing the delayed front section. Furthermore, the process is repeated. However, the investigation performed testifies to the instability of such a regime. It inevitably transforms into either the classic spin regime (Fig. 2) or the above regime with counter motion of the front sections. In experiments when only a limited number of periods are observed, such a regime may seem to be stable. It is possible to find pulsatory-spin waves in the process of burning samples of small radius.

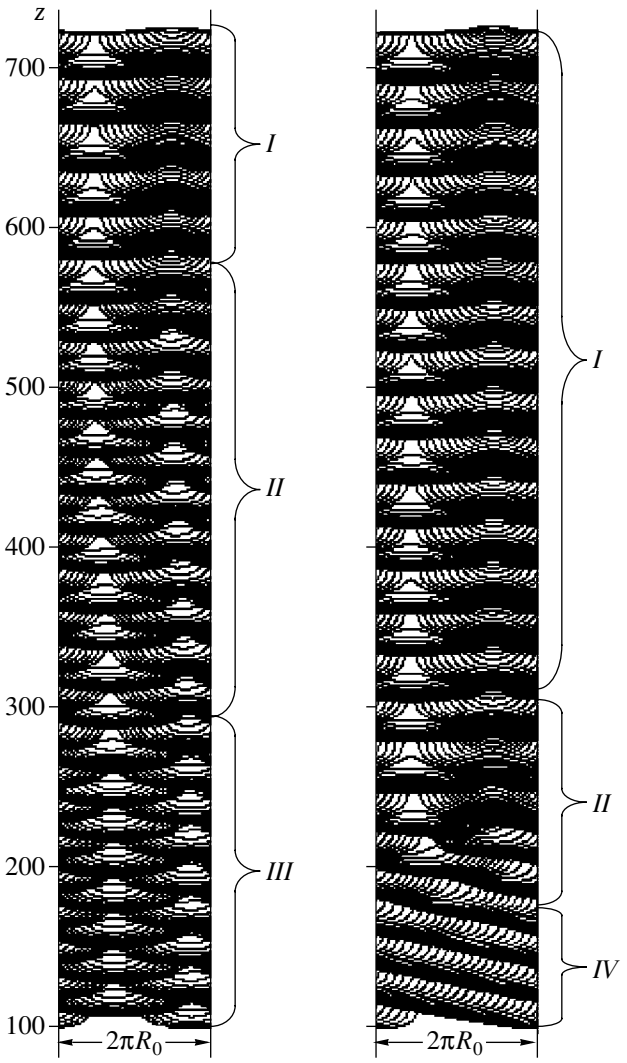

Fig. 2. Positions of the combustion front in successive ($\Delta\tau$ = 10) time moments ($\alpha_{st} \approx 0.75$). Propagation of the combustion front and its transformation at $R_0 \approx 15$ and $R_0 \approx 16$: (*I*) pulsatory-spin combustion propagation; (*II*) regime transformation stage; (*III*) regime of front propagation at the expense of heat inflow from the high-temperature zone formed at the point of merging front sections; (*IV*) spin-combustion regime.

As is well known [3], when increasing the sample radius, a single-center combustion regime initially transforms into a two-center regime. Furthermore, the number of combustion centers can increase. In this case, all the combustion centers move in the same direction (clockwise or counterclockwise). However, in the high-instability region, the situation changes. The increase in the cylinder radius results in the appearance of a second combustion center moving in the opposite direction with respect to the first one (Fig. 3). After both combustion centers meet on the opposite side of the

[1] The front structure is symmetric with respect to a certain (arbitrary) cylinder generatrix.

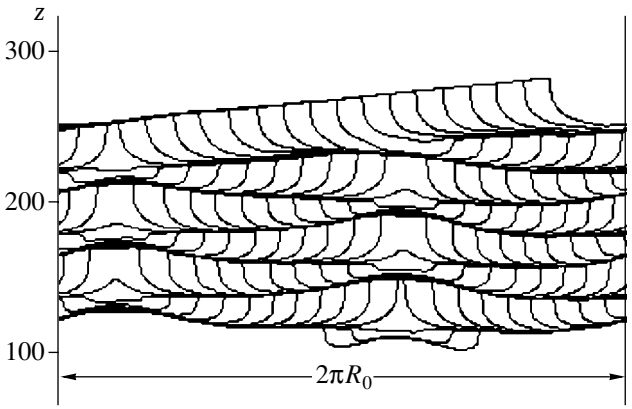

Fig. 3. Positions of the front combustion in successive ($\Delta\tau = 32$) time moments ($\alpha_{st} \approx 0.47$ and $R_0 \approx 75$). In the high-instability region, the given classic regime is unstable and transforms into that of counter combustion-center propagation.

sample, they merge and, as a result, a high-temperature zone arises. It is well known [3] that both an increase in the sample radius and penetration into the instability region lead to an increase in the combustion-center temperature. Therefore, the temperature in this zone is very high. By virtue of this fact, high-temperature combustion centers arise that may move away from the point of their generation without additional heat inflow from the high-temperature zone in which they were formed. Divergent combustion centers removed from this point attain more and more heated layers of fresh reagents. This leads to a continuous rise in both the combustion-center temperature and velocity of motion until the subsequent merging of these centers on the opposite side of the cylinder occurs (Fig. 4). Furthermore, the process repeats itself.

There is no doubt that such a regime of combustion-front propagation is stable. The calculations confirm

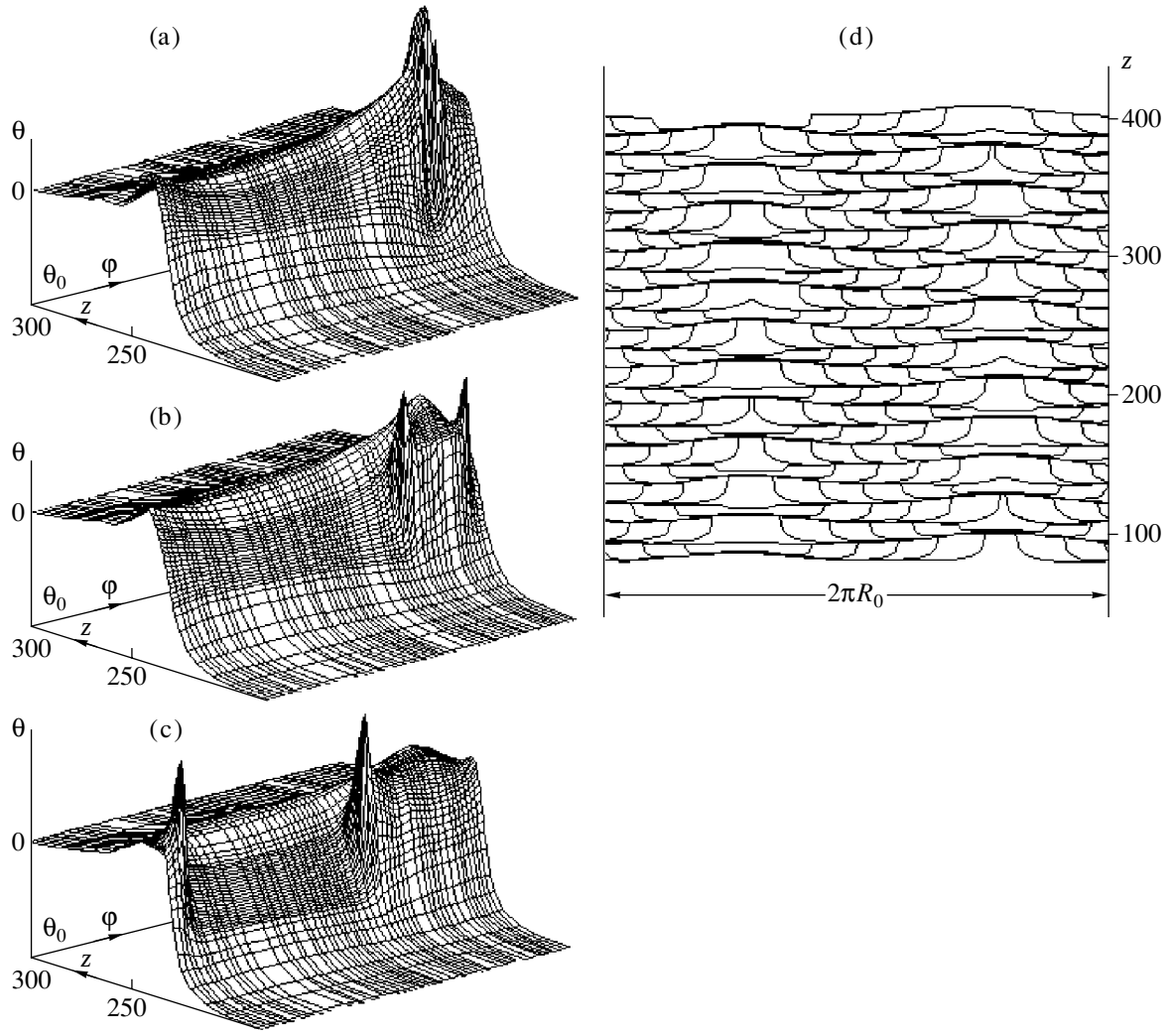

Fig. 4. Counter combustion regimes in the region of strong instability ($\alpha_{st} \approx 0.47$ and $R_0 \approx 48$). Temperature distribution in the combustion front (only the near-front domain is shown): (a) appearance of new combustion centers in the high-temperature zone formed at the point of merging combustion centers; (b) and (c) front propagation from the point of merging combustion centers as a function of the temperature in new combustion centers; (d) position of the combustion front in successive ($\Delta\tau = 32$) time moments.

the viability of this regime. First, it exists during a large number of periods without changing its structure. Second, if within the region of high instability the classic spin regime is taken as the initial condition, then it transforms into the regime of counter-propagating combustion centers (Fig. 3). With further penetration into the instability region and an increase in the sample radius, multiple counter regimes may appear.

Thus, while burning small-radius samples, the merging of combustion centers moving counter to each other can be followed by either depression (if the temperature in the combustion center formed at the merging point is too small to initiate the combustion of the cold layer of reagents that are situated lower) or propagation of the combustion front, which is caused by heat inflow from the formed high-temperature zone. In this case, the temperature in the reaction zone and the rate of its motion decrease as this zone moves away from the high-temperature domain. Within the high-instability region, an increase in the sample radius leads to counter motion of well-pronounced combustion centers, whose temperature and velocity increase as they move away from their point of generation.

ACKNOWLEDGMENTS

The author is grateful to professor I.P. Borovinskaya, who is one of the discoverers of spin waves, for her fruitful participation in discussing the results of this work and valuable advice.

REFERENCES

1. A. G. Merzhanov, A. K. Filonenko, and I. P. Borovinskaya, Dokl. Akad. Nauk SSSR **208**, 892 (1973).
2. A. G. Strunina, A. V. Dvoryankin, and A. G. Merzhanov, Fiz. Goreniya Vzryva **19** (2), 30 (1983).
3. T. P. Ivleva, A. G. Merzhanov, and K. G. Shkadinskiĭ, Fiz. Goreniya Vzryva **16** (2), 3 (1980).
4. Yu. M. Maksimov, A. T. Rak, G. V. Lavrenchuk, *et al.*, Fiz. Goreniya Vzryva **15** (3), 156 (1979).
5. A. S. Mukasyan, S. G. Vadchenko, and I. O. Khomenko, Combust. Flame **111**, 65 (1997).
6. A. G. Merzhanov, V. V. Barzykin, and V. G. Abramov, Khim. Fiz. **15** (6), 3 (1996).
7. K. G. Shkadinskiĭ, V. I. Khaĭkin, and A. G. Merzhanov, Fiz. Goreniya Vzryva **7** (1), 19 (1971).

Translated by Yu. Vishnyakov

Doklady Physics, Vol. 46, No. 5, 2001, pp. 304–306. Translated from Doklady Akademii Nauk, Vol. 378, No. 1, 2001, pp. 38–40.

PHYSICS

On Extremal Entropy Production in the Solid-Body Conductance Theory

A. S. Pleshanov

Presented by Academician G.S. Golitsyn October 31, 2000

Received November 2, 2000

It is shown that, in one-dimensional geometry, the principle of the minimum of entropy production in equilibrium final states is correct in one general situation. Two examples taken from the solid-body conductance theory are considered.

For a solid body with no external loads and no regard for heat expansion, which ensures the constancy of stresses and density, the equations of energy and entropy balance have the form

$$\rho c\frac{\partial T}{\partial t} = -\mathrm{div}\,\mathbf{q} = \mathrm{div}(\kappa\nabla T), \tag{1}$$

$$\rho\frac{\partial s}{\partial t} - \rho\left(\frac{\partial s}{\partial t}\right)_e \equiv \rho\frac{\partial s}{\partial t} + \mathrm{div}\left(\frac{\mathbf{q}}{T}\right) = \rho\left(\frac{\partial s}{\partial t}\right)_i \tag{2}$$
$$\equiv (\mathbf{q}\nabla)\frac{1}{T} = \kappa\left(\frac{\nabla T}{T}\right)^2 \equiv \sigma > 0,$$

where s is the entropy and σ is the entropy production rate. The subscripts e and i are related to the external and internal parts of the variation in the total entropy $S = \int \rho\, s dV$; other designations are the same as in [1]. The entropy balance is described by the equation

$$\frac{\partial S}{\partial t} - \left(\frac{\partial S}{\partial t}\right)_e \equiv \frac{\partial S}{\partial t} + \int\frac{(\mathbf{q}d\mathbf{F})}{T} = \left(\frac{\partial S}{\partial t}\right)_i$$
$$\equiv \int(\mathbf{q}\nabla)\frac{1}{T}dV = \int\kappa\left(\frac{\nabla T}{T}\right)^2 dV \equiv \Sigma > 0. \tag{3}$$

For arbitrary temperature dependences $\kappa(T)$ and $c(T)$, the entropy production rate σ is determined by the equation

$$\frac{\partial\sigma}{\partial t} - \left(\frac{\partial\sigma}{\partial t}\right)_e \equiv \frac{\partial\sigma}{\partial t} - 2\mathrm{div}\left(\frac{\partial T}{T\partial t}\frac{\kappa\nabla T}{T}\right) = \left(\frac{\partial\sigma}{\partial t}\right)_i$$
$$\equiv -2\rho c\left(\frac{\partial T}{T\partial t}\right)^2 + \frac{d(\kappa T^2)}{TdT}\frac{\partial T}{T\partial t}\left(\frac{\nabla T}{T}\right)^2, \tag{4}$$

from which, on account of the condition

$$\kappa T^2 = \mathrm{const}, \tag{5}$$

we obtain

$$\left(\frac{\partial\sigma}{\partial t}\right)_i = -2\rho c\left(\frac{\partial T}{T\partial t}\right)^2 < 0. \tag{6}$$

Note that the differential expression (4) degenerates in the steady-state situation, which suggests the need for its transformation (transition to the integral representation). In the integral form, both for T_e = const and for $q_e = 0$, expression (6) takes the form

$$\frac{\partial\Sigma}{\partial t} = \left(\frac{\partial\Sigma}{\partial t}\right)_i = -2\int\rho c\left(\frac{\partial T}{T\partial t}\right)^2 dV < 0.$$

This means that σ and Σ decrease monotonically in the course of system evolution, tending to the minimum values which are attained in the steady-state condition (the minimum is equal to zero in the equilibrium state). This result is generally known as the minimum entropy production principle [2, 3]. In the case considered here, this principle is realized on the condition that the kinetic coefficient L in the Fourier law

$$\mathbf{q} = L\nabla\left(\frac{1}{T}\right)$$

is constant in accordance with condition (5). Note that this condition is satisfied for metals at low temperatures [4], when $T \ll \theta$ (θ is the Debye temperature). It is asserted in [2, 3] that the discussed principle holds only for L = const. We will show that, in the one-dimensional geometry, this principle is correct in one general situation. We start with the representation of Eq. (4)

OAO Krzhizhanovskiĭ Power Engineering Institute, Leninskiĭ pr. 19, Moscow, 117927 Russia

1028-3358/01/4605-0304$21.00

in the form

$$(\sigma_t)_i = -2\rho c\left(\frac{T_t}{T}\right)^2 + \kappa\chi\frac{d\ln(\kappa T^2)}{d\ln T} \times\left[\frac{T_{xx}}{T} + \frac{d\ln\kappa}{d\ln T}\left(\frac{T_x}{T}\right)^2\right]\left(\frac{T_x}{T}\right)^2, \quad (7)$$

where $\chi = \frac{\kappa}{\rho c}$ and the subscripts t and x denote the partial derivatives. Separating the complete derivative in (7), we obtain

$$(\sigma_t)_i - (\sigma_t)_{ie} \equiv (\sigma_t)_i - \frac{1}{3}\left[\kappa\chi\frac{d\ln(\kappa T^2)}{d\ln T}\left(\frac{T_x}{T}\right)^3\right]_x = (\sigma_t)_{ii} \equiv -2\rho c\left(\frac{T_t}{T}\right)^2 + \frac{1}{3}\kappa\chi K\left(\frac{T_x}{T}\right)^4, \quad (8)$$

with

$$K = \frac{d\ln(\kappa T^2)}{d\ln T}\frac{d\ln(\rho c\kappa T^3)}{d\ln T} - \frac{d^2\ln(\kappa T^2)}{(d\ln T)^2}. \quad (9)$$

When $K < 0$, we have

$$(\sigma_t)_{ii} < 0,$$

which corresponds to the minimum entropy production principle in the final state.

We give here two examples from the solid-body conductance theory. For metals, the power-law temperature dependences are valid [4],

$$\kappa = AT^l, \quad c = BT^m \quad (10)$$

and, on account of (9), parameter K takes the form

$$K = (l + 2)(l + m + 3).$$

This means that the condition $K < 0$ is satisfied for

$$-2 < l < -(m + 3) \text{ or } -(m + 3) < l < -2,$$

while the condition $K > 0$ holds for

$$l > -2, \quad l > -(m + 3) \text{ or } l < -2, \quad l < -(m + 3).$$

The domain of unconditional fulfillment of the minimum entropy production is hatched in Fig. 1. We clearly see the exclusiveness of the value $l = -2$, which is indicated in [2, 3]: this is the only function $\kappa(T)$ ensuring, irrespective of the form of the $c(T)$ dependence, the entropy production minimum in the final state, which, in this case ($l = -2$), is an equilibrium state. As follows from Fig. 1, the domain of unconditional fulfillment of the entropy production minimum

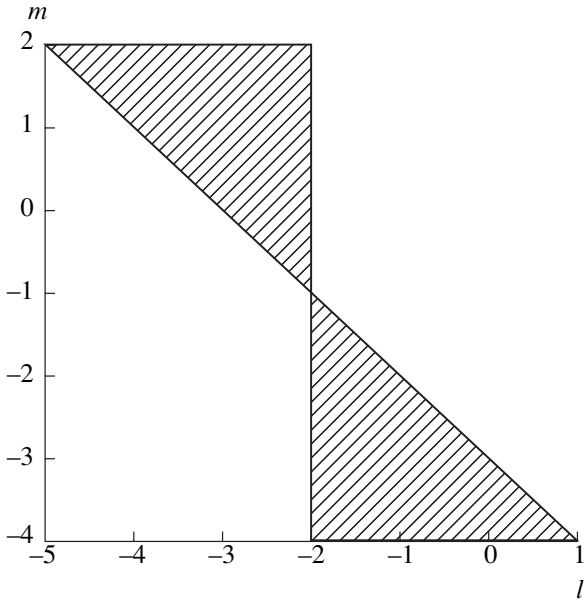

Fig. 1.

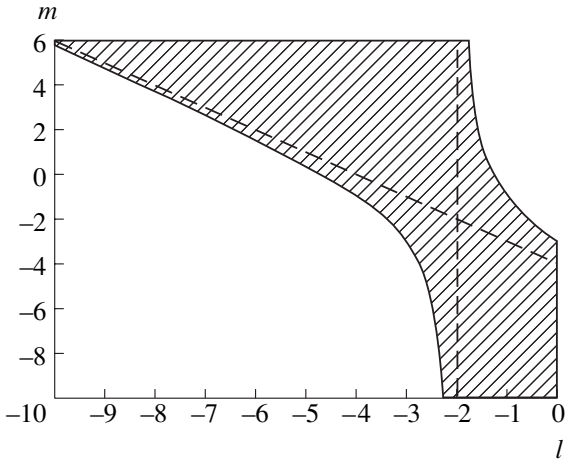

Fig. 2.

in the final state comprises one fourth of the domain occupied by all possible values of l and $m \in (-\infty, \infty)$.

For dielectric substances, the following temperature dependences take place at $T \ll \theta$:

$$\kappa = A\exp\left(\frac{\Delta}{T}\right), \quad c = BT^m \quad (11)$$

($\Delta \sim \theta$ is the photon energy [4]). Taking into account the relationships

$$\frac{d\ln\kappa}{d\ln T} = -\frac{\Delta}{T} = l < 0, \quad \frac{d^2\ln\kappa}{(d\ln T)^2} = \frac{\Delta}{T} = -l > 0,$$

we find from (9)

$$K = (l + 2)m + (l^2 + 6l + 6) = (l - l_1)(m - m_1),$$

where

$$l_1 = -2, \quad m_1 = -(l+4) + \frac{2}{l+2}.$$

The domain located between the branches m_1, where the entropy production minimum is unconditionally attained, is hatched in Fig. 2.

We should make some conclusive remarks. The constraint by one-dimensional geometry is due to the problematic representation of the quantity $(\nabla S)^2 \Delta S$, with an arbitrary scalar S, by the sum of the divergence and the source. Next, the case $\frac{dc}{dT} < 0$ is possible in a chemically reactive medium.

The author is grateful to I.M. Mazilin and N.A. Shevelev for their assistance in performing this study.

REFERENCES

1. L. D. Landau and E. M. Lifshitz, *Course of Theoretical Physics*, Vol. 6: *Fluid Mechanics* (Nauka, Moscow, 1986; Pergamon, New York, 1987).
2. I. Prigogine, *Etude thermodynamique des phénomènes irréversibles* (Dunod, Paris, 1947).
3. S. R. de Groot and P. Mazur, *Nonequilibrium Thermodynamics* (North-Holland, Amsterdam, 1962; Mir, Moscow, 1964).
4. E. M. Lifshitz and L. P. Pitaevskiĭ, *Physical Kinetics* (Nauka, Moscow, 1979; Pergamon, Oxford, 1981).

Translated by A. Kozlenkov

Doklady Physics, Vol. 46, No. 5, 2001, pp. 307–309. Translated from Doklady Akademii Nauk, Vol. 378, No. 1, 2001, pp. 41–43.

PHYSICS

On a Mechanism of Ion Acceleration in Vacuum Arc-Discharge Plasma

G. Yu. Yushkov*, A. S. Bugaev*, I. A. Krinberg, and E. M. Oks*****

Presented by Academician G.A. Mesyats November 11, 2000

Received December 5, 2000

The unremitting attention to the study of vacuum-arc discharge [1, 2] is caused by its wide application in high-current and high-voltage switches, sputtering facilities, and ion sources [3]. At the same time, there exists no conventional concept of the vacuum-arc phenomenon whose specific feature is a rapid transformation of cathode material into the liquid phase, superdense gas, and plasma. (The latter is being subsequently transformed from a dense nonideal state to a moderately rarified one and finally to a collisionless state.)

Among the key experimental facts established while studying vacuum discharge, an important part belongs to the existence of directed flows (jets) of ions moving towards the anode, whose energies exceed the energy determined by the voltage of the discharge burning. At present, there exist three standpoints concerning the mechanism of ion acceleration and its spatial localization:

(i) The acceleration occurs at high densities (nonideal plasma or metal-density gas) in the region of hydrodynamic and electromagnetic discontinuities under phase transitions [4, 5].

(ii) The gas-dynamic acceleration of plasma takes place under the action of a pressure gradient (maintained by Joule heating by the electric-current flow). This occurs at gas densities ensuring the identity of directed velocities for different-charge ions due to electron–ion and ion–ion friction [6–8].

(iii) The ions are accelerated by an electric field towards the anode due to the nonmonotone distribution of the electric potential (potential hump) in the absence of collisions. By virtue of this fact, the ion velocity grows with the ion charge [9, 10].

The available experimental data are of a contradictory nature. For example, Davies and Miller [10] found that the ion velocity linearly increases with the ion charge. At the same time, in a number of other studies (e.g., in the experiments of Tsuruta *et al.* [11]), measured ion velocities, under certain conditions, were virtually independent of ion charge.

Emission methods [12] for studying processes intrinsic to vacuum-arc discharge, which are currently being developed by us, consist in determination of the parameters and characteristics of plasma on the basis of analysis of the ion current extracted from the plasma and the charge components of the current. In this paper, we present the results of an analysis (by the emission method) of directed ion velocities in a vacuum arc. Their comparison with the calculated data allows us to make conclusions on the principal mechanism of ion acceleration in the vacuum arc.

The schematic diagram of the experiment is presented in Fig. 1. When burning the vacuum arc (τ_{arc} = 400–800 μs and I_{arc} = 100–500 A), the plasma flow emitted by cathode spots filled the anode cavity. The ions extracted from the plasma were accelerated by a multiaperture three-grid accelerating–decelerating system with a permanent applied voltage of 10–25 kV. The charge distribution of the accelerated ion flow was analyzed by means of a time-of-flight spectrometer [12].

The ion velocity in the vacuum-arc discharge plasma was measured according to the time delay between the moment of a weak disturbance of the arc current and the reaction of the extracted ion current. In this case, analysis of the evolution of the ion currents with different charges made it possible to measure their directed velocities. The disturbance was formed by either a short-term jump in the arc current or its forced break. The time delay t between the arc-current disturbance and the emission-current response involves the time of flight t_l of the ions having desired directed velocity V_i through the discharge gap, as well as the total time t_g for an ion to be in the accelerating gap and the drift space (in this case, under our experimental

* *Institute of Heavy-Current Electronics, Siberian Division, Russian Academy of Sciences, Akademicheskiĭ pr. 4, Tomsk, 634055 Russia*

** *Irkutsk State University, bul'v. Gagarina 20, Irkutsk, 664003 Russia*

*** *Tomsk State University of Control Systems and Radio Electronics, pr. Lenina 40, Tomsk, 634050 Russia*

1028-3358/01/4605-0307$21.00

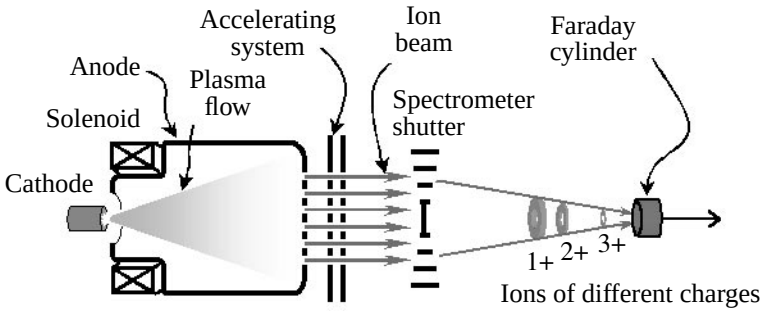

Fig. 1. Schematic diagram of the experimental setup.

conditions, $t \gg t_g$). It is worth mentioning that the basic ionization processes in the vacuum-arc discharge occur near the cathode spots at distances not longer than 1 mm from the cathode surface, which is much smaller than the length l of the discharge gap. Therefore, it is easy to determine the directed ion velocity in plasma according to the measured time t, the calculated value of t_g, and the known distance l: $V_i = \dfrac{l}{t - t_g}$.

As experiments have shown (see Fig. 2), independent of the cathode material, the time responses to the current jump or break were rather similar for ions with different charges. From these results, it follows unambiguously that the values of the directed velocity for ions with different charges and, hence, their kinetic energies turn out to be virtually the same.

This result contradicts the conventional modern data obtained by Davies and Miller [10]. The analysis of the experimental conditions described in [10] testifies to the fact that the pumping equipment employed in these experiments, probably, could not provide a high vacuum due to the intense gas liberation which occurred during arc burning. The elevated pressure of the residual gas in the discharge gap could affect the directed ion velocities. For verifying this suggestion, we have carried out experiments with the goal of measuring the directed ion velocities at an elevated pressure under conditions of forced gas puffing into the discharge gap. As was expected, the elevation of the pressure p led to a different decrease in the velocity V_i for ions with different charges. For relatively high values of pressure, $p > 10^{-2}$ Pa, the measured velocities approach those observed in [10]. Thus, the existence of different directed velocities of ions of different charges is intrinsic to the vacuum-arc plasma only in the case of elevated gas pressure. This fact is, apparently, associated with differences in the processes of deceleration of ions of different charges in a gas rather than with the conditions of their acceleration.

The identity of directed velocities for different ion charges made it possible to considerably simplify the process of measuring ion velocities for various chemical elements without application of a time-of-flight spectrometer. In these experiments, the ion velocities were determined by the time shift between the discharge-current modulation and the total ion-current response. The velocities measured for various cathode materials, including the majority of conducting elements of the periodic system, are presented in Fig. 3.

In [8], the general solution to the problem of expansion of a current-carrying plasma into vacuum from the surface of a sphere with radius r_0 was obtained. This solution can be compared with a cathode microspot of size $a \approx 1$–10 μm [1, 2] that emits a plasma jet. Slightly modifying the results of [8], we can represent the ion velocity in the form $V_i = MV_S$, where $V_S = \left(\dfrac{\gamma \langle Z \rangle T_e}{m_i}\right)^{1/2}$ is the velocity of the (ionic) sound at the critical point $r = r_*$ (where $V_i = V_S$ and M = 1). Here, M is the Mach number; $\gamma = \dfrac{5}{3}$ is the adiabat index; $\langle Z \rangle$ and m_i are the average charge and ion mass, respectively; and T_e is the electron temperature at the point $r = r_*$. The Mach number is a universal function of the dimensionless

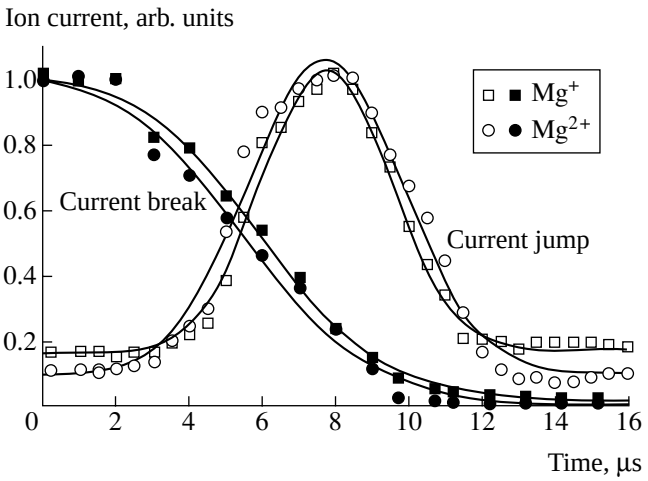

Fig. 2. Mg-ion current as a function of time after a jump or a break of the vacuum-arc current.

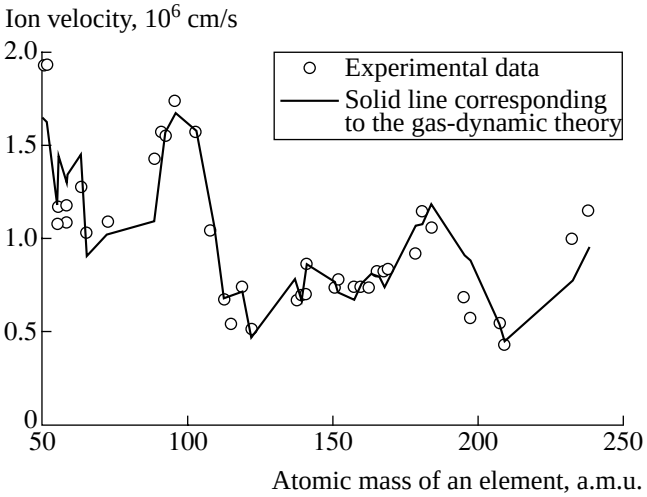

Fig. 3. Experimental and calculated values for velocities of ions of different chemical elements.

length $\frac{r}{r_*}$, where r is the distance from the sphere center. At distances exceeding 1 mm, the Mach number virtually attains its ultimate value $M_{lim} \approx 3.5$. Since all available measurements of ion velocities were certainly performed at longer distances, we can accept for the ion velocity in the main part of the interelectrode gap under the conditions of a vacuum arc that

$$V_i^{lim} = M_{lim} V_S \approx \left(\frac{20\langle Z\rangle T_e}{m_i}\right)^{1/2}.$$

To calculate ion velocities V_i^{lim}, measurements of the ionic composition [13] and values (found from it) of the electron temperature T_e [14] were used. The values of V_i^{lim} obtained are given in Fig. 3. As is seen, they are in good agreement with the measurement data. This fact allows us to draw a conclusion on the prevailing gas-dynamic acceleration mechanism involved in the attainment of the observed velocities by ions. Of course, in the initial stage of motion (when $V_i < V_S$), a certain acceleration of the cathode material in phase transitions to the liquid-metal state or the state of a super-dense gas [4, 5] is also possible. However, the contribution of this mechanism to the final value of the ion velocity does not exceed 20%. As our measurements have shown the absence of velocity differences for ions of various charges, the acceleration at the phase of collisionless plasma expansion turns out to be still less significant.

ACKNOWLEDGMENTS

This work was supported by the Russian Foundation for Basic Research, project no. 99-02-18163.

REFERENCES

1. *Vacuum Arcs: Theory and Application*, Ed. by J. M. Lafferty (Wiley, New York, 1980; Mir, Moscow, 1982).
2. G. A. Mesyats, *Ectons in Vacuum Discharge: Breakdown, Spark, and Arc* (Nauka, Moscow, 2000).
3. *Handbook of Vacuum Arc: Science and Technology*, Ed. by R. L. Boxman, R. J. Martin, and D. M. Sanders (Noyes, Park Ridge, 1995).
4. N. B. Volkov and A. Z. Nemirovskiĭ, J. Phys. D **24**, 693 (1991).
5. A. Z. Nemirovskiĭ and E. A. Litvinov, in *Proceedings of the XII Symposium on High Current Electronics*, Tomsk, 2000, p. 60.
6. G. A. Lyubimov, Dokl. Akad. Nauk SSSR **225**, 1045 (1975) [Sov. Phys. Dokl. **20**, 830 (1975)].
7. C. Wieckert, Contrib. Plasma Phys. **27** (5), 309 (1987).
8. I. A. Krinberg, M. P. Lukovnikova, and V. L. Papernyĭ, Zh. Éksp. Teor. Fiz. **97**, 806 (1990) [Sov. Phys. JETP **70**, 451 (1990)].
9. A. A. Plyutto, V. N. Ryzhkov, and A. T. Kapin, Zh. Éksp. Teor. Fiz. **47**, 494 (1964) [Sov. Phys. Dokl. **20**, 328 (1964)].
10. W. D. Davis and H. C. Miller, J. Appl. Phys. **40**, 2212 (1969).
11. K. Tsuruta, K. Sekiya, and G. Watanabe, IEEE Trans. Plasma Sci. **25**, 603 (1997).
12. A. S. Bugaev, V. I. Gushenets, A. G. Nikolaev, *et al.*, IEEE Trans. Plasma Sci. **27**, 882 (1999).
13. I. G. Brown, J. E. Galvin, R. A. MacGill, and R. T. Wright, Rev. Sci. Instrum. **58**, 1589 (1987).
14. A. Anders, Phys. Rev. E **55** (4), 969 (1997).

Translated by G. Merzon

Doklady Physics, Vol. 46, No. 5, 2001, pp. 310–312. Translated from Doklady Akademii Nauk, Vol. 378, No. 2, 2001, pp. 173–175.

PHYSICS

The Similarity Law and Equation of State for a Liquid in the Vicinity of a Critical Point

G. A. Martynov

Presented by Academician V.E. Fortov November 30, 2000

Received December 4, 2000

In 1873, van der Waals first made the suggestion that the equation of state, when being written in an appropriate coordinate system, must take the same form for all liquids and solutions (similarity law). This hypothesis was confirmed by later experiments. However, the range of validity of the similarity law turned out to involve not the entire phase diagram, as had been initially assumed, but only a certain, sometimes fairly wide, neighborhood of a critical point. Since the correlation radius increases with approaching the critical point, the universality of the equation of state is evidently related to this process. However, attempts to show how an individual equation of state degenerates into a universal one have failed to date. In this paper, we pioneer this type of analysis on the basis of the Ornstein–Zernike equation. In addition, we formulate the so-called critical equations of state in themselves and investigate some of their corollaries.

THE ORIGIN OF THE SIMILARITY LAW

The Ornstein–Zernike equation is known to represent the conventional Gibbs distribution written in the form of an integral equation determining the correlation function $h(r)$, where r is the distance between the particles [1]. The exact solution to this equation can be written out in the form of a series in eigenfunctions of the asymptotic Ornstein–Zernike equation [2]:

$$h(r) = A\frac{\exp(-\lambda_0 r)}{r} + \sum_j \frac{\exp(-\lambda_j r)}{r}[B_j \sin(\mu_j r) + C_j \cos(\mu_j r)]. \quad (1)$$

Here, the constants λ_j and μ_j are the roots of the transcendental equation $1 - \rho\Delta(\lambda, \mu) = 0$; $\rho = \frac{N}{V}$ is the density of the liquid; and A, B_j, and C_j are, in the general case, continuous functions of the density ρ and temperature $\theta = kT$. [The summation in (1) is performed over the entire infinite set of roots for the transcendental equation.]

Substituting (1) into the expression for the isothermal compressibility of the liquid, which is presented in [1],

$$\kappa_\theta = \left(\frac{\partial\rho}{\partial P}\right)_\theta = \frac{1}{\theta}\left\{1 + 4\pi\rho\int_0^\infty h(r)r^2 dr\right\}, \quad (2)$$

we arrive at the expression

$$\frac{\partial\rho}{\partial P} = \frac{1}{\theta}\left\{1 + 4\pi\rho\left[\frac{A}{\lambda_0^2} + \sum_j\left(B_j\frac{2\lambda_j\mu_j}{[(\lambda_j)^2 + (\mu_j)^2]^2} + C_j\frac{(\lambda_j)^2 - (\mu_j)^2}{[(\lambda_j)^2 + (\mu_j)^2]^2}\right)\right]\right\}, \quad (3)$$

where P is pressure.

The derivative $\frac{\partial\rho}{\partial P}$ at the critical point is known to tend to infinity. Since the amplitudes A, B_j, and C_j are always bounded [2], the fact that the compressibility tends to infinity can only be due to the vanishing of the single real root λ_0 of the transcendental equation $1 - \rho\Delta(\lambda_0) = 0$. However, as is seen from formula (3), the compressibility does not exhibit an unbounded increase as λ_j or μ_j with $j > 0$ approach zero (or infinity).

The vanishing of λ_0 is evidently equivalent to the correlation radius becoming infinite:

$$R = \frac{1}{\lambda_0} \longrightarrow \infty. \quad (4)$$

Hence, the term $\frac{\exp(-\lambda_0 r)}{r}$ entering into the general solution to the Ornstein–Zernike equation (1) in the neighborhood of the critical point describes the asymptotic behavior of the general correlation functions. All the remaining terms of the series [in (1), they are under the summation sign] determine the behavior of $h(r)$ at

Institute of Physical Chemistry,
Russian Academy of Sciences,
Leninskiĭ pr. 31, Moscow, 117915 Russia

1028-3358/01/4605-0310$21.00

small distances, i.e., when the general correlation function is independent of the form of the interaction potential $\Phi(r)$. As soon as the contribution of asymptotic distances exceeds that of small distances, we can ignore in (3) both the unity (corresponding to the ideal-gas compressibility) in the braces and the sum (describing the interparticle interaction at small distances) in the square brackets. As a result, Eq. (3) is reduced to the equality

$$\frac{\partial\rho}{\partial P} \approx \frac{4\pi\rho}{\theta}\frac{A}{\lambda_0^2}. \tag{5}$$

Since this expression does not contain a sum allowing for the specific properties of the medium, the behavior of the compressibility becomes universal. Therefore, all the remaining parameters of the medium also begin to behave universally.

The formulas obtained above are easily generalized for solutions [3]. In this case, the transcendental equation determining the roots λ_j and μ_j becomes rather complicated and the constants A, B_j, and C_j in (3) (for a binary solution) are replaced by the sums

$$A = A_{aa} + 2A_{ab} + A_{bb}, \quad B_j = B^j_{aa} + 2B^j_{ab} + B^j_{bb}, \quad C_j = C^j_{aa} + 2C^j_{ab} + C^j_{bb}. \tag{6}$$

Nevertheless, the basic conclusion remains valid. We imply that the behavior of a solution in the neighborhood of a critical point is determined by the single real root λ_0. This fact is a reason for the universal behavior of solutions.

THE CRITICAL EQUATION OF STATE

More rigorous analysis of the compressibility in the neighborhood of a critical point indicates that $A = \lambda_0^\eta A_0$ at this point, where $\eta \approx 0.05$ is one of the critical indices and $A_0 = \text{const}$ is independent of λ_0 [4]. Moreover, since $\lambda_0 = \text{const}\ \varepsilon_\theta^\nu$, where $\nu \approx 0.63$ is another critical index and $\varepsilon_\theta = \dfrac{\theta - \theta_c}{\theta_c}$ is a small parameter characterizing the distance from the critical point, then equalities (6) can be written out in the form [4]

$$\frac{\partial\rho}{\partial P} = \frac{4\pi\rho}{\theta}\frac{A_0}{\varepsilon_\theta^\gamma} = \kappa_0\varepsilon_\theta^{-\gamma} \quad \text{for} \quad \rho = \rho_c, \tag{7}$$

where $\gamma = \nu(2 - \eta)$ and κ_0 is a constant independent of λ_0. In the same manner according to the theory developed in [1], the pressure P and specific heat c_ρ at a constant volume are given by

$$P - P_c = \pi_0\varepsilon_\rho^\delta \quad \text{for} \quad \theta = \theta_c, \quad \text{and} \quad c_\rho = c_0\varepsilon_\theta^{-\alpha} \quad \text{for} \quad \rho = \rho_c. \tag{8}$$

Here, $\varepsilon_\rho = \dfrac{\rho - \rho_c}{\rho_c}$ is the second small parameter, π_0 and c_0 are certain constants, $\alpha \approx 0.11$ and $\delta \approx 4.6$ are the critical indices, and the subscript "c" related to different functions implies that the value of the function is taken at the critical point.

In essence, the expression $P - P_c = \pi_0\varepsilon_\rho^\delta$ represents an equation of state; this equation is valid, however, only along the isotherm $\theta = \theta_c$. In the general case, when $\theta \neq \theta_c$, the equation of state must take the form $P - P_c = \pi_0\varepsilon_\rho^\delta + f(\varepsilon_\rho, \varepsilon_\theta)$, where an unknown function $f(\varepsilon_\rho, \varepsilon_\theta)$ must vanish for $\theta = \theta_c$.[1] It is natural to define this function in such a manner that condition (7) for the compressibility will be satisfied in the neighborhood of the critical point. Hence,

$$P - P_c = \pi_0\varepsilon_\rho^\delta + k_0^{-1}\varepsilon_\rho\varepsilon_\theta^\gamma, \qquad \kappa_\theta = \frac{\partial\rho}{\partial P} = \rho_c\frac{\partial\varepsilon_\rho}{\partial P} = \frac{1}{\pi_0\delta\varepsilon_\rho^{\delta-1} + k_0^{-1}\varepsilon_\theta^\gamma}. \tag{9}$$

Introducing the variables $p = \dfrac{P - P_c}{P_0}$, $P_0 = \pi_0$, $q = \varepsilon_\rho$, and $t = (k_0\pi_0)^{-1/\gamma}\varepsilon_\theta$, we arrive at

$$p = q^\delta + qt^\gamma, \quad \kappa = \frac{\partial q}{\partial p} = \frac{\tilde\kappa_0}{\delta q^{\delta-1} + t^\gamma}, \tag{10}$$

where $\tilde\kappa_0 = \dfrac{\rho_c}{P_0}$.

Since for $\theta = \theta_c$, the chemical potential μ obeys the identity $d\mu = \dfrac{dP}{\rho}$, then the equalities

$$\frac{d\mu}{d\rho} = \frac{\mu_0}{\rho_c}\frac{dm}{dq} = \frac{P_0}{\rho_c(1+q)}\frac{dp}{dq}$$

are valid, where $m = \dfrac{\mu - \mu_c}{\mu_0}$. Assuming that $\mu_0 = \dfrac{P_0}{\rho_c}$, we have

$$\frac{dm}{dq} = \frac{t^\gamma}{1+q} + \frac{\delta q^{\delta-1}}{1+q}.$$

[1] In the neighborhood of a critical point, both ε_ρ and ε_θ are small parameters. Therefore, the correction $f(\varepsilon_\rho, \varepsilon_\theta)$ to the degenerate equation of state (8) can also be sought in the form of a small addition.

Ultimate laws for various directions of approaching a critical point

Parameter	$q = 0$	$q = t$	$t = 0$
Pressure	Const	$\sim t^{\gamma+1}$	$\sim q^{\delta}$
Compressibility	$\sim t^{-\gamma}$	$\sim t^{-\gamma}$	$\sim q^{\delta-1}$
Chemical potential	Const	$\sim t^{\gamma+1}$	q^{δ}
Specific heat	$\sim t^{-\alpha}$	$\sim t^{-\alpha}$	∞

Integrating this expression within the limits $q = 0$ and q yields

$$m = \frac{\mu - \mu_c}{\mu_0} = t^{\gamma}\ln(1+q) + \int_0^q \frac{\delta q^{\delta-1} dq}{1+q} \quad (11)$$
$$= (t^{\gamma} + \delta q^{\delta-1})\ln(1+q) - \delta(\delta-1)\int_0^q q^{\delta-2}\ln(1+q)dq.$$

Expanding $\ln(1+q)$ in (11) in terms of a power series of q, we now obtain, within an accuracy to linear terms, that $\mu - \mu_c = \frac{P - P_c}{\rho_c}$. The allowance for the quadratic terms yields

$$m = q^{\delta} + qt^{\gamma} - \frac{\delta}{1+\delta}q^{\delta+1} - \frac{1}{2}q^2t^{\gamma} + \ldots \quad (12)$$
$$\approx p - \frac{\delta}{1+\delta}q^{\delta+1} - \frac{1}{2}q^2t^{\gamma} + \ldots$$

We, finally, consider the behavior of the specific heat in the vicinity of a critical point. The specific heat $c_\rho = \left(\frac{\partial e}{\partial \theta}\right)_\rho$ at a constant volume is known to be related to pressure by the equality [5]

$$\rho^2\left(\frac{\partial c_\rho}{\partial \rho}\right)_\theta = -\theta\left(\frac{\partial^2 P}{\partial \theta^2}\right)_\rho.$$

Taking into account that $\rho \equiv \rho_c(1+\varepsilon_\rho)$, $\theta \equiv \theta_c(1+\varepsilon_\theta)$, $d\rho = \rho_c d\varepsilon_\rho$, and $d\theta = \theta_c d\varepsilon_\theta$ and ignoring the small quantities $\varepsilon_\rho, \varepsilon_\theta \ll 1$, we arrive at the relation

$$\frac{\partial c_\rho}{\partial \varepsilon_\rho} = -\frac{P_0}{\rho_c\theta_c}\frac{\partial^2 p}{\partial \varepsilon_\theta^2}.$$

We set $c = \frac{c_\rho - c_c}{c_0}$, where $c_0 = \frac{P_0^{1-(2/\gamma)}}{\rho_c\theta_c k_0^{2/\gamma}}$. In this case, the equation for the dimensionless specific heat takes the form

$$\frac{\partial c}{\partial q} = -\frac{\partial^2 p}{\partial t^2} = -\gamma(\gamma-1)qt^{\gamma-2}. \quad (13)$$

This equation determines the function c with an accuracy to the arbitrary function $f(t)$ of temperature. In order for the solution to Eq. (13) at $q = 0$ to transform into formula (8), the function $f(t)$ must take the form $t^{-\alpha}$. As a result, we arrive at

$$c \equiv \frac{c - c_c}{c_0} = -\frac{1}{2}\gamma(\gamma-1)q^2t^{\gamma-2} + t^{-\alpha}. \quad (14)$$

Thus, we obtain equations that describe the behavior of the pressure, compressibility, chemical potential, and specific heat in the entire critical region, in which the asymptotic contribution into the compressibility isotherm exceeds the other remaining contributions. All the equations obtained, being written in dimensionless form, become universal because they do not contain parameters which characterize the specific properties of the medium. It should be emphasized that these results are valid for both pure liquids and multicomponent solutions because formula (3) for the compressibility is applicable to the latter and the former.

Until now, all known equations of states (7), (8) described the behavior of a medium along either the critical isotherm with $t = 0$ or the critical isochore with $q = 0$. The equations of state obtained above make it possible to approach a critical point along an arbitrary direction. The critical indices corresponding to three directions of approaching a critical point are listed in the table; namely, for $t = 0$ (i.e., along the isotherm $\theta = \theta_c$), $t = q$ (along the bisectrix of the right angle between this isotherm $\theta = \theta_c$ and the isochore $\rho = \rho_c$), and $q = 0$ (along this isochore). It is seen that these indices significantly differ from their generally accepted values given by (7) and (8). Thus, the neighborhood of a critical point can be imagined as a certain mountain whose slope depends on the direction of approaching. This feature of a critical point appears to have been first indicated in [6].

REFERENCES

1. G. A. Martynov, *Fundamental Theory of Liquids* (Adam Hilger, Bristol, 1992).
2. R. Evans, R. J. Leote de Carvalcho, and D. C. Hoyle, J. Chem. Phys. **100**, 591 (1994).
3. G. A. Martynov, Teor. Mat. Fiz. **123**, 500 (2000).
4. G. A. Martynov, Usp. Fiz. Nauk **169**, 595 (1999).
5. L. D. Landau and E. M. Lifshitz, *Statistical Physics* (Nauka, Moscow, 1976; Pergamon, Oxford, 1980).
6. V. A. Rabinovich and Yu. E. Sheludyak, *Thermodynamics of Critical Phenomena: New Analysis of the Evolution of Properties* (Begell House, New York, 1998).

Translated by V. Chechin

Doklady Physics, Vol. 46, No. 5, 2001, pp. 313–316. Translated from Doklady Akademii Nauk, Vol. 378, No. 2, 2001, pp. 176–178.

PHYSICS

Magnetic Depolarization and Overlapping 3*d* Orbitals in Crystals of Transition Elements

N. N. Sirota

Presented by Academician V.V. Osiko December 21, 2000

Received December 25, 2000

In accordance with the Hund rules, when filling with electrons 3*d* orbitals of free atoms within the range from Sc(d^1) to Mn(d^5), the magnetic moment of an atom increases up to $5\mu_B$. Then, it lowers from Fe(d^6) to Cu(d^{10}) (from $4\mu_B$ to zero, respectively) due to the formation of electron pairs with opposite spin directions.

It was established in [1–4] that the mean magnetic moments for atoms of elements in crystals are substantially lower than those for free atoms. This phenomenon has not been reasonably explained to date.

The difference of magnetic moments of free atoms and those bound in crystals in the case of elements with unfilled 3*d* orbitals depends on the electron-density distribution in them, on the degree of orbital overlapping, and the probability of magnetic depolarization [5]. The "tails" of the distributions indicated play, evidently, the most essential role in this case.

In order to describe the density distribution for electrons with uncompensated spins, we employ, as before, the Gaussian function

$$\rho = \frac{dn}{dV} = Ae^{-\gamma r^2}, \qquad (1)$$

in which the factor A is determined from the normalization condition, and $\gamma = \frac{1}{r_0^2}$ is the inverse value of the orbital radius squared. The use of the Gaussian function allows us to find, within reasonable accuracy, analytical expressions that determine the number of electrons in the overlapping region and to evaluate the probabilities of formation among them of electron pairs with compensated spins.

The numbers N_d and n_0 of 3*d* electrons and 3*d* electrons with uncompensated spins for isolated atoms, respectively, and the equilibrium distances δ_1 between nearest neighboring atoms in the crystal lattices of the elements studied are listed in the table. The numbers n_P of electrons per atom, which were experimentally determined (these electrons have compensated spins in the overlapping region), and the rest number n_F of electrons with uncompensated spins are also indicated in the table. (In this case, $n_0 = n_P - n_F$.) The number n_F expressed in Bohr magnetons corresponds to the mean atomic magnetic moment in a crystal for a given degree of orbital overlapping, which is determined by δ_1. The equilibrium values of δ_1 are calculated according to data taken from [8, 9].

The number n_P of electrons with compensated spins that are present in the overlapping region is determined by the degree of overlapping orbitals with the corresponding effective electron density

$$\rho_{\text{eff}} = e^{-C_2\gamma r^2}. \qquad (2)$$

The presence of the coefficient C_2, which takes the probability of magnetic depolarization into account, can be considered formally as an increase of 3*d*-orbital radii in the crystal lattice compared to those in isolated atoms.

The ratio of the number n_P of electrons with compensated spins in the overlapping region to the number n_0 of electrons with uncompensated spins of an isolated atom is, in this case,

$$\frac{n_P}{n_0} = \frac{\int_{\delta/2}^{\infty} \rho_{\text{eff}} dV}{\int_0^{\infty} \rho_{\text{eff}} dV}. \qquad (3)$$

We can take, approximately, [5] that

$$\frac{n_P}{n_0} \approx e^{-C_2\gamma\delta^2}. \qquad (4)$$

Moscow State University of Environmental Engineering, ul. Pryanishnikova 19, Moscow, 127550 Russia

1028-3358/01/4605-0313$21.00

Radii of 3*d* orbitals, coefficients γ_w and γ_{GZ}, magnetic moments n_0 for isolated atoms and atoms in crystals, the structure type A_j, the nearest interatomic distances δ_1, and the number N_d of 3*d*-electrons for transition elements with Z = 23–28

No.	Z	Element	N_d	n_0	Radius of the 3*d* orbital		γ_w, a.m.u.$^{-1}$	γ_{GZ}, a.m.u.$^{-1}$	Structure type
					r_{d_w}, a.m.u.	$r_{d_{GZ}}$, a.m.u.			
1	23	V	3	3	0.84877	0.91	1.3881	1.2076	A_2
2	24	Cr	5	5	0.8053	0.892	1.542	1.2568	A_2
3			(4)	(4)					
4	25	Mn	5	5	0.73346	0.8236	1.8589	1.4742	A_1
5	26	Fe	6	4	0.68620	0.7823	2.1237	1.6340	A_2
6	27	Co	7	3	0.6465	0.7446	2.3925	1.8036	A_1
7	28	Ni	8	2	0.6106	0.7100	2.6822	1.9837	A_1

No.	Experimental data						Calculated data			
	$C_{2_w} \times 10^4$	$C_{2_{GZ}} \times 10^4$	δ_1, a.m.u.	n_{P_1}	$\bar{n}_{F_1}$	$-\ln\frac{n_{P_1}}{n_0}$	$C_{2_w} \times 10^4$	$-\ln\frac{n_{P_1}}{n_0}$	n_{P_1}	$\bar{n}_{F_1}$
1	10	11.5	4.95	2.99	0.1	0.034	0.01	0.0003	2.999	0.001
2	(36)		4.722	(4.4)	(0.6)	0.127	78	0.268	3.824	1.176
3	24	29		(3.8)	(0.2)	0.083	15.7	0.054	1.79	0.21
4	72	91	5.163	3.5	1.5	0.357	81.1	0.394	3.4	1.6
5	172	224	4.692	1.782	2.218	0.808	177	0.827	1.748	2.251
6	160	210	4.737	1.28	1.72	0.85	168	0.902	1.2172	1.782
7	59	82	4.71	1.40	0.604	0.358	67	0.399	1.34	0.66

The quantity $\ln\frac{n_P}{n_0} = \ln\left(1 - \frac{n_F}{n_0}\right) = -C_2\gamma\delta^2$ is associated with the ratio of the atomic magnetic moment (n_F, μ_B) in the crystal lattice to the magnetic moment (n_0, μ_B) of the isolated atom and depends on the interatomic distance squared.

The values of $-\ln\frac{n_P}{n_0}$, which are determined in accordance with experimental mean atomic magnetic moments of 3*d* transition elements in crystals for equilibrium nearest interatomic distances δ_1, as well as the radii r_w and r_{GZ} of 3*d* orbitals, are presented in the table. These radii were calculated by the Hartree–Fock method [6] and by methods of the atom statistical theory [7], respectively. The values of γ_w and γ_{GZ} corresponding to these radii are also indicated in the table.

It is worthwhile noting that the orbital radii given in the table and those of other authors, as well as the radii of several types of hybridized orbitals (3*d* etc.), significantly differ from each other. However, the general dependence on the ordinal number of elements is conserved. The coefficients C_{2r_w} and $C_{2r_{GZ}}$ calculated according to the values of γ_w and γ_{GZ}, as well as the experimental values for $-\ln\frac{n_{P_1}}{n_0} \approx C_2\gamma\delta_1^2$, are also given in the table.

The probability coefficient C_2 depending on the filling N_d of the 3*d* orbital can be described by a semiempirical expression:

$$C_2(x) = \frac{1}{N_{d_m}\sqrt{x_m}}x^{\nu}(1-x)\exp\left(-\frac{N_{d_m}^2}{2\sqrt{2}}(x_m - x)^2\right), \quad (5)$$

where $x = \frac{N_d}{N_{d_m}}$, $N_{d_m} = 10$, the exponent ν ranges within the limits of 1 to 2 (we have accepted $\nu = 2$), and x_m is within the range from 0.62 to 0.67 (we assume x_m = 0.64, which, to a larger extent, corresponds to the experimental data).

The curve $C_2(x)$ calculated by the expression given above is shown in Fig. 1. Dots corresponding to the values of C_{2_w}, which were determined according to the

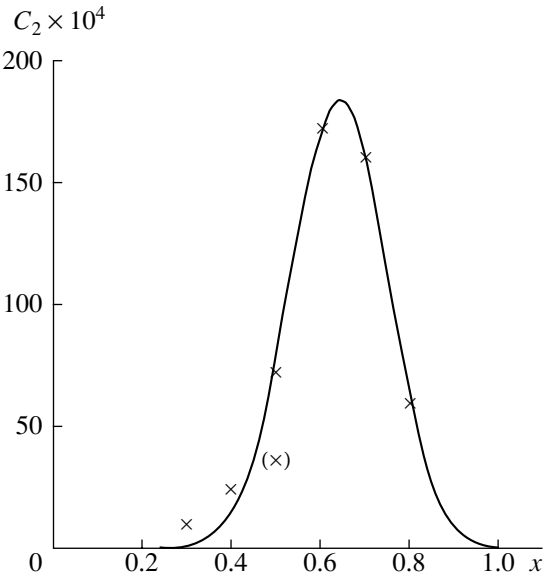

Fig. 1. The coefficient C_2 as a function of $x = \frac{N_d}{N_{d_m}}$ for $x_m = 0.64$ and $\nu = 2$. The dots corresponding to the experimental data are plotted together with the calculated curve.

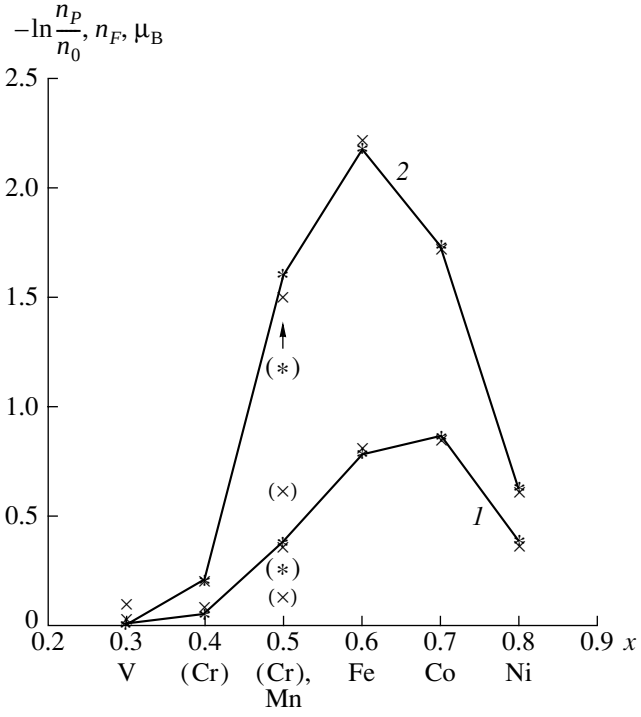

Fig. 2. (*1*) Values of $-\ln\frac{n_{P_1}}{n_0}$ for elements with $Z = 23$–28. The calculated dots (∗) are connected by a solid line; the dots (×) correspond to the experimental data. In the calculations, the values of γ_w and δ_1 are used corresponding to $x_m = 0.64$, $\nu = 2$. (*2*) Atomic moments $\bar{n}_F$ for elements with $Z = 23$–28. The experimental dots (∗) are plotted together with the curve drawn according to calculated data (×). In the calculations, the values of γ_w and δ_1 used correspond to $x_m = 0.64$.

experimental data for $\ln\frac{n_{P_1}}{n_0}$, δ_1, and for the values of γ_w, are plotted together with the curve. As is seen from Fig. 1, the dots calculated by the experimental data fit the theoretical curve for $C_2(x)$ relatively well.

In this case, the values of $\ln\frac{n_P}{n_0}$, depending on the filling of the *d* orbital in 3*d*-transition elements, are described by the expression

$$\ln\frac{n_P}{n_0} = -\frac{1}{N_{d_m}\sqrt{x_m}}x^2(1-x)\left[\exp\left(-\frac{N_{d_m}^2}{2\sqrt{2}}(x_m-x)^2\right)\right]\gamma\delta^2. \quad (6)$$

As is seen from Fig. 2, the experimental values for $\ln\frac{n_P}{n_0}$ correspond well to those calculated by this expression.

The mean atomic magnetic moments are expressed by the relationship

$$\frac{\overline{n_F}}{n_0} = 1 - e^{-C_2(x)\gamma\delta_1^2}. \quad (7)$$

In Fig. 2, the calculated curve $\overline{n_F}(x)$ together with experimental data on the magnetic moments of 3*d* elements with atomic number $Z = 23$–28 is also shown. As is seen, the experimental values agree rather well with the calculated curve.

Thus, in this paper, we have derived expressions for the probability of the magnetic depolarization of electrons in the region of *d* orbital overlapping. These expressions allow us to establish the semiquantitative dependences for the mean magnetic moments of transition elements on both the number of electrons filling 3*d* orbitals and the interatomic distances between the nearest neighboring atoms in the crystal lattice.

The allowance for the probability of spin compensation (magnetic depolarization) when overlapping 3*d* orbitals of neighboring atoms is equivalent to the concept of an increase (compared to isolated atoms) in the effective radii of *d* orbitals in atoms that residue in a crystal lattice.

REFERENCES

1. S. V. Vonsovskiĭ, *Magnetism* (Nauka, Moscow, 1971; Wiley, New York, 1974).

2. S. V. Tyablikov, *Methods in the Quantum Theory of Magnetism* (Nauka, Moscow, 1975, 2nd ed.; Plenum, New York, 1967).
3. R. M. White, *The Quantum Theory of Magnetism* (Springer-Verlag, Berlin, 1983; Mir, Moscow, 1985).
4. J. B. Goodenough, *Magnetism and the Chemical Bond* (Interscience, New York, 1963; Metallurgiya, Moscow, 1968).
5. N. N. Sirota, Dokl. Akad. Nauk **368**, 328 (1999) [Dokl. Phys. **44**, 600 (1999)].
6. J. Waber and T. Cromer, J. Chem. Phys. **42**, 4116 (1965).
7. P. Gombás and T. Szondy, *Solutions of the Simplified Self-Consistent Field for All Atoms of the Periodic System of Elements from Z = 2 to Z = 92* (Akadémiai Kiadó, Budapest, 1970).
8. G. V. Samsonov, *Properties of Metals. A Handbook* (Metallurgiya, Moscow, 1976), Part 1.
9. J. Emsley, *The Elements* (Clarendon Press, Oxford, 1989; Mir, Moscow, 1993).

Translated by T. Galkina

Doklady Physics, Vol. 46, No. 5, 2001, pp. 317–320. Translated from Doklady Akademii Nauk, Vol. 378, No. 2, 2001, pp. 179–182.

PHYSICS

An Effect of Nucleation Processes on the Thermal-Destruction Rate of Materials under Intense Thermal Actions

O. F. Shlenskiĭ

Presented by Academician V.V. Osiko November 27, 2000

Received December 8, 2000

High-intense thermal flows (induced by radiation heating, laser irradiation, etc.) give rise to thermal destruction and evaporation in near-surface layers of a material. The mass velocity for the motion of the thermal-destruction boundary is determined by an approximate relationship [1]:

$$G = \frac{\sqrt{B\rho\frac{RT_w^2}{E}\lambda_s\exp\left(-\frac{E}{RT_w}\right)}}{\sqrt{H^* - \frac{Q}{2}}}. \quad (1)$$

Here, E, B, and Q are the activation energy, the preexponential factor, and the thermal effect of the thermal-decomposition reaction, respectively; T_0 and T_w are the initial temperature and surface temperature; C_s and ρ are the heat capacity and density of the material; $H^* = C_s(T_w - T_0) + Q$; and λ_s is the heat conduction of the material, which is assumed to be constant.

Similar relationships are used when calculating the propagation rate $u = \frac{G}{\rho}$ of the combustion front in condensed systems [2].

Equation (1) is based on the assumptions that the material structure is invariable and homogeneous and that the coefficient λ_s is constant. A number of other simplifications are also used in the derivation of Eq. (1), which may be considered to be reasonable to some extent for processes occurring in gas mixtures (when nucleation is absent), at low temperatures, and in the case of a free outflow of gaseous thermal-decomposition products. However, in heat-protective materials characterized by a sufficient stiffness, in composite materials, and in thermoplastic, reactive-plastic, and other nonvolatile substances, the heterogeneous reaction inevitably passes through the nucleation stage of the thermal-decomposition products (usually consisting of gaseous compounds) and, as a result, is accompanied by the destruction of the initial structure.

The goal of this study is to determine the rate of thermal destruction of a material under intense heating with allowance for a significant drop in the thermal conduction of heated near-surface layers and to determine the destruction and dispersion of the substance. This destruction is implied to proceed in the presence of the other processes accompanying nucleation. In the most general formulation, this problem is set for the first time.

Formula (1) is based on the heat-conduction equation

$$\frac{d}{dx}\lambda_s\frac{dT}{dx} - F(T) + \rho C_s u\frac{dT}{dx} = 0. \quad (2)$$

Below, the last term is ignored because of its smallness [1, 2]. By integrating the equation, we find (disregarding, furthermore, that $\lambda_s = \text{const}$)

$$\frac{dT}{dx} = -\left(2\int_{T_0}^{T}\frac{F(T)dT}{\lambda_s(T)}\right)^{1/2}. \quad (3)$$

The heat conduction of a porous medium depends on the reaction rate and, due to the similarity of temperature and concentration fields, like the function of the heat absorption F, depends on temperature and the quantity $\lambda_s \simeq \frac{\lambda_0\rho}{\rho_0}$. Approximating the ratio $\frac{F(T)}{\lambda_s(T)}$ by an exponential function in the form

$$\frac{B\rho Q}{\lambda_0}\exp\left(-\frac{E_\lambda}{RT}\right),$$

where λ_0 is the heat conduction of the initial material, we obtain the approximate solution

$$\frac{dT}{dx} = -\frac{2B\rho_0 QRT^2}{\lambda_0 E_\lambda}\exp\left(-\frac{E_\lambda}{RT}\right)^{1/2}. \quad (4)$$

Equation (4) defines the steeply dropping exponential temperature profile $T(x)$ near the surface (Fig. 1) to

Mendeleev University of Chemical Technology, Miusskaya pl. 9, Moscow, 125190 Russia

1028-3358/01/4605-0317$21.00 © 2001 MAIK “Nauka/Interperiodica”

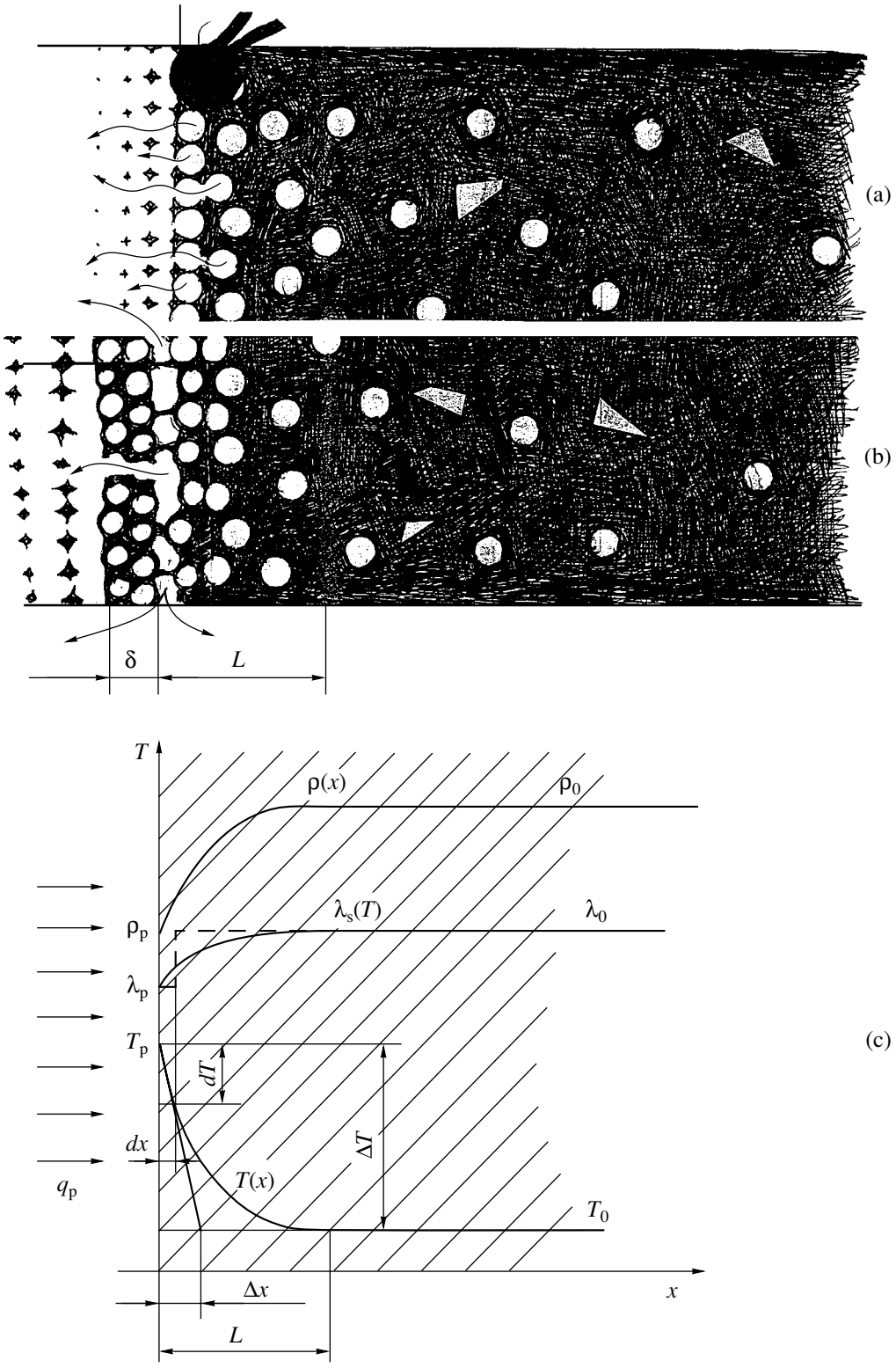

Fig. 1. Schematic diagram of the destruction of near-surface layers in a material heated as a result of the nucleation of thermal-decomposition products and evaporation of the components: (a) positions of nuclei (porous inclusions of gaseous thermal-decomposition products) in the case of a free outflow of gases through the surface owing to their diffusion or molar transfer. On the top, the thermocouple junction for measuring the near-surface temperature T_w is shown; (b) separation of a near-surface layer with thickness δ due to the action of elevated pressure in the pores (in the absence of gas filtration to the surface; a triangular hollow is a heterogeneous nucleus); (c) distributions of the temperature $T(x)$, density $\rho(x)$, and heat-conduction coefficient in the vicinity of the surface of a body heated by a thermal flow q_p. Dashed line is the adopted steplike approximation for $\lambda_s(T)$.

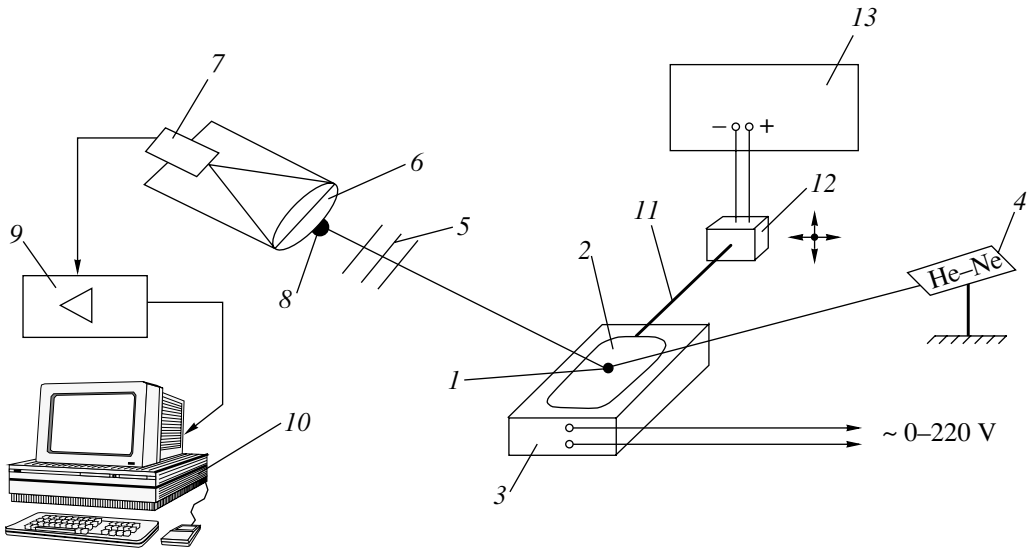

Fig. 2. Schematic drawing of the setup for determining the kinetic characteristics of a material's thermal decomposition and of the ultimate thickness δ for a near-surface layer exfoliated by gas pressure: (*1*) film (sample) of a material, (*2*) substrate, (*3*) heater, (*4*) laser, (*5*) optical filters, (*6*) lens, (*7*) photodetector, (*8*) point screen, (*9*) amplifier, (*10*) computer, (*11*) glass rod, (*12*) removable emitter, (*13*) oscillator.

which the heat flow $q_p = \lambda_p\left(\frac{dT}{dx}\right)$ is delivered. Let λ_p be the heat conduction of a surface layer with pores filled with the products of thermal decomposition ($\lambda_p < \lambda_0$). It is evident that the material boundary should be considered as a surface ($x = 0$), which is characterized by the maximum number of pores. While exceeding this number, their merging and, as a result, material-continuity violation occur. According to [3], the maximum relative volumetric content of spherical inclusions in the case of a dense chaotic (random) porosity distribution is 0.64 of the entire volume ($\Pi = 0.64$). In accordance with the heat conduction theory of disperse media [4–6], the heat conduction of a porous medium and the heat conduction λ_0 of a matrix substance are bound by a simple relation. For the surface $x = 0$, it takes the form

$$\lambda_p = \lambda_0\kappa. \tag{5}$$

The evaluation of the proportionality factor κ by various theories yields close results. For example, at $\Pi = 0.64$, according to the Missenard formula, $\kappa = 1 - \Pi^{2/3} = 0.2573$. As is seen from Fig. 1a, a certain fraction $(1 - \zeta)$ of the nonreacting near-surface material filling the space between the pores is separated from the basic layer in the form of small disperse particles, thereby increasing the rate of the surface motion.

We now equate the flow q_p to the total amount of heat spent on heating the fraction ζ of the reacting material, which, in the case under consideration, is equal to Π ($\zeta = \Pi$):

$$q_p = \kappa\lambda_0\left(\frac{dT}{dx}\right)_{x=0} = u\rho(C_s(T_p - T_0) + \zeta Q), \tag{6}$$

where T_p is the calculated value of T_w. Whence it follows that the thickness L of the well-heated layer increases with decreasing q_p. The value of L is proportional to the segment Δx cut off by a tangent to the curve $T(x)$ at the point $x = 0$. Therefore, the filtration and diffusion of gases to the surface is hampered. As a result, under the action of gas pressure, this can lead to the separation of a layer with thickness δ (see Fig. 1b). Then, the fraction ζ of the reacting material decreases ($\zeta < \Pi$) and the regime can acquire a pulsating form [7]. Substituting $\frac{dT}{dx}$ from Eq. (6) into Eq. (4), we obtain

$$G = u\rho = \frac{\kappa T_p}{C_s(T_p - T_0) + \zeta Q} \times \sqrt{\frac{2B\rho_0 Q\lambda_0 R\exp(-E_\lambda/RT_p)}{E}}. \tag{7}$$

In the particular case of $\kappa = 1$, $\zeta = 1$, $C_s(T_p - T_0) \ll Q$, and $E_\lambda = E$, this equation transforms into relationship (1). For $\zeta = 0$, Eq. (7) transforms into the well-known Belyaev–Zel'dovich equation applied in calculating the combustion rate u of volatile power-consuming compounds [2]. However, the results of calculating the quantity G on the basis of traditional formulas (without regard for the above factors) significantly disagree (by a factor of 2 to 3) with the available experimental data. We imply the thermal destruction of energy-consuming compounds [8], linear polymers [9], composites [1], and other materials in the case of intense surface heating [2, 7, 13]. The allowance for the corrections κ and ζ makes it possible to avoid this disagreement in the results.

There is another essential drawback of Eq. (1). Using it, we need to experimentally determine the surface temperature T_w, which is unknown *a priori*. This fact decreases the predictive significance of the equation, since the quantity G, in itself, is usually determined in the same experiments. Employing a thermocouple reduces the accuracy of the measurements of T_p, because the temperature along the thermocouple length is averaged to $T_w \neq T_p$. The above problems may be solved, if all parameters involved in Eq. (7) are determined by the contact thermal-analysis method [7]. Using this method, it is possible to record the decrease in the mass kinetics of samples placed on a substrate heated to a constant temperature (Fig. 2).

The method and the setup used were updated. To improve the setup time resolution, we used a laser system for signal recording. The setup makes it possible to determine the effective activation energies E_1 and E_2 not only for moderate temperatures (E_1), in which heterogeneous nucleation dominates, but also at high temperatures, where homogeneous nucleation (E_2) occurs (with allowance for vibrations) [11]. In accordance with the theory of heterogeneous reactions [12, 13], both these characteristics are taken into account in the heat-absorption function $F(T)$. Hence, substituting them into Eq. (3), we obtain the final result, which can be written out in simplified form [at $E_\lambda = E$, $\lambda_s = \lambda_0$, $C_s(T_p - T_0) \ll Q$, and $\lambda_p = \kappa\lambda_0$] as

$$G = \frac{\kappa\sqrt{B\rho_0 R T_p^2 \lambda_0 \left[\frac{\exp(-E_1/RT_p)}{E_1} + \frac{\exp(-E_2/RT_p)}{E_2}\right]}}{\sqrt{\frac{\zeta^2 Q}{2} + \zeta C_s(T_p - T_0)}}. \quad (8)$$

In addition, the method of contact thermal analysis allows us to determine the admissible temperature T_l of overheating a material [3] and the minimum thickness of the surface layer δ, which is separated under the action of the gaseous-product pressure. These quantities make it possible to calculate the surface temperature T_p of the material. Since $\frac{dT}{dx} = \frac{q_p}{\lambda_p} \approx \frac{\Delta T}{\Delta x}$, it follows that $T_p = T_l - q_p\frac{\delta}{\lambda_p}$ [7]. For example, for linear polymers, such as PMMA, PS, and PE, it was established that $\delta \sim 20$ μm. This fact results in a reduction ($\Delta T \sim$ 15–20 K) of the temperature when testing by the linear pyrolysis method. Such a reduction was found previously in [9, 14]. Other examples of the analysis of thermal-destruction processes with allowance for nucleation and admissible overheating, as applied to technological processes, are given in [7, 15].

The above analysis makes it possible to conclude that the processes of nucleation, secondary-pore formation, and the accompanying reasons for their occurrence essentially influence the physical properties of near-surface layers and, ultimately, the rate of material thermal destruction. Allowance for the nucleation parameters enables significant (in a number of cases, by an order of magnitude) improvements of the results of numerical simulations to be made. The relationships derived include certain additional parameters. For their determination, we have proposed employing the updated contact thermal-analysis method combined with a high-speed signal-recording system.

REFERENCES

1. Yu. V. Polezhaev and F. B. Yurevich, *Thermal Protection* (Énergiya, Moscow, 1976).
2. K. K. Andreev, *Thermal Decomposition and Combustion of Explosive Materials* (Nauka, Moscow, 1966).
3. V. P. Skripov and V. P. Koverda, *Spontaneous Crystallization of Supercooled Liquids* (Nauka, Moscow, 1984).
4. H. S. Carslaw and J. C. Jaeger, *Conduction of Heat in Solids* (Clarendon Press, Oxford, 1959; Nauka, Moscow, 1964).
5. A. Missenard, *Conductivité termique des solides, liquides, gaz et de leurs mélamges* (Editions Eyrolles, Paris, 1965; Mir, Moscow, 1968).
6. G. N. Dul'nev and Yu. P. Zarichnyak, *Heat Conduction of Mixtures and Compositions* (Énergiya, Leningrad, 1974).
7. O. F. Shlenskiĭ, N. V. Afanas'ev, and A. G. Shashkov, *Thermodestruction of Materials* (Énergoatomizdat, Moscow, 1996).
8. A. F. Belyaev, Dokl. Akad. Nauk SSSR **129**, 635 (1959).
9. A. S. Shteĭnberg, *Linear Pyrolysis*, Preprint, IKhF im. N.N. Semenova (Semenov Institute of Chemical Physics, Academy of Sciences of USSR, Chernogolovka, 1977).
10. D. N. Yundev, D. A. Rogatkin, and L. G. Moiseeva, Teplofiz. Vys. Temp. **36**, 161 (1998).
11. M. E. Brown, D. Dollimore, and A. K. Galwey, in *Reactions in the Solid State*, Ed. by C. Tipper and C. Bamford (Elsevier, Amsterdam, 1980; Mir, Moscow, 1983).
12. D. A. Young, *Decomposition of Solids* (Pergamon, New York, 1966; Mir, Moscow, 1969).
13. O. F. Shlenskiĭ, A. G. Shashkov, and L. N. Aksenov, *Thermal Physics of Decomposing Materials* (Énergoatomizdat, Moscow, 1985).
14. N. P. Novikov and A. A. Kholodilov, Inzh.-Fiz. Zh. **23**, 257 (1972); **22**, 618 (1972).
15. N. A. Zyrichev and O. F. Shlenskiĭ, Khim. Vys. Énerg. **33**, 484 (1999).

Translated by Yu. Vishnyakov

Doklady Physics, Vol. 46, No. 5, 2001, pp. 321–325. Translated from Doklady Akademii Nauk, Vol. 378, No. 3, 2001, pp. 326–330.

PHYSICS

Change-Over of the Conductivity Mechanism in a Nonperfect Helium Plasma on Cooling to ~5 K

É. I. Asinovskiĭ*, A. V. Kirillin, V. V. Markovets*, and Academician V. E. Fortov****

Received January 25, 2001

Three possible trends in experimental investigations of the strong Coulomb interaction in plasma can be associated with the plasma-imperfection parameter [1]:

$$\Gamma = \frac{Z_1 Z_2 e^2 n_e^{1/3}}{kT}. \quad (1)$$

Different methods of obtaining a dense nonperfect plasma with a charged-particle concentration $n_e \sim 10^{20}$–10^{23} cm^{-3} can be assigned to a traditional trend of increasing Γ. The second trend is associated with dust plasma in which the Coulomb interaction between microparticles is enhanced because of the high values of particle charges $Z \sim 10^3$–10^5 [2]. In this paper, we consider cryogenic plasma in which the parameter Γ can be increased by decreasing the temperature of charged particles in the plasma to cryogenic temperatures. One of the reasons why this trend should be considered is the results of experiments with ions accumulated in electrostatic traps and cooled by laser radiation to temperatures of ~10 mK [3]. Although the confined ionic formation is not a plasma in itself because of the absence of electrical neutrality, it is worthwhile noting that the correlation effects observed in the system of Coulomb particles are attained at the expense of decreasing the temperature of these particles.

To date, three cycles of investigations are known in which the problem of obtaining an imperfect cryogenic plasma is formulated. In [4], microwave methods were used to investigate helium afterglow plasma cooled in a cryostat at gas densities lower than 1.2×10^{19} cm^{-3}. The temperature and the electron-collision frequency were measured when the electrons were cooled to 5 K. It was found that, in a late afterglow, the frequency of electron–atom collisions becomes independent of gas density in the range 4.5×10^{18}–1.1×10^{19} cm^{-3}. The authors presumed that this effect is caused by the presence of a large number of atoms in spheres with radius equal to the de Broglie wavelength for cooled electrons.

A decaying cryogenic plasma with a particle number $N = 2$ in the Debye sphere was obtained in experiments [5]. The theoretical estimates showed that the value of N can be reduced to ~0.4 in the afterglow; i.e., a value of $\Gamma \approx 0.8$ can be attained.

A steady cryogenic plasma was first investigated in [6]. A tube with a glow discharge was immersed in cryogenic fluid—liquid nitrogen or helium (Fig. 1). The pressure in the tube and discharge current were chosen such that the ionic temperature T_i in the tube was close to the cooling-fluid temperature. At the same time, the electron temperature T_e in the discharge plasma can attain several tens of thousands of degrees. Theory [7] makes it possible to estimate the interval of parameters in which a heavy component has a mean temperature close to the tube temperature. This theory relates internal plasma parameters T_e, E, and n_e to external discharge parameters: a tube radius R, a gas type, its pressure P, a tube temperature T_w, and a current strength i. The possibility of cooling ions to cryogenic temperatures follows from the energy balance for particles in a nonequilibrium positive-column plasma:

$$W_{e,i} = eEu_{e,i} = \delta_{e,i} k(T_{e,i} - T_a)\nu_{e,i,a}. \quad (2)$$

Here, $u_{e,i}$, $\delta_{e,i}$, $\nu_{e,i}$, and $\mu_{e,i}$ are the drift velocity, the energy fraction lost in collisions, the frequency of collisions with neutral atoms, and the mobilities of electrons and ions, respectively. If we exclude E from the power balance, it is possible to obtain the relationship for temperatures of plasma components:

$$\frac{T_e(T_e - T_a)}{T_i(T_i - T_a)} \approx \frac{m_i m_a^2}{m_e(m_i + m_a)^2}\left(\frac{\lambda_e}{\lambda_i}\right)^2. \quad (3)$$

From this formula, it is possible to determine the range of parameters for the glow discharge in which the ionic component can be cooled to cryogenic temperatures.

The neutral-gas temperature in a weakly ionized plasma is lower than the temperature of ions and is approximately equal to the temperature of tube walls. A neutral gas can be heated mainly by the electrons that loose their energy in elastic collisions. The energy flux

* *Joint Institute for High Temperatures, Russian Academy of Sciences, Izhorskaya ul. 13/19, Moscow, 127412 Russia*

** *Research Center for Thermal Physics of Pulse Effects, Russian Academy of Sciences, Izhorskaya ul. 13/19, Moscow, 127412 Russia*

1028-3358/01/4605-0321$21.00

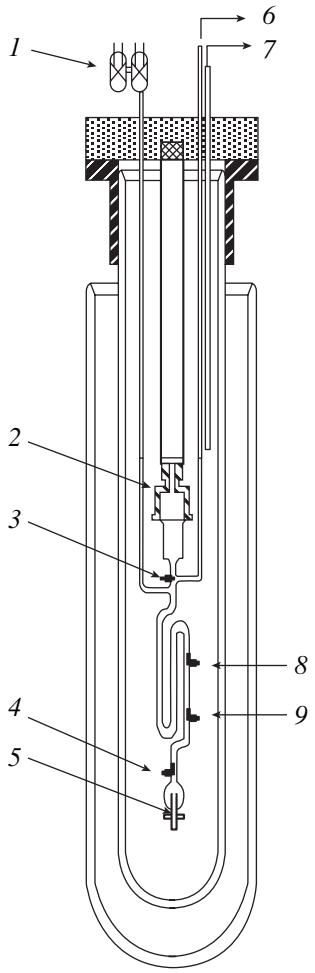

Fig. 1. Design of the discharge tube with a cryostat for investigating steady cryogenic plasma at T = 4.2 K: (*1*) Pirani manometer; (*2*) cathode; (*3*) discharge tube; (*4*), (*8*), (*9*) probes; (*5*) anode; (*6*) outlet for pumping out and for filling the tube by gaseous helium; (*7*) pipe for filling the cryostat with liquid helium.

from electrons per atom is approximately equal to $q_{e,a} = \nu_{e,a}\left(\frac{2m_e}{m_a}\right)kT_e\left(\frac{n_e}{n_a}\right)$. The heat outflow to the wall is determined by the gas heat conductivity, and the corresponding heat flow amounts to $q_a = \frac{k(T_a - T_w)D}{\Lambda^2}$. Making these quantities equal, we obtain the relationship

$$T_a - T_w = \left(\frac{R}{\Lambda}\right)^2\left(\frac{n_e}{n_a}\right)^2\left[\frac{T_e}{T_a}\frac{m_e}{m_a}\right]^{1/2}T_e; \qquad (4)$$

i.e., at a reasonably low ionization degree of 10^{-8} and low pR = 5–10 torr cm, a neutral gas and, thus, the ionic component are heated negligibly in a steady discharge even at T_e = 5 eV. Because the glow-discharge plasma is strongly nonequilibrium, the cooling does not directly affect the character of the electron–atomic interaction; therefore, in the investigation of cryogenic plasma of this type, the methods commonly used in investigating glow discharge at room temperatures are applicable.

In the case of a two-component quasineutral electron–ion plasma with single-charged ions, it is necessary to take the following parameter as a criterion for a strong Coulomb interaction:

$$\Gamma = \frac{e^2 n_e^{1/3}}{k\left(\frac{T_e T_i}{T_e + T_i}\right)}. \qquad (5)$$

Thus, in steady discharges of low and moderate pressure, which are cooled to cryogenic temperatures, it is possible to investigate the effects of imperfect behavior associated with the ionic component for the Γ value close to unity, whose maximum is limited by the heating of ions in the discharge.

It is known that the present view of the low-pressure glow discharge at room temperatures (see, for example, [7]) does not suggest any dependence of ionization processes on the neutral-component temperature. However, for the glow discharge occurring at cryogenic temperatures, the region of parameters in which such an approach is invalid was found experimentally [6, 8, 9].

The strongest influence of liquid-nitrogen cooling of discharge-tube walls on discharge was found for low currents and the electric fields indicated above. At $p \geq$ 5 mm Hg, i < 1 mA, and $\frac{E}{p}$ > 2.5 V/(cm mm Hg), a modification in the behavior of the $E(i)$ dependence is observed: a decrease in the current by 15–20% is accompanied by a drop of E by more than a factor of two; respectively, $\frac{dE}{di} > 0$ (Fig. 2). This segment of the current–voltage characteristic was termed an *H–T* transition by analogy with study [10], in which a similar shape of the current–voltage characteristic was observed for oxygen. The regime with i < 1 mA (T-form of discharge) is characterized by an increase in the strength of the He_2^* molecular bands and by a modification in the shape of probe characteristics—their electron branch is identical to the ionic branch within the ±30 V range near the point $j_p = 0$. A comparison of the characteristics at T_w = 300 K and T_w = 77 K shows that, for currents in the range from 5 to 130 mA and for neutral-atom concentrations $n_a = (1–20) \times 10^{16}$ cm^{-3}, the results of measurements are closely allied if they are referred to the same neutral-gas concentration in the tube irrespective of whether the tube is cooled or not. The change to a low temperature at high discharge currents also does not lead to essential changes in the longitudinal electric field in plasma.

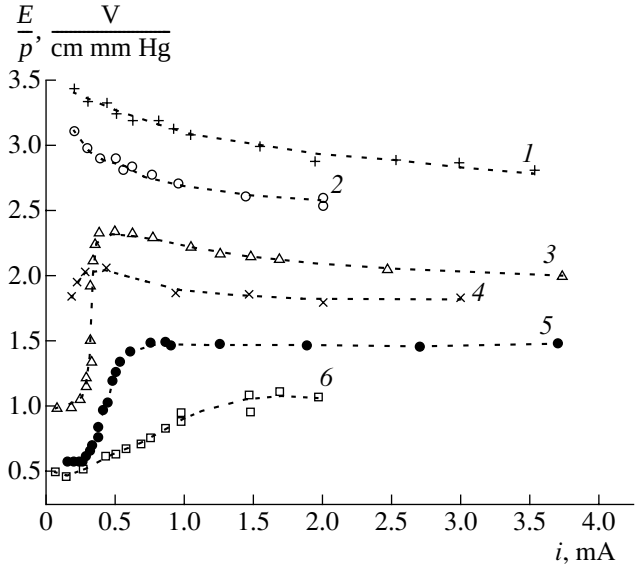

Fig. 2. Reduced electric-field strength in the discharge column as a function of current for various pressures and temperatures: p = 5.35 (*1*); 5.12 (*2*); 9.40 (*3*); 9.28 (*4*); 19.4 (*5*); and 19.3 (*6*) mm Hg. T = 77 (*1*, *3*, *5*) and 4.2 K (*2*, *4*, *6*).

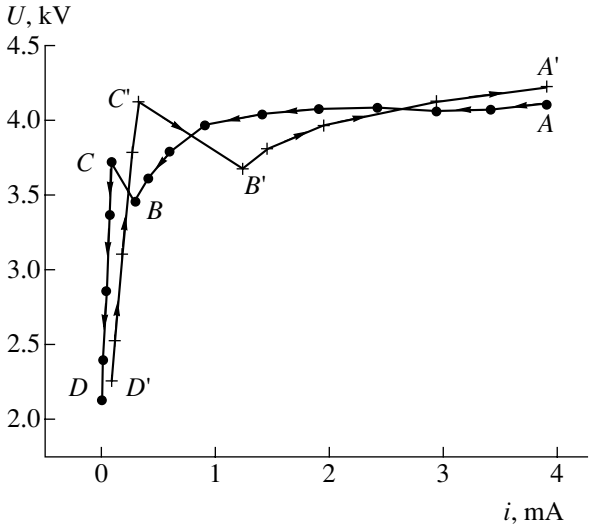

Fig. 3. Current–voltage characteristic of discharge at helium temperatures: *A* and *A*' are the beginning and the end of the direct and the reverse run of the characteristic, respectively; *DC* and *D*'*C*' are the segments where no optical radiation was observed from the positive column [6, 9].

In spite of the low absolute values of power released in this range of currents in a unit length of the plasma column (10^2–10^3 mW/cm), this power turns out to be sufficient for heating a gas to the temperature (lower than 300 K) at which special features of elementary processes at low temperatures still fail to influence the field strength. A decrease in the current and specific power of the discharge leads to the appearance of the $E(T)$ dependence, although the values of $E(p)$ ($i >$ 1 mA) are close to those known for room temperature. Moreover, the shape of the $E(i)$ characteristics is retained.

Theoretical and experimental investigations [11, 12] show that the nature of *H*–*T* transitions is closely related to the so-called *S*-source of fast electrons in the cryogenic glow-discharge plasma; such electrons originate in reactions with participation of helium metastable atoms and molecules. To such processes, we assign the reactions

$$\mathrm{He}(2^3S) + \mathrm{He}(2^3S) \xrightarrow{\beta} \mathrm{He}_2^+ + e(17.4\ \mathrm{eV}), \qquad (6)$$

$$\mathrm{He}(2^1S) + \mathrm{He}(2^1S) \longrightarrow \mathrm{He}_2^+ + e(19.0\ \mathrm{eV}), \qquad (7)$$

$$\mathrm{He}(2^1S) + \mathrm{He}(2^3S) \longrightarrow \mathrm{He}_2^+ + e(18.2\ \mathrm{eV}), \qquad (8)$$

as well as collisions between electrons and metastable atoms for which the excitation energy is transferred to electrons. The theoretical model of cryogenic glow-discharge plasma [11] involving an *S*-source of electrons shows that, for $\frac{E}{N} < 4 \times 10^{-17}\ \mathrm{V\ cm^2}$, the excitation constant is equal to $(0.5\text{–}2.0) \times 10^{-14}\ \mathrm{V\ cm^3\ s^{-1}}$ and exceeds, therefore, by four orders of magnitude, the constant calculated for the case when the birth of fast electrons is ignored. Thus, in the region of small $\frac{E}{N}$, the excitation constant depends not only on $\frac{E}{N}$, but also on the metastable-particle concentration, which increases with decreasing plasma temperature because the breakup of metastable atoms by ground-state atoms does not occur at T_a < 88–100 K due to the presence of a low activation barrier in their interaction [13]. Therefore, when the temperature of the heavy plasma component passes from room temperature to the liquid-nitrogen temperature, spectral measurements show an increase in the metastable-atom concentration by more than an order of magnitude, while the ratio of the metastable-atom density in the triplet state to the electron density attains a value of 10^2 and is much higher than for other excited states [12]. The addition of small amounts of argon to the discharge leads to a decrease in the density of metastable helium atoms owing to their deexcitation in the Penning-ionization reaction, and the *H*–*T* transition disappears for sufficiently high quantities of the additive. The *H*–*T* transition can also be observed in pure neon and in a helium–neon mixture.

The glow discharge cooled to helium temperatures in the region of parameters where the imperfection parameter has a maximum ($\Gamma \approx 0.3$–0.4) reveals other features as well [8]. To these features we should assign, first of all, the appearance of cathode drops of potential which exceed normal drops by an order of magnitude. In this case, a break in the current–voltage characteristic and its hysteresis are observed (Fig. 3).

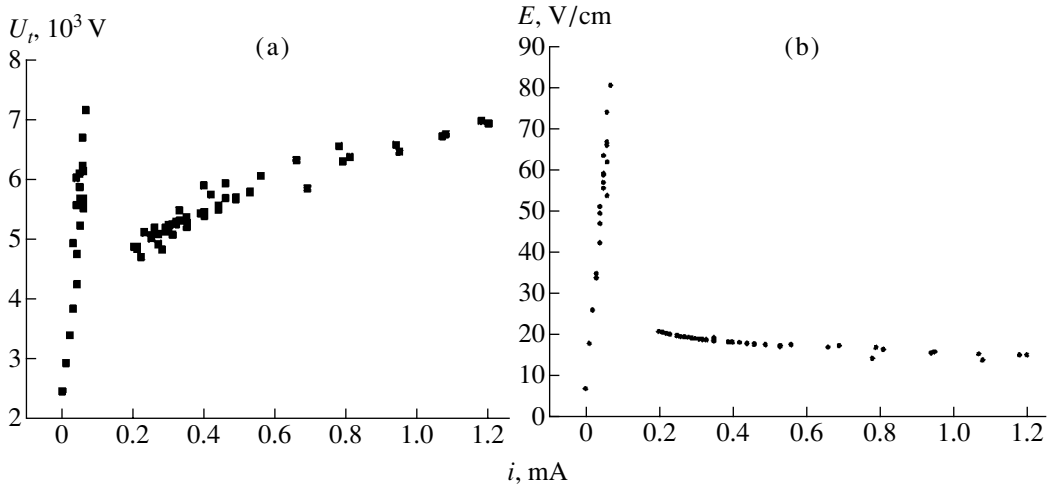

Fig. 4. Electrical characteristics of the discharge cooled to T = 4–5 K (this work): (a) current–voltage characteristic of the discharge; (b) strength of the longitudinal electric field in plasma.

When the discharge ignites in point *A* and the current reduces to 0.4 mA (point *B*), the voltage and current in the tube change in a jumplike manner to the values corresponding to point *C*. The segments *CD* and *C'D'* are linear. In the reverse run, the current–voltage characteristic undergoes the discontinuity once again. It has the same appearance, but does not coincide with the curve *ABCD*; i.e., the hysteresis is observed. The discontinuity in polarity of electrodes is retained for the same discharge currents. The measured temperature *T* of the gas in the tube at the moment of discontinuity is equal to 5–6 K. The peculiar feature of the discharge at the segments *DC* and *D'C'* is the complete absence of optical glow of the positive column in the cryogenic plasma.

In this study, we confirmed this effect on a newly built setup (Fig. 4a) and measured the electric field in plasma (Fig. 4b) using probes. The characteristic obtained points to a jumplike change in the mechanism of plasma conductivity in the region of 5 K and to its independence from the value of discharge current. In connection with this, it is of interest to compare the measured conductivity with the corresponding value for a strongly imperfect "cold" plasma [1, 14]:

$$\sigma_e = \frac{\omega_0}{4\pi}, \qquad (9)$$

where ω_0 is the plasma frequency. On the left-hand branch of the characteristic, the value $\sigma_e \approx 10^{-4}$ Ohm^{-1} cm^{-1} averaged over the cross section agrees well with the conductivity of an imperfect cold plasma under the assumption of the electron concentration $n_e \approx 10^9$ cm^3 being the same as on the right-hand branch near the transition.

Thus, the available experimental data confirm the possibility of transition of cryogenic plasma into a new state, the study of which calls for the development of special methods of diagnostics and methods of increasing the parameter Γ. From this point of view, of interest are the experiments with a glow discharge cooled to several kelvin, in which high-amplitude ionization waves are excited by high-voltage nanosecond pulses. In these waves, the value $\frac{E}{p}$ of the reduced electric field is optimal for accumulating both the metastable states and the charged component and for obtaining the values of $\Gamma \gg 1$ for the ionic and electron components.

The transition discovered in plasma near 5 K (Figs. 3, 4) testifies to the change-over of the conductivity mechanism. This transition is of interest itself irrespective of whether it is caused by the plasma imperfection or by the accumulation of the metastable states within it.

ACKNOWLEDGMENTS

We thank V.I. Platonov and V.I. Kiselev for their help in carrying out the experiments.

This work was supported by the Russian Foundation for Basic Research, project no. 09-02-16182.

REFERENCES

1. V. E. Fortov and I. T. Yakubov, *Nonideal Plasma* (Énergoatomizdat, Moscow, 1994).
2. H. Thomas, G. E. Morfill, and V. Demmel, Phys. Rev. Lett. **73**, 652 (1994).
3. S. L. Gilbert, J. J. Bollinger, and D. J. Wineland, Phys. Rev. Lett. **60**, 2022 (1988).
4. P. D. Goldan and L. Goldstem, Phys. Rev. **138** (1), 39 (1965).
5. J.-E. Delpech and J.-C. Gauthier, *Plasmas cryogeniques a fortes correlations*, Rapport de Groupe d'Electronique dans les gaz (IEF-Orsay, 1972), p. 46.
6. A. V. Kirillin and V. V. Markovets, Teplofiz. Vys. Temp. **11**, 706 (1973).

7. V. L. Granovskiĭ, *Electric Current in a Gas* (GITTL, Moscow, 1952), p. 432.
8. V. V. Markovets, Author's Abstract of Candidate's Dissertation in Mathematical Physics (Mosk. Fiz.-Tekh. Inst., Moscow, 1974), p. 20.
9. É. I. Asinovskiĭ, A. V. Kirillin, and V. V. Markovets, Teplofiz. Vys. Temp. **13**, 933 (1975).
10. P. D. Edgley and A. von Engel, in *Proceedings of the 10th International Conference on Phenomena in Ionized Gases, Oxford, 1971*, p. 116.
11. A. A. Belevtsev and A. Kh. Mnatsakanyan, Teplofiz. Vys. Temp. **13**, 943 (1975).
12. É. I. Asinovskiĭ, A. V. Kirillin, and A. A. Rakovets, *Cryogenic Discharges* (Nauka, Moscow, 1988), p. 62.
13. I. Ya. Fugol', Usp. Fiz. Nauk **97**, 423 (1969).
14. É. I. Asinovskiĭ and A. V. Kirillin, *Nontraditional Methods for Research of Thermodynamic Properties of Matter under High Temperatures* (Yanus-K, Moscow, 1997), p. 158.

Translated by V. Bukhanov

Doklady Physics, Vol. 46, No. 5, 2001, pp. 326–327. Translated from Doklady Akademii Nauk, Vol. 378, No. 3, 2001, pp. 331–332.

PHYSICS

An Accelerated Frame of Reference Is Not a Particular Case of a Gravitational Field

Academician A. A. Logunov and M. A. Mestvirishvili

Received December 28, 2000

In the general relativity (GR) theory, in the case of the absence of a medium, an arbitrary metric field of Minkowski space, which corresponds to an accelerated frame of reference, is a solution to the Gilbert–Einstein equation. This is what made it possible for A. Einstein to consider such a metric field a particular case of a gravitational field [1]. In the relativistic gravitation theory [2], the gravitational field, in contrast to general relativity, is a physical field possessing energy-momentum density. By virtue of the universality of this field, it is natural to consider the conserving energy-momentum tensor of the medium and the gravitational field taken together to be a field source. As the medium, we imply all forms of matter except the gravitational field. This approach ensures the existence, in the theory of fundamental conservation laws, of both the energy-momentum and moment of momentum in a closed physical system. In this case, there arises, as a consequence, an effective Riemann space of the field origin that has a simple topology. Moreover, a nonzero graviton mass also inevitably arises. Furthermore, we use a system of units in which the constants $\hbar$, c, and G are equal to unity.

The equations of the relativistic gravitation theory in Minkowski space, which are written out in an arbitrary frame of reference determined by the metric tensor $\gamma^{\alpha\beta}$, have the form

$$\gamma^{\alpha\beta}D_\alpha D_\beta\tilde{\Phi}^{\mu\nu} + m^2\tilde{\Phi}^{\mu\nu} = 16\pi t^{\mu\nu}, \tag{1}$$

$$D_\mu\tilde{\Phi}^{\mu\nu} = 0. \tag{2}$$

Here, the following notation is employed: D_μ is the covariant derivative in the Minkowski space, $\gamma^{\alpha\beta}(x)$ is the metric tensor of the Minkowski space, $t^{\mu\nu}$ is the tensor of the energy-momentum density for the entire matter, $\tilde{\Phi}^{\mu\nu}$ is the density of the tensor gravitational field, and m is the graviton mass.

Institute of High-Energy Physics,
Protvino, Moscow oblast, 142284 Russia

The effective metric of the Riemann space and the gravitational field turn out to be bound by the relationship

$$\tilde{g}^{\mu\nu}(x) = \tilde{\gamma}^{\mu\nu}(x) + \tilde{\Phi}^{\mu\nu}(x). \tag{3}$$

The densities of the tensors are equal to

$$\tilde{g}^{\mu\nu} = \sqrt{-g}g^{\mu\nu}, \quad \tilde{\gamma}^{\mu\nu} = \sqrt{-\gamma}\gamma^{\mu\nu}, \quad \tilde{\Phi}^{\mu\nu} = \sqrt{-\gamma}\Phi^{\mu\nu}. \tag{4}$$

Here, $g^{\mu\nu}$ is the metric tensor of the effective Riemann space and $\Phi^{\mu\nu}$ is the tensor gravitational field,

$$g = \det(g_{\mu\nu}), \quad \gamma = \det(\gamma_{\mu\nu}). \tag{5}$$

The system of equations of the relativistic gravitation theory in the effective Riemann space has the form [3]

$$R_{\mu\nu} + \frac{m^2}{2}(\gamma_{\mu\nu} - g_{\mu\nu}) = 8\pi\left(T_{\mu\nu} - \frac{1}{2}g_{\mu\nu}T\right), \tag{6}$$

$$D_\nu\tilde{g}^{\mu\nu} = 0. \tag{7}$$

To solve particular problems, we should add the equation of state to Eqs. (6), (7). It is particularly worth emphasizing that the system of equations (6), (7) is, generally, covariant with respect to arbitrary coordinate transformations. At the same time, it is form-invariant with respect to coordinate transformations that remain the functionally invariant metric $\gamma_{\mu\nu}(x)$. In other words,

$$d\sigma^2 = \gamma_{\mu\nu}(x)dx^\mu dx^\nu = \gamma_{\mu\nu}(x')dx'^\mu dx'^\nu. \tag{8}$$

Physical solutions to Eqs. (6), (7) must satisfy the conditions $g < 0$ at each point of the K_ν space $T^{\mu\nu}K_\mu K_\nu \geq 0$ for an arbitrary timelike vector K_ν. At the same time, the quantity $T^{\mu\nu}K_\nu$ must form a nonspacelike vector.

On the other hand, the causality principle must be valid:

$$\begin{aligned}\gamma_{\mu\nu}(x)V^\mu V^\nu &= 0,\\ g_{\mu\nu}(x)V^\mu V^\nu &\leq 0.\end{aligned} \tag{9}$$

It follows from the causality conditions (9) that if the

1028-3358/01/4605-0326$21.00

inequality

$$\gamma_{\mu\nu}L^\mu L^\nu < 0 \tag{10}$$

is fulfilled by definition for an arbitrary spacelike vector L^μ, then the inequality

$$g_{\mu\nu}L^\mu L^\nu < 0 \tag{11}$$

must also be valid.

According to the causality principle, the gravitational field does not extract a tentative body out from the causality cone of the Minkowski space with metric $\gamma_{\mu\nu}(x)$. At the same time, this condition always makes it possible to compensate the three-dimensional gravitation force by the inertia force in the case of the corresponding choice of a reference system.

In the case of ideal liquid, the energy-momentum tensor of the medium has the form

$$\begin{aligned} T_{\mu\nu} &= (\rho + p)U_\mu U_\nu - pg_{\mu\nu}, \\ T &= T_{\mu\nu}g^{\mu\nu} = (\rho - 3p), \quad U^\nu = \frac{dx^\nu}{ds}. \end{aligned} \tag{12}$$

Here, ds is an interval of the effective Riemann space:

$$ds^2 = g_{\mu\nu}(x)dx^\mu dx^\nu. \tag{13}$$

In Eqs. (6), (7), as in all other physical theories, the metric $\gamma_{\mu\nu}(x)$ of the Minkowski space is chosen by the researcher. Usually, an inertial reference frame is used in the calculations.

It follows from Eqs. (6), (7) that in the case when the medium is absent, among all possible metrics of the Minkowski space in the given reference frame, only one metric $\gamma_{\mu\nu}(x)$ chosen previously satisfies the equations. We now show that in this reference frame and in the presence of a medium, none of the metrics of the Minkowski space is the solution to gravitational equations (6), (7). With this goal in mind, we perform the convolution of Eq. (6) with the help of a spacelike vector determined by inequality (10):

$$\begin{aligned} \frac{m^2}{2}\gamma_{\mu\nu}L^\mu L^\nu &= 8\pi\left(T_{\mu\nu} - \frac{1}{2}g_{\mu\nu}T\right)L^\mu L^\nu \\ &- R_{\mu\nu}L^\mu L^\nu + \frac{m^2}{2}g_{\mu\nu}L^\mu L^\nu. \end{aligned} \tag{14}$$

As long as we consider only metric fields of the Minkowski space, relation (14) is simplified and takes the form

$$\begin{aligned} &m^2\gamma_{\mu\nu}L^\mu L^\nu \\ &= 16\pi\left(T_{\mu\nu} - \frac{1}{2}g_{\mu\nu}T\right)L^\mu L^\nu + m^2 g_{\mu\nu}L^\mu L^\nu. \end{aligned} \tag{15}$$

Substituting expression (12) into this equation, we arrive at the formula

$$\begin{aligned} m^2\gamma_{\mu\nu}L^\mu L^\nu &= 16\pi(\rho + p)(U_\mu L^\mu)^2 \\ &- 8\pi g_{\mu\nu}L^\mu L^\nu\left(\rho - p - \frac{m^2}{8\pi}\right). \end{aligned} \tag{16}$$

By virtue of conditions (10), (11), we see that the right-hand side of Eq. (16) is strictly positive as long as the inequality

$$\rho > p + \frac{m^2}{8\pi} \tag{17}$$

is fulfilled. At the same time, the left-hand side of Eq. (16) is strictly negative. Whence it follows that in the presence of a medium, none of the metric fields of Minkowski space satisfies the gravitational equations. Therefore, metric fields arising in noninertial frames of reference in Minkowski space cannot be considered gravitational fields. Equation (16) has a solution only if $p = \rho = 0$. However, in this case, only one solution, which was discussed above, takes place:

$$g_{\mu\nu}(x) = \gamma_{\mu\nu}(x). \tag{18}$$

Since Eq. (16) also is valid in the case of a nonzero tensor of the Riemannian curvature but with the zero $R_{\mu\nu}$ tensor, it follows from this equation that it has no solution satisfying the causality principle. In particular, such a conclusion relates to that region of space in which the effect of the graviton mass is significant. This implies that in this region, a substantial change in the character of the solution takes place. We were convinced of this conclusion previously when studying, as an example, the solution for a static spherically symmetric body in the region close to the Schwarzschild sphere [4].

REFERENCES

1. A. Einstein, *Collection of Scientific Papers* (Nauka, Moscow, 1966), Vol. 2, Paper 133, p. 662.
2. A. A. Logunov, Theor. Math. Phys. **104**, 1184 (1995).
3. A. A. Logunov, Fiz. Élem. Chastits Atom. Yadra **29**, 5 (1998) [Phys. Part. Nucl. **29**, 1 (1998)].
4. A. A. Logunov and M. A. Mestvirishvili, Teor. Mat. Fiz. **121**, 4 (1999).

Translated by G. Merzon

Doklady Physics, Vol. 46, No. 5, 2001, pp. 328–330. Translated from Doklady Akademii Nauk, Vol. 378, No. 1, 2001, pp. 44–46.

THEORETICAL PHYSICS

Transmission Coefficient for Excitations Passing through a One-Dimensional Barrier Described by the Nonlinear Schrödinger Equation

D. L. Kovrizhin and Academician L. A. Maksimov

Received December 6, 2000

1. It has long been known that studying nonlinear phenomena is one of the most interesting and challenging problems in theoretical physics [1]. Recently, this problem became even more urgent since supercold gases in the Bose-condensate state were observed in magnetic traps [2–4]. Many of the properties of such gases are adequately described by the nonlinear Schrödinger equation which, for nearly ideal Bose gases, is referred to as the Gross–Pitaevskiĭ equation [5, 6]. In this paper, we consider the problem of scattering Bose-condensate excitations by a one-dimensional barrier. This problem is nontrivial even in the case of a low barrier because both the variation of the condensate density in the neighborhood of the barrier and the barrier itself play an equally important role. In contrast to a bare particle, for which any repulsive potential becomes impermeable in the long-wave limit, the transmission coefficient for phonons passing through a δ-shaped barrier tends in this limit to unity, and, hence, the barrier becomes transparent.

2. The Gross–Pitaevskiĭ equation in dimensionless variables $\left(t = \frac{t_s\mu}{\hbar},\ x = \frac{x_{cm}\sqrt{m\mu}}{\hbar},\ \psi = \psi_{dim}\sqrt{\frac{U}{\mu}},\ \text{and}\ V(x) = \frac{V_{erg}}{\mu}\right)$ takes the form

$$i\frac{\partial\Psi}{\partial t} = -\frac{1}{2}\Psi'' - \Psi + |\Psi|^2\Psi + V(x)\Psi. \qquad (1)$$

Here, we restrict ourselves to the evaluation of scattering by using only the localized δ-shaped potential barrier

$$V(x) = V_0\delta(x),\ \text{with}\ V_0 = \frac{\sqrt{m\mu}}{\hbar\mu}V_{dim} > 0.$$

The wave function $\psi(x)$ for the ground state of the condensate has, to the left and to the right of the barrier, the well-known form

$$\psi(x) = t(x) \equiv \tanh(|x| + X_0), \quad |x| > a. \qquad (2)$$

The derivative jump at the barrier determines the wave-function amplitude at the point $x = 0$:

$$1 - \xi^2 = V_0\xi,\ \xi = \tanh X_0 = -\frac{1}{2}V_0 + \sqrt{\left(\frac{1}{2}V_0\right)^2 + 1}. \qquad (3)$$

In the limits of small and large barriers, we obtain, respectively,

$$\xi = 1 - \frac{1}{2}V_0 = 1 - 2e^{-2X_0},\quad X_0 = \frac{1}{2}\ln\frac{4}{V_0},\quad V_0 \ll 1,$$

$$\xi = X_0 = \frac{1}{V_0},\quad V_0 \gg 1.$$

The states with negative values of ξ have a higher energy.

The odd state $\psi = \tanh x$ has no derivative jump, but the energy of this state is even higher.

3. The Bose-condensate excitations $\tilde{\psi} = \Psi - \psi$ are described by the Gross–Pitaevskiĭ linearized equation

$$i\frac{\partial\tilde{\psi}}{\partial t} = h\tilde{\psi} + g(x)\tilde{\psi}^*,$$
$$h = \left(-\frac{1}{2}\frac{d^2}{dx^2} + V(x) + 2g(x) - 1\right), \qquad (4)$$

where the interaction potential for the excitation and the condensate is given by formulas (1) and (2):

$$g(x) = \psi^2 = \tanh^2(|x| + X_0). \qquad (5)$$

We do not consider inelastic processes, and the calculation of the excitation scattering on the basis of quasi-classical equation (4) yields the same result as that within the framework of the secondary quantization.

Russian Research Centre, Kurchatov Institute, pl. Akademika Kurchatova 1, Moscow, 123182 Russia

1028-3358/01/4605-0328$21.00

As is well known, Eq. (4) can be reduced to a diagonal form by the Bogolyubov–de Jean transformation:

$$\tilde{\psi} = \sum_k (u_k(x)e^{-i\varepsilon t} - v_k^*(x)e^{i\varepsilon t}),$$
$$(h-\varepsilon)u_k - g v_k = 0, \quad (h+\varepsilon)v_k - g u_k = 0. \tag{6}$$

At long distances from the barrier, we have

$$v_k = u_k\left(\sqrt{\varepsilon^2+1}-\varepsilon\right) \sim e^{ikx},$$
$$\varepsilon^2 = \left(\frac{1}{2}k^2+1\right)^2 - 1, \quad [\varepsilon]_{k\ll 1} \simeq k. \tag{7}$$

It is easy to prove that the excitation-energy flux far from the barrier is

$$Q = \mathrm{Re}\left\{(\hat{p}\tilde{\psi})^*\left(\left(\frac{\hat{p}^2}{2}+1\right)\tilde{\psi} + \tilde{\psi}^+\right)\right\}$$
$$= \sum_k k\varepsilon^2\left(\sqrt{\varepsilon^2+1}-\varepsilon\right)|u_k|^2. \tag{8}$$

In the secondary-quantization representation,

$$\hat{u}_k = e^{ikx}\hat{b}_k\sqrt{\frac{1}{2}\left(\frac{\sqrt{\varepsilon^2+1}}{\varepsilon}+1\right)}$$

and quasi-classical expression (8) for the energy flux takes the conventional form

$$Q = \sum_k k\varepsilon n_k, \quad n_k = \langle \hat{b}_k^+ \hat{b}_k \rangle.$$

Whence it is clear that, when solving the problem of the excitation scattering within the framework of quasi-classical equation (4), the function $u(x)$ must, naturally, be considered. However, the functions $u(x)$, $v(x)$, and $f(x) = u(x) + v(x)$ are asymptotically mutually proportional to each other and we may use any of them to evaluate the transmission coefficient.

If $V_0 \ll 1$ and $V_0 \ll \varepsilon$, we can ignore in (6) the condensate-density perturbance in the neighborhood of the barrier and use the approximation $g(x) = 1$ to solve the scattering problem.

Then, at the point $x = 0$, we can directly sew together the wave outgoing from the right side and a superposition of the incident and reflected waves on the left side:

$$f_+ = Ae^{ikx}, \quad x > 0, \tag{9}$$

$$f_- = e^{ikx} + Be^{-ikx}, \quad x < 0. \tag{10}$$

As a result, we obtain the reflection coefficient

$$D = \frac{k^2}{k^2 + V_0^2}, \tag{11}$$

which differs from the known expression for a bare particle only in the dependence $k(\varepsilon)$. At high energies ($k \gg V_0$), the barrier is nearly completely transparent. At the lower boundary of the application range for this formula, when $V_0 \simeq \varepsilon \simeq k$, semitransparency takes place.

4. However, even small density variations in the vicinity of the barrier can significantly affect the low-energy phonon scattering (for $\varepsilon < V_0$) by the barrier.

In the neighborhood of the barrier, a phonon moves in the effective potential [whose size is on the order of the correlation length, see (5)]

$$V_{\mathrm{eff}}(x) = V(x) + g(x). \tag{12}$$

For long-wave excitations (phonons), the sum $f = u + v$ is large, while the difference $F = u - v$ is smaller by a factor of ε:

$$\left(-\frac{1}{2}\frac{d^2}{dx^2} + V_{\mathrm{eff}}(x) - 1\right)f = \varepsilon F, \tag{13}$$

$$\left(-\frac{1}{2}\frac{d^2}{dx^2} + V_{\mathrm{eff}}(x) + 2g(x) - 1\right)F = \varepsilon f. \tag{14}$$

In the linear (with respect to ε) approximation, the function f is described by the equation

$$\left(-\frac{1}{2}\frac{d^2}{dx^2} + V_{\mathrm{eff}}(x) - 1\right)f = 0 + O(\varepsilon^2). \tag{15}$$

According to [8], within the range of the action of potential (12), the function f can be written out as a superposition of two independent exact solutions to Eq. (15):

$$f_1 = \tanh x, \quad f_2 = x\tanh x - 1.$$

Thus, for $|x| \ll k^{-1}$, we obtain

$$f_+ = A_1\tanh(x + X_0) + B_1[(x + X_0)\tanh(x + X_0) - 1], \quad x > 0,$$

$$f_- = A_2\tanh(|x| + X_0) + B_2[(|x| + X_0)\tanh(|x| + X_0) - 1], \quad x < 0.$$

For $1 \ll |x| \ll k^{-1}$, the asymptotic representation of these functions,

$$f_+ = A_1 + B_1[x + X_0 - 1],$$
$$f_- = A_2 + B_2[(-x + X_0) - 1],$$

must have the form [see (9) and (10)]

$$f_+ = A + ikAx,$$
$$f_- = (1 + B) + (1 - B)ikx.$$

Sewing together these functions on the left and on the right of the barrier, we arrive at the expressions

$$A_1 = A[1 - ik(X_0 - 1)], \quad B_1 = ikA, \tag{16}$$

$$A_2 = (1 + B) + ik(X_0 - 1)(1 - B),$$
$$B_2 = -ik(1 - B). \tag{17}$$

Sewing these functions at the barrier ($x = 0$) yields, with due regard to equality (3),

$$A_1\xi + B_1(X_0\xi - 1) = A_2\xi + B_2(X_0\xi - 1),$$
$$A_1(-V_0\xi) + A_2(V_0\xi) + B_1(-X_0V_0\xi + \xi + 2V_0) \tag{18}$$
$$+ B_2(X_0V_0\xi + \xi) = 0.$$

Multiplying the first equation in (18) by V_0 and adding it to the second one, we obtain the simple relationship

$$B_1 = -B_2, \tag{19}$$

which allows the set of equations (16)–(19) to be easily solved. As a result, the transmission and reflection amplitudes are, respectively,

$$A = \frac{1}{1 - ikL}, \quad B = -\frac{ikL}{1 - ikL}.$$

Here, we introduce the effective barrier length

$$L = \frac{1 - \xi}{\xi} = \frac{1}{2}V_0 + \sqrt{\left(\frac{1}{2}V_0\right)^2 + 1} \simeq V_0. \tag{20}$$

Thus, for the δ-shaped barrier, the transmission and reflection coefficients for phonons are, respectively,

$$D = \frac{1}{1 + (kL)^2}, \quad R = \frac{(kL)^2}{1 + (kL)^2}. \tag{21}$$

The dependence of scattering on the wavelength of a bare particle is opposite to that for a phonon [see (11)]. In the long-wave limit, a particle is completely reflected, while the barrier is transparent for long-wave phonons. It is worth noting that formulas (21) are valid only for low-energy quasi-particles ($\varepsilon \ll 1$).

In the case of small ε, the use of Eqs. (13) and (14) instead of (15) to describe the scattering can lead to the appearance of an insignificant weak ε-dependence of the transmission coefficient; i.e.,

$$D = \frac{d(\varepsilon)}{1 + k^2L(\varepsilon)^2}, \quad d(0) = 1, \quad L(0) = L.$$

In the range of application of formulas (21), small barriers ($L \simeq V_0 \ll 1$) are nearly transparent. Larger barriers, for which formula (11) is applicable, are semitransparent and become completely transparent for high-energy quasi-particles. The transparency of large barriers ($L \simeq V_0 \gg 1$) drops twice even within the range of application of formula (21). The question on barrier transparency in a wide range ($1 < k < V_0$) yet remains open.

ACKNOWLEDGMENTS

The authors are grateful to Academician Yu.M. Kogan for his attention to this work. This work was supported by the Russian Foundation for Basic Research and the INTAS Foundation.

REFERENCES

1. V. E. Zakharov, S. Novikov, S. V. Manakov, and L. P. Pitaevskiĭ, *Theory of Solitons: The Inverse-Problem Method* (Nauka, Moscow, 1980; Consultants Bureau, New York, 1984).
2. M. H. Anderson, J. R. Ensher, M. R. Matthews, *et al.*, Science **269**, 198 (1995).
3. C. Bradley, C. Sackett, J. Tolett, and R. Hulet, Phys. Rev. Lett. **75**, 1687 (1995).
4. K. Davies, Phys. Rev. Lett. **75**, 3969 (1995).
5. F. Dalfovo, S. Giorgini, L. P. Pitaevskii, and S. Stringari, Rev. Mod. Phys. **71**, 463 (1999).
6. V. Hakim, Phys. Rev. E **55**, 2835 (1997).
7. D. N. Zubarev, *Nonequilibrium Statistical Thermodynamics* (Nauka, Moscow, 1971; Consultants Bureau, New York, 1974).
8. P. O. Fedichev, A. E. Muryshev, and G. V. Shlyapnikov, Phys. Rev. A **60**, 3220 (1999).

Translated by V. Chechin

Doklady Physics, Vol. 46, No. 5, 2001, pp. 331–335. Translated from Doklady Akademii Nauk, Vol. 378, No. 2, 2001, pp. 183–186.

TECHNICAL PHYSICS

Unsteady Diffraction by a Nonclosed Cone

V. A. Doroshenko* and V. F. Kravchenko**

Presented by Academician Yu.V. Gulyaev December 7, 2000

Received December 7, 2000

A method for solving a stationary problem of wave scattering by a semi-infinite circular cone with slots periodically cut along its generating lines is presented in [1]. In this paper, we pioneer the presentation of an algorithm for constructing an unsteady Green's function of a cone with longitudinal slots.

FORMULATION AND THE METHOD OF SOLUTION OF THE PROBLEM

The conic structure under consideration represents a perfectly conducting semi-infinite thin cone with N slots periodically cut along its generatrices. We introduce a spherical coordinate system r, ϑ, φ with the origin at the vertex of the cone; its axis coincides with the oz-axis of the Cartesian coordinate system (see the figure). Furthermore, we use the following notation: 2γ is the cone opening angle, $l = \dfrac{2\pi}{N}$ is the structure period, and d is the slot width (d and l are the values of the dihedral angles formed by intersections of planes drawn through the cone axis and edges of conic strips). In the coordinate system chosen, the cone is determined by a set of points:

$$\Sigma = \{(r, \vartheta, \varphi) \in R^3:\ r \in [0, +\infty),\ \vartheta = \gamma,\ \varphi \in L\},$$

where

$$L = \bigcup_{p=1}^{N} L_p, \quad L_p = \left((p-1)l + \frac{d}{2},\ pl - \frac{d}{2}\right),$$

$$CL = [0, 2\pi)\backslash L.$$

The desired Green's function $G(\mathbf{r}, \mathbf{r}_0, t, t_0)$ satisfies (*1*) the equation

$$\left(\Delta - \frac{1}{c^2}\frac{\partial^2}{\partial t^2}\right)G(\mathbf{r}, \mathbf{r}_0, t, t_0) = -\delta(\mathbf{r} - \mathbf{r}_0)\delta(t - t_0);$$

(*2*) the boundary condition at the cone strips

$$G(\mathbf{r}, \mathbf{r}_0, t, t_0)\big|_\Sigma = 0; \text{ and}$$

(*3*) the initial conditions

$$G = \frac{\partial G}{\partial t} \equiv 0 \quad \text{for} \quad t < t_0.$$

We represent the function G in the form

$$G(\mathbf{r}, \mathbf{r}_0, t, t_0) = G_0(\mathbf{r}, \mathbf{r}_0, t, t_0) + G_1(\mathbf{r}, \mathbf{r}_0, t, t_0),$$

$$G_0(\mathbf{r}, \mathbf{r}_0, t, t_0) = \frac{\delta(\hat{t} - R/c)}{4\pi R}, \tag{1}$$

$$\hat{t} = t - t_0, \quad R = |\mathbf{r} - \mathbf{r}_0|.$$

Here, c is the speed of light; the function G_1 is conditioned by the presence of the cone surface. For find-

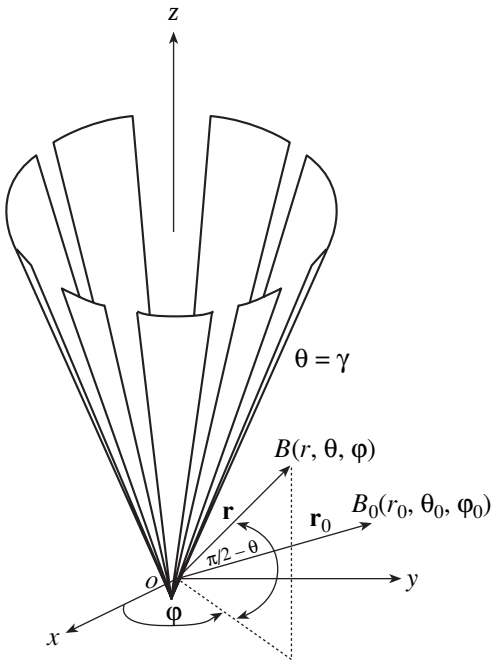

Geometry of the problem.

* *Kharkov Technical University of Radio Electronics, pr. Lenina 14, Kharkov, 310726 Ukraine*

** *Institute of Radio Engineering and Electronics, Russian Academy of Sciences, ul. Mokhovaya 18, Moscow, 103907 Russia*

1028-3358/01/4605-0331$21.00

ing G, we use the Laplace transformation

$$G^s(\mathbf{r}, \mathbf{r}_0, t_0) = \int_0^{+\infty} G(\mathbf{r}, \mathbf{r}_0, t, t_0)e^{-st}dt, \quad s > 0, \quad (2)$$

where G^s is the Green's function for the corresponding steady boundary value problem. This function satisfies the inhomogeneous Helmholtz equation, the first boundary condition on the cone strips, the condition at infinity in space, and the condition near the boundary irregularities (the cone vertex and the strip edges).

In accordance with (1),

$$G^s(\mathbf{r}, \mathbf{r}_0, t, t_0) = G_0^s(\mathbf{r}, \mathbf{r}_0, t, t_0) + G_1^s(\mathbf{r}, \mathbf{r}_0, t, t_0),$$

$$G_0^s(\mathbf{r}, \mathbf{r}_0, t, t_0) = e^{-st_0}\frac{e^{-qR}}{4\pi R}, \quad q = \frac{s}{c}.$$

To solve the steady problem, we invoke the Kontorovich–Lebedev integral transformation

$$F(\tau) = \int_0^{+\infty} f(r)\frac{K_{i\tau}(qr)}{\sqrt{r}}dr, \quad (3)$$

$$f(r) = \frac{2}{\pi^2}\int_0^{+\infty} \tau\sinh\pi\tau F(\tau)\frac{K_{i\tau}(qr)}{\sqrt{r}}d\tau. \quad (4)$$

Here, $K_\mu(z)$ is the Macdonald function. Taking into account the representation

$$G_0^s = \frac{2}{\pi^2}\int_0^{+\infty} \tau\sinh\pi\tau \sum_{m=-\infty}^{+\infty} a_{m\tau}^s U_{m\tau}^{(0)} e^{im\varphi}\frac{K_{i\tau}(qr)}{\sqrt{r}}d\tau,$$

$$U_{m\tau}^{(0)}(\vartheta, \vartheta_0)$$

$$= \begin{cases} P_{-1/2+i\tau}^m(\cos\vartheta)P_{-1/2+i\tau}^m(-\cos\vartheta_0), & \vartheta < \vartheta_0 \\ P_{-1/2+i\tau}^m(-\cos\vartheta)P_{-1/2+i\tau}^m(\cos\vartheta_0), & \vartheta_0 < \vartheta, \end{cases}$$

we seek the function G_1^s in the form of Kontorovich–Lebedev integral (3), (4):

$$G_1^s = \frac{2}{\pi^2}\int_0^{+\infty} \tau\sinh\pi\tau \sum_{m=-\infty}^{+\infty} b_{m\tau}^s U_{m\tau}^{(1)}\frac{K_{i\tau}(qr)}{\sqrt{r}}d\tau, \quad (5)$$

$$U_{m\tau}^{(1)} = \sum_{n=-\infty}^{+\infty} x_{m, n+m_0}(\tau)\frac{P_{-1/2+i\tau}^{m+nN}(\pm\cos\vartheta)}{P_{-1/2+i\tau}^{m+nN}(\pm\cos\gamma)}e^{i(m+nN)\varphi}. \quad (6)$$

Here, $P_\mu^m(\cos\vartheta)$ is the associated Legendre function of the first kind; $a_{\nu\tau}^s$ and $b_{\nu\tau}^s$ are known coefficients, and x_m and x_n are unknown coefficients; the superscripts of the Legendre-function arguments in (6) correspond to the region $0 < \vartheta < \gamma$, and the subscripts correspond to the region $\gamma < \vartheta < \pi$; and $\frac{m}{N} = \nu + m_0, -\frac{1}{2} \le \nu < \frac{1}{2}$, m_0 being the integer closest to $\frac{m}{N}$. As a result of using the boundary condition, the conjunction condition for G_1^s in the slots, and the semiconversion method [1], the steady problem is reduced to the solution of an infinite set of linear Fredholm-type algebraic equations of the second kind with respect to the coefficients $y_{m, n}$ related to $x_{m, n}$:

$$A_\nu(u)y_{m, 0} = V^{m_0}(u) + \sum_{p=-\infty}^{+\infty}\frac{|p|}{p}\varepsilon_{m, p}V^p(u)y_{m, p}, \quad (7)$$

$$y_{m, n} = V_{n-1}^{m_0-1}(u) + \sum_{p=-\infty}^{+\infty}\frac{|p|}{p}\varepsilon_{m, p}y_{m, p}V_{n-1}^{p-1}(u) + y_{m, 0}P_n(u), \quad n \ne 0, \quad (8)$$

$$y_{m, n} = (-1)^{n-m_0}\frac{n+\nu}{m_0+\nu}\frac{|n|}{n}\frac{x_{m, n}}{1-\varepsilon_{m, n}},$$

$$A_\nu(u) = \frac{2P_{\nu-1}(-u)}{\nu(P_{\nu-1}(-u) + P_\nu(-u))},$$

$$u = \cos\delta, \quad \delta = \frac{l-d}{d}\pi,$$

where $V^m(u)$ and $V_{n-1}^{p-1}(u)$ are known functions [1]. For the matrix elements $\varepsilon_{m, n}$ of the system, in the case of $N(n + \nu) \gg 1$, the estimate holds:

$$\varepsilon_{m, n} = O\left(\frac{\sin^2\gamma}{N^2(n+\nu)^2}\right).$$

It should be emphasized that the desired coefficients $y_{m, n}$ (and, consequently, $x_{m, n}$) are independent of parameter q. This is essential for conversing and solving the unsteady problem. A solution to the system of equations (7), (8) exists and is unique. For arbitrary parameters of the problem, this solution can be obtained by the reduction method. In the case of a semitransparent cone, a cone with narrow slots, and a narrow cone, the norm of the system matrix operator is smaller than unity. This allows the method of successive approximations to be employed for solving the system of equations. Using the procedure of a steady-problem conversion for a continuous cone [2], we obtain representations for the Green's function G_1 in

the case of a cone with longitudinal slots:

$$G_1 = \frac{c}{4\pi r r_0}\eta\left(\hat{t} - \frac{r + r_0}{c}\right)\sum_{m=-\infty}^{+\infty} e^{im\varphi} \times \int_0^{+\infty} g_{m\tau} U^{(1)}_{m\tau} P_{-1/2+i\tau}(\cosh b)\, d\tau, \quad \gamma < \vartheta < \vartheta_0. \tag{9}$$

Here,

$$g_{m\tau} = (-1)^{m+1} e^{-im\varphi_0}\tau\tanh\pi\tau\frac{\Gamma(1/2 - m + i\tau)}{\Gamma(1/2 + m + i\tau)} \times P^m_{-1/2+i\tau}(-\cos\vartheta_0)P^m_{-1/2+i\tau}(\cos\gamma),$$

$$\cosh b(\hat{t}) = \frac{\hat{t}^2c^2 - r^2 - r_0^2}{2rr_0},$$

$\eta(x)$ is the Heaviside function, and $\Gamma(z)$ is the gamma-function.

REPRESENTATIONS FOR THE GREEN'S FUNCTION

Semitransparent cone. In the case of a semitransparent cone determined by the existence of the limit

$$\lim_{\substack{N\to+\infty \\ d/l\to 1 \\ (\delta\to 0)}}\left[\frac{2}{N}\ln\frac{2}{\delta}\right] = Q > 0,$$

we obtain from (9) the following integral representations for the unsteady Green's function:

$$G_1 = \frac{c}{4\pi r r_0}\eta\left(\hat{t} - \frac{r + r_0}{c}\right)\sum_{m=-\infty}^{+\infty} e^{im\varphi}\int_0^{+\infty} w_{m\tau} \times P^m_{-1/2+i\tau}(\cos\vartheta)P_{-1/2+i\tau}(\cosh b)\, d\tau, \quad 0 < \vartheta < \gamma, \tag{10}$$

$$G_1 = \frac{c}{4\pi r r_0}\eta\left(\hat{t} - \frac{r + r_0}{c}\right)\sum_{m=-\infty}^{+\infty} e^{im\varphi}\int_0^{+\infty} w_{m\tau} \times \frac{P^m_{-1/2+i\tau}(\cos\gamma)}{P^m_{-1/2+i\tau}(-\cos\gamma)}P^m_{-1/2+i\tau}(-\cos\vartheta)P_{-1/2+i\tau}(\cosh b)\, d\tau, \quad \gamma < \vartheta < \pi, \tag{11}$$

$$w_{m\tau} = \frac{(1 - \varepsilon_{m,0})g_{m\tau}}{(1 - \varepsilon_{m,0}) + 2mQ}.$$

If the source is placed on the cone axis ($\vartheta_0 = \pi$, $\varphi_0 = 0$; $m = 0$), expressions (10) and (11) are simplified:

$$G_1 = -\frac{c}{4\pi r r_0}\eta\left(\hat{t} - \frac{r + r_0}{c}\right)\int_0^{+\infty}\frac{\tau\tanh\pi\tau}{D_{i\tau}}P_{-1/2+i\tau}(\cos\gamma) \times P_{-1/2+i\tau}(-\cos\gamma)P_{-1/2+i\tau}(\cos\vartheta)P_{-1/2+i\tau}(\cosh b)\, d\tau, \quad 0 < \vartheta < \gamma,$$

$$G_1 = -\frac{c}{4\pi r r_0}\eta\left(\hat{t} - \frac{r + r_0}{c}\right)\int_0^{+\infty}\frac{\tau\tanh\pi\tau}{D_{i\tau}}[P_{-1/2+i\tau}(\cos\gamma)]^2 \times P_{-1/2+i\tau}(-\cos\vartheta)P_{-1/2+i\tau}(\cosh b)\, d\tau, \quad \gamma < \vartheta < \pi, \tag{12}$$

$$D_{i\tau} = \pi P_{-1/2+i\tau}(\cos\gamma)P_{-1/2+i\tau}(-\cos\gamma) + 2Q\cosh\pi\tau.$$

Passing to integrating over the imaginary axis ($\mu = i\tau$) in (12) and using the fundamental residue theorem, we arrive at a representation for G_1 in the form of a series:

$$G_1 = \frac{c}{2\pi r r_0}\sum_{j=0}^{+\infty}\frac{\mu_j}{\dfrac{d}{d\mu}D_{\mu_j}}P_{-1/2+\mu_j}(\cos\gamma) \times P_{-1/2+\mu_j}(-\cos\gamma)P_{-1/2+\mu_j}(\cos\vartheta)Q_{-1/2+\mu_j}(\cosh b), \tag{13}$$

$$0 < \vartheta < \gamma, \quad c\hat{t} > r + r_0, \quad D_{\mu_j} = 0,$$

where $Q_\zeta(z)$ is the Legendre function of the second kind. Thus, the spectrum for the unsteady boundary value problem is the same as that for the corresponding steady one; it depends on the angular parameters of the conic structure [1]. In the particular case of a semitransparent cone ($Q \gg 1$), the spectrum is determined by the set $\{\mu_j\}_0^{+\infty}$:

$$\mu_j = \frac{1}{2} + j + \frac{1}{2Q}[P_j(\cos\gamma)]^2 + O(Q^{-2}),$$

$$j = 0, 1, 2, \ldots$$

In the case of a steady-state mode ($\hat{t} \gg 1$), we can restrict ourselves to approximation (13) for G_1:

$$G_1 \sim \frac{c}{2\pi r r_0}\frac{\mu_0}{\dfrac{d}{d\mu}D_{\mu_0}}P_{-1/2+\mu_0}(\cos\gamma)P_{-1/2+\mu_0}(-\cos\gamma) \times P_{-1/2+\mu_0}(\cos\vartheta)Q_{-1/2+\mu_0}\left(\frac{\hat{t}^2c^2 - r^2 - r_0^2}{2rr_0}\right).$$

For a semitransparent cone with the filling parameter $Q \gg 1$ and $\hat{t} \gg 1$,

$$\mu_0 = \frac{1}{2} + \frac{1}{2Q} + O(Q^{-2}), \quad G_1 \sim -\frac{c}{4\pi^2 Q}(\hat{t}c)^{-2},$$

$$0 < \vartheta < \gamma$$

under the condition that $\dfrac{1}{Q}|\ln(0.5\sin\gamma)| \ll 1$.

Narrow slots. In the case of a cone with narrow slots $\left(\frac{d}{l} \ll 1; 1+u \ll 1\right)$, the asymptotic expansion of the Green's function in terms of the parameter $1+u$, which holds far from the slots, has the form ($\vartheta_0 = \pi$, $\varphi_0 = 0$)

$$G_1 = -\frac{c}{4rr_0}\int_0^{+\infty}\frac{\tau\tanh\pi\tau}{\cosh\pi\tau}\frac{[P_{-1/2+i\tau}(\cos\gamma)]^2}{\Omega_\tau}$$

$$\times P_{-1/2+i\tau}(-\cos\vartheta)P_{-1/2+i\tau}(\cosh b)d\tau + \frac{c}{8\pi rr_0}\frac{1+u}{N}$$

$$\times\sum_{n\neq 0}e^{inN\varphi}\int_0^{+\infty}\tau\tanh\pi\tau\frac{\widehat{W}_\tau P_{-1/2+i\tau}(\cos\gamma)}{\Phi_\tau}$$

$$\times\frac{P^{nN}_{-1/2+i\tau}(-\cos\vartheta)}{P^{nN}_{-1/2+i\tau}(-\cos\gamma)}P_{-1/2+i\tau}(\cosh b)d\tau$$

$$+ O((1+u)^2\ln(1+u)),$$

$$\gamma < \vartheta < \pi,$$

$$\Omega_\tau = B_\tau - \frac{1}{N}\ln\frac{1-u}{2}, \quad \Phi_\tau = \widehat{W}_\tau + \frac{1}{N}\frac{1+u}{2}(B_\tau + \widehat{W}_\tau),$$

$$B_\tau = \frac{\pi}{\cosh\pi\tau}P_{-1/2+i\tau}(\cos\gamma)P_{-1/2+i\tau}(-\cos\gamma),$$

$$\widehat{W}_\tau = \frac{1-\varepsilon_{0,n}}{N|n|\varepsilon_{0,n}}.$$

A similar representation also holds in the case of $0 < \vartheta < \gamma$. The spectrum of eigenvalues is determined by the roots of the equation with a small right-hand side:

$$\frac{\pi}{\cos\pi\mu}P_{-1/2+\mu_k^\pm}(\cos\gamma)P_{-1/2+\mu_k^\pm}(-\cos\gamma) = \frac{1}{N}\ln\frac{1-u}{2},$$

where

$$\mu_k^\pm = \alpha_k^\pm - \frac{1+u}{2N}$$

$$\times\frac{\cos\pi\mu}{\pi\frac{d}{d\mu}[P_{-1/2+\mu}(\cos\gamma)P_{-1/2+\mu}(-\cos\gamma)]\big|_{\mu=\alpha_k^{\pm+}}}$$

$$+ O((1+u)^2),$$

$$P_{-1/2+\alpha_k^+}(\cos\gamma) = 0, \quad P_{-1/2+\alpha_k^-}(-\cos\gamma) = 0,$$

$$k = 0, 1, 2, \ldots$$

In the limiting case of vanishing slots ($d \longrightarrow 0$, $u \longrightarrow -1$), the expressions obtained coincide with the results for the continuous cone [2].

Narrow cone. In the case of a narrow cone ($\gamma \ll 1$), the asymptotic representation for G_1 has the form ($\vartheta_0 = \pi$, $\varphi_0 = 0$)

$$G_1 = G_1^{\mathrm{istr}} + G_1^{\mathrm{slt}} + O\left(\ln^{-3}\left(\frac{2}{\gamma}\right)\right), \quad \gamma < \vartheta < \pi. \quad (14)$$

Here,

$$G_1^{\mathrm{istr}} = \frac{c}{8\pi rr_0}\frac{1}{\ln(2/\gamma)}\eta\left(\hat{t} - \frac{r+r_0}{c}\right)$$

$$\times\left[\frac{1}{\pi(\cosh b - \cos\vartheta)} - \Phi_1(\hat{t}, r, r_0, \vartheta)\right]$$

is the asymptotic form of the Green's function for the continuous cone:

$$\Phi_1 = \frac{1}{2}\int_0^{+\infty}\frac{\tau\tanh\pi\tau}{\cosh\pi\tau}\left[\Psi\left(-\frac{1}{2}+i\tau\right) + C - \frac{1}{2}\pi i\tanh\pi\tau\right]$$

$$\times P_{-1/2+i\tau}(-\cos\vartheta)P_{-1/2+i\tau}(\cosh b)d\tau,$$

where $\Psi(z)$ is the psi-function, C is the Euler constant, and the term

$$G_1^{\mathrm{slt}} = -\frac{c}{8\pi rr_0}\frac{1}{\ln^2(2/\gamma)}\frac{1}{N}\ln\left(\frac{1-u}{2}\right)\frac{1}{\cosh\pi\tau - \cos\vartheta}$$

accounts for the effect of the slots. Representation (14) for G_1 is valid far from the slots and the cone vertex.

CONCLUSIONS

In this paper, we proposed and substantiated an algorithm for constructing an unsteady Green's function of a first boundary value problem for a semi-infinite circular cone with periodic longitudinal slots. The problem of finding the Green's function for the wave equation was reduced to solving a system of linear algebraic equations with respect to the Fourier coefficients of the desired function. For the cases of a semitransparent cone, a cone with narrow slots, and a narrow cone, both integral representations and representations in the form of a series are obtained for the Green's function. The spectrum of the unsteady first boundary value problem is shown to be the same as that for the corresponding steady one. The algorithm proposed can be used in solving boundary value problems with a more complicated conic geometry.

The results of this study were reported in part at the Second International Conference "Urgent Problems of Computational Physics" (July 24–29, 2000, Dubna, Russia) [3].

ACKNOWLEDGMENTS

The authors are grateful to Academician Yu.V. Gulyaev, Corresponding Member of the RAS V.I. Pustovoĭt, and Professors E.G. Zelkin and Ya.S. Shifrin for their participation in discussing the results of this work.

REFERENCES

1. V. A. Doroshenko and V. F. Kravchenko, Dokl. Akad. Nauk **375**, 611 (2000) [Dokl. Phys. **45** (12), 659 (2000)].
2. K.-K. Chan and L. B. Felsen, IEEE Trans. Antennas Propag. **AP-25**, No. 6, 802 (1977).
3. V. A. Doroshenko, in *Abstracts of the II International Conference on Modern Trends in Computational Physics, Dubna, 2000*, p. 60.

Translated by V. Tsarev

Doklady Physics, Vol. 46, No. 5, 2001, pp. 336–339. Translated from Doklady Akademii Nauk, Vol. 378, No. 1, 2001, pp. 47–50.

MECHANICS

Behavior of Stresses near the Tip of a Crack in an Inhomogeneous Anisotropic Aging Body

S. A. Nazarov* and J. Sokolowski**

Presented by Academician N.F. Morozov

Received November 3, 2000

1. Problem statement. Let $\Omega = \Omega_0 \backslash M$ be a two-dimensional inhomogeneous anisotropic aging body containing a crack represented by the segment $M = \{x: |x_1| < l, |x_2| = 0\}$. In the creep theory, the stress column $\sigma = (\sigma_{11}, \sigma_{22}, 2^{1/2}\sigma_{12})^t$ is determined as

$$\sigma(u; x, t) = A(x, t)D(\nabla_x)u(x, t) + \int_0^t B(x, t, \tau)D(\nabla_x)u(x, \tau)d\tau. \quad (1)$$

We use the matrix representation of equations in Cartesian coordinates $x = (x_1, x_2)^t$, i.e., interpret the displacement vector u as the column $(u_1, u_2)^t$ (where "t" is transposition). In addition, $\nabla_x = (\partial_1, \partial_2)^t$, $\partial_i = \dfrac{\partial}{\partial x_i}$, and

$$D(\nabla_x) = \begin{pmatrix} \partial_1 & 0 \\ 0 & \partial_2 \\ 2^{-1/2}\partial_2 & 2^{-1/2}\partial_1 \end{pmatrix},$$
$$d(x) = \begin{pmatrix} 1 & 0 \\ 0 & 1 \\ 2^{-1/2}x_2 & -2^{-1/2}x_1 \end{pmatrix}. \quad (2)$$

Equation (1) includes the strain column $\varepsilon = D(\nabla_x)u$, as well as the positive definite matrix A of elastic constants and the relaxation kernel B; these are symmetric 3×3 matrices smoothly dependent on variables x, which, however, are only measurable and bounded in the time parameters t and τ. The behavior of these matrices near the tips $P^\pm = (0, \pm l)$ is described by the formula

$$\left|\nabla_x^p(A(x, t) - A^\pm(t))\right| + \left|\nabla_x^p(B(x, t, \tau) - B^\pm(\varphi_\pm, t, \tau))\right| \le c_p r_\pm^{1-p}, \quad (3)$$

where $p = 0, \ldots, s + 1$; $(r_\pm, \varphi_\pm)$ are the polar coordinates with origin $P^\pm$. The matrices $A^\pm$ and $B^\pm$ retain the properties of the matrices A and B, with a smooth dependence on $\varphi_\pm \in [-\pi, \pi]$. The factors $2^{-1/2}$ are introduced in formulas (2) in order to equalize the natural norms of the strain column ε and the strain tensor $[\varepsilon_{ij}]$. The column $c \in \mathbb{R}^3$ forms a rigid displacement $d(x)^t c$. The equilibrium equations and boundary conditions take the form

$$D(-\nabla_x)^t\sigma(u; x, t) = f(x, t), \quad x \in \Omega,$$
$$D(n(x))^t\sigma(u; x, t) = g(x, t), \quad x \in \partial\Omega, \quad (4)$$

where n is a unit vector (column) of the external normal to $\partial\Omega$; f characterizes the mass forces; and g characterizes the external efforts, which are assumed to be self-balanced for nearly all $t \in (0, t_0)$:

$$\int_\Omega d(x)f(x, t)dx + \int_{\partial\Omega} d(x)g(x, t)ds_x = 0. \quad (5)$$

The main objective of this paper is to indicate the asymptotic formulas for solving problem (4), which isolate stresses and give residuals bounded everywhere in Ω. As was verified in [1–5] and in some other works, the root singularities of stresses typical of the linear problems of elasticity theory are also retained in problem (4) on the condition that the instant elastic properties and the relaxation kernel are isotropic. This is explained by the conformity principle (see [6, 7], etc.), which establishes the independence of the stress field from Poisson's ratio. This principle is realized in the creep theory as the Volterra integral operator. Thus, the reason for the retention of the singularity is revealed: the viscoelastic integral operator cancels the principal elastic-solution term at any time t! Such an effect dis-

* *Smirnov Research Institute of Mathematics and Mechanics, St. Petersburg University, Bibliotechnaya pl. 2, St. Petersburg, 198904 Russia*

** *Universite Henri Poincare Nancy I, Vandoeuvre-Les-Nancy, France*

1028-3358/01/4605-0336$21.00

appears in the anisotropic case, and the root singularities gain an additional factor which depends analytically on the logarithmic variable. Similar complications were encountered in the problem with Laplacian operator [8], where direct calculations were possible.

2. Solvability of the problem and its asymptotic behavior. To ensure the uniformity of residuals in the asymptotic formulas, it is convenient to use the Hölder weight space with the norm

$$\begin{aligned}\|v;\Lambda_\beta^{s,\alpha}(\Omega)\| &= \sum_{k=0}^{s}\sup_\Omega\{\rho(x)^{\beta-s-\alpha+k}|\nabla_x^k v(x)|\}\\ &+\sup_{\cdots}\{\rho(x)^\beta|x-y|^{-\alpha}|\nabla_x^s v(x)-\nabla_y^s v(y)|\},\end{aligned}\tag{6}$$

where $s\in\{0,1,\ldots\}$, $\alpha\in(0,1)$, and $\beta\in\mathbb{R}$ are the smoothness and weight indices; $\rho(x)=\min\{1,r_\pm\}$; and dots mean $x,y\in\Omega$: $2|x-y|<\rho(x)$, where x and y lie on one side of M, when $|x_1|<l$. Let us additionally introduce the space $L_\infty([0,t^\circ]\longrightarrow\Lambda_\beta^{s,\alpha}(\Omega))$ of the functions dependent on parameter $t\in[0,t^\circ]$ and having the finite norm

$$|||v;\Lambda_\beta^{s,\alpha}(\Omega)|||_{t^\circ}=\operatorname*{ess\,sup}_{t\in[0,t^\circ]}\|v(\bullet,t);\Lambda_\beta^{s,\alpha}(\Omega)\|.$$

We assume that

$$\begin{aligned}f&\in L_\infty([0,t^\circ]\longrightarrow\Lambda_\beta^{s-1,\alpha}(\Omega)),\\ \tilde g&\in L_\infty([0,t^\circ]\longrightarrow\Lambda_\beta^{s,\alpha}(\partial\Omega)),\\ g(x,t)&=\tilde g(x,t)+\sum_\pm\chi_\pm(x)b^\pm(t),\quad b^\pm\in L_\infty(0,t^\circ),\\ s&\in\{1,2,\ldots\},\quad\alpha\in(0,1),\quad\beta-s-\alpha\in(-1/2,0).\end{aligned}\tag{7}$$

Here, $\chi_\pm$ are smooth cutoff functions that are equal to unity near "their own" tips $P^\pm$ and vanish near the "foreign" tips $P^\mp$; $\chi_\pm(x)=0$ for $r_\pm>l$. Formulas (7) admit any right-hand side f, smooth up to the bound, but the boundary data g must have the same limits at the vertices $P^\pm$ along the crack shore. The point is that, for $\beta-s-\alpha<0$, norm (6) estimates the value of $|v(x)|$ at any point $x\in\Omega$ and, moreover, the weight $\rho(x)^{\beta-s-\alpha}$ with a negative exponent causes the norm to tend to zero at $x\longrightarrow P^\pm$.

Theorem. *Under the constraints* (3), (5), *and* (7), *problem* (4) *has a solution representable as*

$$\begin{aligned}u(x,t)&=\tilde u(x,t)+\sum_\pm\chi_\pm(x)\Big\{a^{0\pm}(t)+\sum_{i=1}^{2}x_ia^{i\pm}(t)\\ &+r_\pm^{1/2}\sum_{j=0}^{\infty}\frac{1}{j!}(\log r_\pm)^j\mathcal{U}^{j\pm}(\varphi_\pm,t)\Big\},\end{aligned}\tag{8}$$

where

$$a^{p\pm}\in L_\infty(0,t^\circ),\quad p=0,1,2,$$

$$\tilde u\in L_\infty([0,t^\circ]\longrightarrow\Lambda_\beta^{s+1,\alpha}(\Omega))$$

and, for any fixed $q\in\{1,2,\ldots\}$, $q\ge s+1$,

$$\mathcal{U}^{j\pm}\in L_\infty([0,t^\circ]\to C^{q+1}[-\pi,\pi]).\tag{9}$$

This solution possesses a finite elastic energy at nearly all $t\in(0,t^\circ)$ *and is defined up to the rigid displacement* $d(x)^{\mathrm t}c(t)$. *Provided that the orthogonality conditions*

$$\int_\Omega d(x)u(x,t)dx=0$$

are fulfilled at nearly all $t\in(0,t^\circ)$, *the solution becomes unique and the values of* $C_i>0$ *and* $\delta_i>0$ *exist such that, for any* $t\le t^\circ$, *the relations*

$$\begin{aligned}\|a^{p\pm};L_\infty(0,t)\|+|||\tilde u;\Lambda_\beta^{s+1,\alpha}(\Omega)|||_t&\le C_1e^{\delta_1t}N(t),\\ |||\mathcal{U}^{j\pm};C^{q+1}[-\pi,\pi]|||_t&\le C_2\frac{1}{j!}\Big(\frac{\delta_2}{\delta_1}t\Big)^je^{\delta_2t}N(t),\\ N(t)&=|||f;\Lambda_\beta^{s-1,\alpha}(\Omega)|||_t\\ &+|||\tilde g;\Lambda_\beta^{s,\alpha}(\partial\Omega)|||_t+\sum_\pm\|b^\pm;L_\infty(0,t)\|\end{aligned}\tag{10}$$

are valid.

Let us make some comments on the outcome formulated here. As usual (see, e.g., [9]), the solution to problem (4) is sought as a series:

$$u(x,t)=\sum_{q=0}^{\infty}u^q(x,t),\tag{11}$$

where u^q are the solutions of the elasticity theory with parameter t:

$$\begin{aligned}D(-\nabla_x)^{\mathrm t}AD(\nabla_x)u^q&=\delta_{q,0}f-D(-\nabla_x)^{\mathrm t}F^q\quad\text{in}\quad\Omega;\\ D(n)^{\mathrm t}AD(\nabla_x)u^q&=\delta_{q,0}g-D(n)^{\mathrm t}F^q\quad\text{on}\quad\partial\Omega,\end{aligned}\tag{12}$$

where

$$F^q(x,t)=\int_0^t B(x,t,\tau)u^{q-1}(x,\tau)d\tau,\quad q\ge1,\quad F^0=0.$$

The existence of solutions to problems (12) and their asymptotic representations are established using the theory of boundary-value problems in domains with angular and conical points (see [10, 11] and also [12–14], where the theory is adapted to the problems of crack mechanics). Since the asymptotic representations are constructed iteratively (one has to solve the tasks with right-hand sides of a special kind; see theorem 4.5.12 in [12]), logarithms accumulate and the $\mathbf{U}^{q\pm}(\varphi_\pm, t, \log r_\pm)$ factors at $r_\pm^{1/2}$ in the asymptotics of the solution u^q turn out to be polynomials of $\log r_\pm$ of degree q. Multistep estimates of the coefficients of these polynomials (due to the presence of the four selected constants C_i and δ_i) make it possible to sum up series (11).

The sums $\mathcal{U}^\pm(\varphi_\pm, t, \log r_\pm)$ involved in (8) are, in general, infinitely large as compared to any power of $|\log r_\pm|$. At the same time, for arbitrary $J \in \{1, 2, \ldots\}$, we deduce from (10) the relationship

$$\left|\left|\left|\mathcal{U}^\pm(\bullet, \bullet, \log r); C^{q+1}(-\pi, \pi)\right|\right|\right|_t \le C_2 e^{\delta_2 t} N(t)$$

$$\times \sum_{j=0}^{\infty} \left(\frac{1}{j!}\right)^2 \left(\frac{\delta_2}{\delta_1} t|\log r|\right)^j$$

$$\le C_2 \kappa(J) N(t) \exp\{\delta_2 t[1 + (J\delta_1)^{-1}|\log r|]\},$$

where $\kappa(J) = \min\{J^j/j!|\ j = 0, 1, \ldots\} < \infty$. Therefore, $\mathcal{U}^\pm(\varphi_\pm, t, \log r_\pm)$ grows more slowly than any power of $r_\pm$ and does not change the power order of the stress singularity.

The stresses $\sigma(\tilde{u})$ calculated from the asymptotic residue belong to the space $L_\infty([0, t^\circ] \longrightarrow \Lambda_\beta^{s,\alpha}(\Omega))$ and, therefore, as was mentioned before the theorem statement, are bounded everywhere in Ω at nearly all $t \in (0, t^\circ)$.

3. Conditions for appearance and disappearance of logarithms. Let $X^{i\pm}(x, t) = r_\pm^{1/2} \Phi^{i\pm}(\varphi_\pm, t)$ and $Y^{i\pm}(x, t) = r_\pm^{-1/2} \Psi^{i\pm}(\varphi_\pm, t)$ $(i = 1, 2)$ be solutions to the problem of elasticity theory in the homogeneous plane with a semi-infinite crosscut $\{x: \mp x_1 > 0, x_2 = 0\}$. The elastic properties of the plane are described by the matrix $A^\pm(t)$. The singularities $Y^{i\pm}(x, t)$ of the weight functions are found from the main singularities $X^{i\pm}(x, t)$ using simple operations (see [15]).

Lemma. *If for any $t \in [0, t^\circ]$ and $\tau \in [0, t]$ the 2×2 matrix $Q^\pm(t, \tau)$ with elements*

$$Q_{in}^\pm(t, \tau) = \int\limits_{\{1 < r_\pm < 2\}} (D(\nabla_x) Y^{i\pm}(x, t))^t \times B^\pm(\varphi_\pm, t, \tau) D(\nabla_x) X^{n\pm}(x, \tau) dx \quad (13)$$

is nonsingular, the polynomials $\log r_\pm \mapsto \mathbf{U}^{q\pm}(\varphi_\pm, t, \log r_\pm)$ with nonzero coefficients in $(\log r_\pm)^q$ appear in the asymptotics of the solutions u^q to problems (12). *Moreover, if A and B are independent of the time parameters t and τ and $\mathcal{U}^{j\pm} = 0$ for large numbers j, then $\mathcal{U}^{j\pm} = 0$ for all $j = 0, 1, \ldots$ and, therefore, $\mathcal{U}^\pm(\varphi_\pm, t, \log r_\pm)$ is never a nontrivial polynomial of the variable $\log r_\pm$.*

We should emphasize that the ring $\{x: 1 < r < 2\}$ in formula (13) can be replaced by any concentric ring, because the integrand is a homogeneous function of the variable $r_\pm$ of degree –2.

For any sets $\{D(\nabla_x) Y^{i\pm}\}$ and $\{D(\nabla_x) X^{n\pm}\}$, we can construct the matrix-function $B^\pm(\varphi_\pm, t, \tau)$ so that $\det Q^\pm(t, \tau) \ne 0$. In other words, the condition defined by the lemma can be satisfied at even instant elastic isotropy of the material if the relaxation kernel is suitably chosen. In this case, the product $r_\pm^{1/2} \sigma(u; x, t)$ has no limit when $r \longrightarrow +0$! This unexpected result calls for reconsideration of the classical force criterion in the creep theory, which appeals to the notion of the stress intensity coefficients expressed through such a limit.

The equality $Q^\pm(t, \tau) = 0$ does not provide for the absence of logarithms in the asymptotic formula (8). Certainly, logarithms disappear on the condition that the matrices $B^\pm(\varphi_\pm, t, \tau)$ and $A^\pm(t)$ are similar to the matrix $A^\pm(0)$. However, all possible variants are not exhausted by such a simple case. Indeed, using the algebraic equivalence of two-dimensional problems of elasticity theory [15], one can assure that the logarithms are absent if the matrices $B^\pm(\varphi_\pm, t, \tau)$ and $A^\pm(t)$ fall into a certain two-parameter class generated by the matrix $A^\pm(0)$.

The stabilization condition (3) implies that the $A^\pm(t)$-matrices are independent of $\varphi_\pm$. This requirement is necessary because the exponents of the stress singularities in the elasticity problem with matrix $A^\pm(\varphi_\pm, t)$ may differ from –1/2 and vary with time. No detailed asymptotic formulas are, however, known for such a situation.

This study was supported by the Lyapunov French–Russian Center for Applied Mathematics and Informatics, project no. 00-01.

REFERENCES

1. N. Kh. Arutyunyan, S. A. Nazarov, and B. A. Shoĭkhet, Dokl. Akad. Nauk SSSR **266**, 1365 (1982).
2. V. P. Zhuravlev, S. A. Nazarov, and B. A. Shoĭkhet, Prikl. Mat. Mekh. **47**, 200 (1983).
3. S. E. Mikhaĭlov, Izv. Akad. Nauk, Mekh. Tverd. Tela, No. 2, 126 (1984).
4. C. Atkinson and J. P. Bourne, Int. J. Eng. Sci. **28**, 615 (1990).
5. S. E. Mikhailov, Math. Methods Appl. Sci. **20**, 13 (1997).
6. G. S. Vardanyan and V. D. Sheremet, Izv. Akad. Nauk Arm. SSR, Mekh. **26** (4), 60 (1973).
7. S. A. Nazarov, L. P. Trapeznikov, and B. A. Shoĭkhet, Prikl. Mat. Mekh. **51**, 504 (1987).
8. S. A. Nazarov and B. A. Shoĭkhet, Mat. Zametki **33**, 583 (1983).
9. M. A. Krasnosel'skiĭ, G. M. Vaĭnikko, P. P. Zabreĭko, Ya. B. Rutitskiĭ, and B. Ya. Stetsenko, *Approximate Solutions of Operator Equations* (Nauka, Moscow, 1967).
10. V. A. Kondrat'ev, Tr. Mosk. Mat. O–va **16**, 219 (1967).
11. V. G. Maz'ya and B. A. Plamenevsky, Math. Nachr. **76**, 29 (1977).
12. S. A. Nazarov and B. A. Plamenevsky, *Elliptic Problems in Domains with Piecewise Smooth Boundaries* (Walter de Gruyter, Berlin, 1994).
13. S. A. Nazarov and O. R. Polyakova, Tr. Mosk. Mat. O–va **57**, 16 (1996).
14. S. A. Nazarov, Prikl. Mat. Mekh. **62**, 489 (1998).
15. A. A. Kulikov, S. A. Nazarov, and M. A. Narbut, Vestn. S.-Peterb. Univ., No. 8, 58 (2000).

Translated by A. Kozlenkov

Doklady Physics, Vol. 46, No. 5, 2001, pp. 340–345. Translated from Doklady Akademii Nauk, Vol. 378, No. 1, 2001, pp. 51–57.

MECHANICS

Nonlinear Variations of the Level of the Caspian Sea and the Global Climate

V. I. Naĭdenov* and I. A. Kozhevnikova**

Presented by Academician V.V. Kozlov October 24, 2000

Received October 25, 2000

In 1958, the well-known American scientist E. Lorentz proposed a hypothesis on climate intransitivity (ambiguity) [1]. This hypothesis claims the existence of several steady states of a dynamical system under identical external actions and is well known in mechanics (cf., the famous Euler problem on equilibrium of an elastic rod). We show that similar phenomena of multiplicity and instability of steady-state regimes are characteristic for many natural processes, and they can be described in terms of the theory of nonlinear dynamical systems. The observed abrupt variations in the level of the Caspian Sea and global warming are explained by the nonlinear dependence of thermal-physical properties (heat capacity and albedo) of dry land on moisture reserves.

1. BISTABILITY OF THE SEA LEVEL

The equations of water balance for the Caspian-Sea basin, the dynamics of the river run-off, and the water balance of the sea in itself are

$$\frac{dW}{dt} = P - E(W) - Q + \sigma_1\xi_1(t) - \sigma_2\xi_2(t),$$

$$\tau\frac{dQ}{dt} = G(W) - Q, \qquad (1)$$

$$\frac{dH}{dt} = \frac{S_r Q}{S(H)} - \tilde{E}(H) - q(H) + \sigma_3\xi_3(t).$$

Here, W, Q, H are the moisture capacity of the basin volume, the river run-off, and the sea level, respectively; S_r, $S(H)$ are the areas of the water-collection basin and the sea; P, E, $\tilde{E}$, q are the quantities characterizing atmospheric precipitations in the sea basin, evaporation from both the basin and the water area, and the run-off into the Gulf of Kara-Bogaz-Gol, respectively; $G(W)$ is the run-off dependence on the moisture reserves (above all, on the volume of underground waters actively drained by rivers); τ is the relaxation time of the river run-off (i.e., the setting time for a new regime as a reaction to an external perturbation); ξ_1, ξ_2, ξ_3 are the delta-correlated independent random processes; and σ_1, σ_2, and σ_3 are their intensities.

The second equation of set (1) can be obtained in the following method. Let $K = \frac{Q^2}{2}$ be the kinetic energy of the river run-off, $\Pi = G(W)\tau^{-1}Q$ be the power developed by the gravity force while displacing river-basin waters into the locking section of a river, and $\Phi = \tau^{-1}Q^2$ be the power of dissipative forces (friction forces and other resistance forces).

The second equation of set (1) is derived from the change of the kinetic energy for the river run-off: $\frac{dK}{dt} = \Pi - \Phi$.

As a result of vast investigations [2] (over 56 stations of the East-European Plain, Kazakhstan, and Central Asia), it was found that the estimate of the correlation between the annual atmospheric precipitations and evaporability is negative at a reasonable significance level. Thus, for the zone of formation of the river run-off in sufficiently moistened territories, it is possible to assume that evaporation decreases with increasing moisture reserves. In [3], it was shown (over 125 stations of Eurasia and North America in the zone of 35°–65° N.L.) that the amplitude of the annual temperature variation is a decreasing function of the annual amount P(mm/year) of precipitation, $\Delta\theta_a = 470P^{-0.63}$.

The fundamental effects indicated explain the dependence of evaporation on moisture reserves and lead to a high negative correlation between the river run-off and the apparent evaporation in the Caspian Sea, as was found in [4]. A rise in precipitation in the Volga and Ural basins leads to a simultaneous growth in the run-off and moistening. This, in turn, reduces the evaporation both from the river basin and sea surface. Here, the mechanism of positive feedback is in action,

* *Institute of Water Problems, Russian Academy of Sciences, Mytishchi, Moscow oblast, Russia*

** *Moscow State University, Vorob'evy gory, Moscow, 119899 Russia*

1028-3358/01/4605-0340$21.00

Table 1. Parameters obtained by the Box–Jenkins method for the discrete ARMA(2, 1) model and the corresponding continuous mode

Parameter	ϕ_1	ϕ_2	θ	$2h$	ω^2
Nile run-off (1900–1960)	0.66	−0.26	0.32	1.347	1.205
Residual sequence $\{\gamma^{(5)}(t)\}$ for the Caspian-Sea model (1830–1989)	0.49	−0.13	−0.01	2.040	1.719

which is responsible for the abrupt variation in the level of the Caspian Sea and other basins without outflow.

In [5], nonlinear dependences of the evaporation and run-off on the moisture reserves of river basins were proposed. For them, the following relationships are characteristic:

$$G'_W > 0, \quad E'_W > 0, \quad W < W_*,$$
$$E'_W < 0, \quad W > W_*, \quad E'_W(W_*) = 0. \tag{2}$$

From the set of relationships (1), without allowance for the stochastic components, it is possible to obtain an equation for the Duffing-type nonlinear oscillator:

$$\frac{d^2W}{dt^2} + (E'_W + \tau^{-1})\frac{dW}{dt} + \tau^{-1}\Psi(W) = 0,$$
$$\Psi(W) = G(W) - (P - E(W)).$$

This oscillator has three equilibrium states: W_S^i, $Q_S^i = G(W_S^i)$, $\Psi(W_S^i) = 0$; $i = 1, 2, 3$. It is easy to show that, under assumptions (2), W_S^1 and W_S^3 are stable (or unstable) focuses and W_S^2 is a saddle.

The set of equations (1) has stable self-oscillatory regimes. The conditions for the excitation of self-oscillations are $E'_W(W_S^j) + \tau^{-1} < 0$.

We would like to emphasize that the nonlinear oscillators with two stable states of equilibrium with the presence of a periodic excitation demonstrate a determinate chaos.

For example, from this set, we can obtain the equations for a linear oscillator with friction:

$$q = Q - Q_S^j,$$
$$\frac{d^2q}{dt^2} + 2h\frac{dq}{dt} + \omega^2 q = \tau^{-1}G'_W(\sigma_1\xi_1(t) - \sigma_2\xi_2(t)), \tag{3}$$
$$2h = E'_W(W_S^j) + \tau^{-1},$$
$$\omega^2 = \tau^{-1}(E'_W(W_S^j) + G'_W(W_S^j)), \quad j = 1, 3.$$

In the vicinity of stable equilibrium states, we have two frequencies ω^j with periods $\Omega^j = \frac{2\pi}{\omega^j}$.

Since the available models of the hydrologic cycle [6] fail to describe even the regional climatic systems, we determine the parameters h and ω for the model of a river run-off from the full-scale data for the mean annual run-off. If an original continuous process is subjected to white noise (3) in its right-hand side (at the input), then the discrete autoregression process is described by a differential equation with a moving average whose order of magnitude is smaller by unity than that for the differential equation describing the system under consideration [7, 8]. We put in correspondence to Eq. (3) a discrete autoregression model, i.e., the moving-average model ARMA(2, 1) $q_t - \phi_1 q_{t-1} - \phi_2 q_{t-2} = \varepsilon_t - \theta\varepsilon_{t-1}$, where ε_t is the white noise, $E\varepsilon_t = 0$, and $E\varepsilon_t\varepsilon_{t+u} = \delta(u)\sigma_\varepsilon^2$ {$\delta(u)$ is the Dirac delta function}. The parameters ϕ_1, ϕ_2, and θ of this model are obtained by minimizing the function

$$\Omega = \sum_{t=3}^{n}\varepsilon_t^2 = \sum_{t=3}^{n}(q_t - \phi_1 q_{t-1} - \phi_2 q_{t-2} + \theta\varepsilon_{t-1})^2$$

over ϕ_1 and ϕ_2 with the Box–Jenkins method and by recalculating θ with the help of the formula from [8], which was adapted to the case of complex roots $\lambda_1 = |\lambda|e^{i\varphi}$ and $\lambda_2 = |\lambda|e^{-i\varphi}$, $\varphi \neq 0$ for the discrete-model characteristic equation

$$\theta = \frac{|\lambda|\varphi(|\lambda|^2[\ln|\lambda|\sin\varphi - \varphi\cos\varphi] - [\ln|\lambda|\sin\varphi + \varphi\cos\varphi])}{|\lambda|^2[\ln|\lambda|\sin\varphi - \varphi\cos\varphi] + |\lambda|[\ln^2|\lambda| + \varphi^2]\sin^2\varphi - \varphi^2}.$$

The parameters $2h$ and ω^2 of Eq. (3) can be expressed in terms of the ARMA(2, 1) parameters:

$$2h = -\frac{\ln(-\phi_2)}{\Delta},$$
$$\omega = \frac{1}{\Delta}\sqrt{\frac{\ln^2\sqrt{-\phi_2}}{4} + \arccos^2\left(\frac{\phi_1}{2\sqrt{-\phi_2}}\right)}.$$

In the case under consideration, $\Delta = 1$ year. The results of calculations for certain time series are displayed in Table 1.

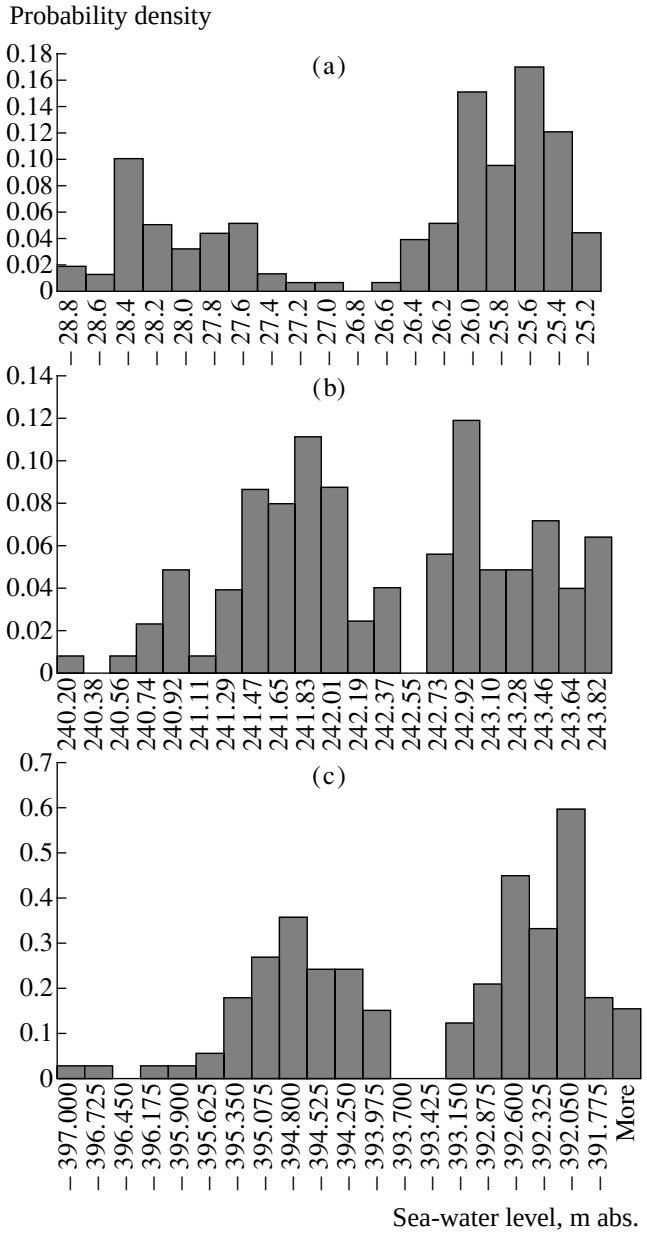

Fig. 1. Histograms for variations in water levels in the case of (a) the Caspian Sea, (b) Lake Chad; and (c) the Dead Sea.

The characteristic feature of the steady-state probability density for the moisture reserves of the Caspian basin and the Volga run-off is its bimodal distribution.

Indeed, the time-independent solution to the Fokker–Planck–Kolmogorov equation for set (1),

$$\frac{\partial p}{\partial t} + \frac{\partial}{\partial W}[(P - E(W))p]$$

$$+ \frac{\partial}{\partial Q}[\tau^{-1}(G(W) - Q)P] - \frac{1}{2}\bar{\sigma}^2\frac{\partial^2 p}{\partial W^2} = 0,$$

$$\bar{\sigma}^2 = \sigma_1^2 + \sigma_2^2,$$

as $\tau \longrightarrow 0$, has the form

$$p(W) = N\exp\left\{-\int_0^W \frac{2\Psi(\xi)}{\bar{\sigma}^2}d\xi\right\}.$$

Hence, it follows that $\frac{dp}{dW}(W_S^i) = 0$ corresponds to the maximum for $i = 1, 3$ and to the minimum for $i = 2$.

Analysis of observational data showed that, for the modern climate, in the case of the same value of atmospheric precipitates in the sea basin, there are two steady equilibrium values of the annual river run-off into the Caspian Sea, namely, 320 and 270 km^3/year and two levels of the Caspian Sea equal to –25.47 and –27.92 m abs., respectively. The equilibrium states of the sea level are determined as

$$S_r Q_S^i = [\tilde{E}(H_S^i) + q(H_S^i)]S(H_S^i).$$

In fact, the histograms for the level of the Caspian Sea and for certain other closed basins (the Dead Sea, Lake Chad, the Great Salt Lake, etc.) are bimodal (Fig. 1). In [9], it is stated that the bimodal character of the histogram for the level of the Caspian Sea is only an occasion. However, it is unlikely that Nature is so occasional. In our opinion, the Caspian Sea represents a complicated and poorly studied nonlinear system, which should be investigated instead of claiming that its properties are occasional.

We present here the regression model [10] for the variation of the level of the Caspian Sea:

$$\begin{aligned} Z(t+1) - Z(t) &= \Phi_1^{(5)}(Z(t)) + \gamma^{(5)}(t), \\ \gamma^{(5)}(t) &= 0.459\gamma^{(5)}(t-1) + 0.060\delta^{(5)}(t), \\ \Phi_1^{(5)}(Z(t)) &= -0.021 + 0.0021Z(t) + 0.1441Z^2(t) \\ &+ 0.057Z^3(t) - 0.1231Z^4(t) - 0.1176Z^5(t). \end{aligned} \quad (4)$$

Here, $Z(t)$ is the dimensionless level, $\gamma^{(5)}(t)$ is the residual sequence of the regression model of the fifth order, and $\delta^{(5)}(t)$ is the sequence of mutually independent and identically distributed random values with zero mean and unit variance.

The full-scale data $X(t)$, $t = 1, 2, \ldots, N$ were normalized using the transformation

$$Z(t) = \frac{2X(t) - X_{\max} - X_{\min}}{X_{\max} - X_{\min}}, \quad X_{\max} = \max_{1 \le t \le N} X(t),$$
$$X_{\min} = \min_{1 \le t \le N} X(t), \quad |Z(t)| \le 1,$$

where $X_{\max} = -25.21$ and $X_{\min} = -28.92$ m abs.

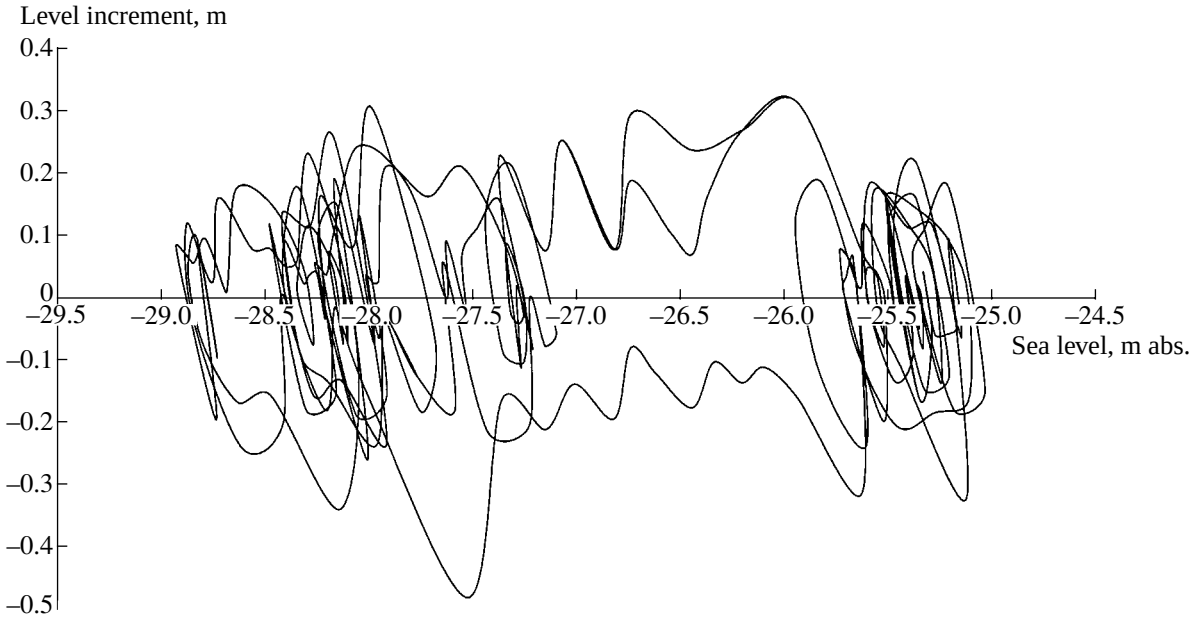

Fig. 2. Phase portrait of the nonlinear model for variations in the level of the Caspian Sea.

The attractor of nonlinear model (4) is shown in Fig. 2.

2. ON A PROBABILISTIC PREDICTION OF SEA-LEVEL OSCILLATIONS

We now put forth a question: what is the probability that a sea initially at a fixed level H_c (for example, H_c can be the sea level observed in 1999) attains a high level H_3 (–25.47 m abs.) prior to a lower level H_1 (–27.92 m abs.), and what is the average time of attaining a new position of equilibrium? The solution to this problem is based on solving the Kolmogorov inverse equation and is displayed in Table 2. This is the probabilistic prognosis of the sea-level variations for the nearest 15–20 years, which is obtained on the basis of the analytical solution to the Kolmogorov inverse equation. [This result can also be obtained by the method of mathematical simulation of the solution to nonlinear discrete equation (4).]

In the long-term time scale, the number of transitions of the Caspian Sea from one equilibrium level to another is determined by the Poisson law with a parameter of 0.01–0.002 $\frac{1}{\text{year}}$. We emphasize that the processes of the heat exchange and moisture exchange in the sea basin are strongly unstable and are nonlinear dynamic processes whose description is possible only at the probabilistic level. Thus, only the ensemble evolution can be predicted. As to the individual trajectory over a period of 100 years, this prediction is incorrect [11].

3. ON THE PROBLEM OF INSTABILITY OF THE GLOBAL CLIMATE

We write out the equations of the thermal-energy balance for the terrestrial climatic system, the land water balance, and the dynamics of the global river run-off:

$$c\frac{dT}{dt} = \frac{S_0}{4}[1 - \alpha(T, W)] - I(T),$$
$$\frac{dW}{dt} = P(T) - E(T, W) - Q, \qquad (5)$$
$$\tau\frac{dQ}{dt} = G(W) - Q.$$

Here, $\mathbf{R} = \{T, W, Q\}$ are the global air temperature, the moisture reserves of continents, and the river run-off

Table 2. Probabilities and durations of transitions from a fixed sea level to the upper and lower levels

Level, m abs.	Probability of the transition to the lower level	Transition time, years	Probability of the transition to the upper level	Transition time, years
–27.74	0.98	5	0.02	34
–27.55	0.96	10	0.04	33
–27.36	0.93	13	0.07	32
–27.17	0.89	17	0.11	29
–26.99	0.83	20	0.17	27
–26.81	0.75	22	0.25	24
–26.62	0.64	25	0.36	20
–26.44	0.50	28	0.50	17
–26.25	0.35	30	0.65	13
–26.07	0.22	32	0.78	10
–25.88	0.12	33	0.88	7
–25.69	0.05	34	0.95	3

into the ocean, respectively; S_0, $I(T)$, $\alpha(T, W)$ are the solar constant, the amount of the heat radiation outgoing from the atmosphere upper boundary, and the planetary albedo of the Earth; c is the heat capacity of the system consisting of both the atmosphere and the functional layer of the underlying surface; and $P(T)$ and $E(T, W)$ are the amount of precipitates and evaporation from the continental surface.

These equations are obtained provided that the amount of water and the total ice mass on the Earth are constant (land and island polar-ice sheets and the underground ice of permafrost are steady formations and do not participate in short-period oscillations of the climate).

Let $\mathbf{R}_S = \{T_S, W_S, Q_S\}$ be the time-independent solution to the set of equations (5). It is easy to show that, with allowance for the dependence of planetary albedo and evaporation of the land moisture reserves, this solution turns out to be unstable. The character of the climate instability is specified by the spectrum of the matrix $\frac{\partial \mathbf{F}}{\partial \mathbf{R}}(\mathbf{R}_S^i)$ of the nonlinear dynamical system $\partial_t \mathbf{R} = \mathbf{F}(\mathbf{R})$. For example, for $c = 9.6$ W year/m^2, $\frac{\partial \alpha}{\partial T} = 0$,

$$-\frac{S_0}{4}\frac{\partial \alpha}{\partial W} = 0.2\ \frac{\mathrm{W}}{\mathrm{m}^3}, \quad \frac{dP}{dT} - \frac{\partial E}{\partial T} = 0.035 \frac{\mathrm{m}}{\mathrm{year\ K}},$$

$$\frac{dI}{dT} = 2\frac{\mathrm{W}}{\mathrm{m}^2\ \mathrm{K}}, \quad \frac{dG}{dW} = 0.05\frac{1}{\mathrm{year}},$$

$$\frac{\partial E}{\partial W} = -0.06\frac{1}{\mathrm{year}}, \text{ and } \tau = 4 \text{ years},$$

where the derivatives are calculated for modern climatic conditions (T_S = 15°C, Q_S = 0.3 m/year, P_S = 0.8 m/year, E_S = 0.5 m/year, $\alpha_S = 0.33$, $S_0 = 1370$ W/m^2) and the eigenvalues of this matrix are 1.63×10^{-2} 1/year, $-2.07 \times 10^{-1} \pm 1.15 \times 10^{-2}\ i$/year (saddle–focus). It is easy to show that, for $\frac{\partial \alpha}{\partial W} < 0$ and $\frac{\partial E}{\partial W} < 0$, the nonlinear set of equations (5) can have several solutions. The central problem relevant to the properties of this set consists in the possibility of existence of a strange attractor, because there exists a hypothesis that the climatic evolution for the last million years can be considered a manifestation of the deterministic dynamics possessing a chaotic small-dimensional attractor.

Thus, the modern climate turns out to be unstable with a characteristic oscillation period of hundreds of years.

The observed global warming of the Earth takes place due to increased solar-energy absorption, owing to a progressing decrease in the land albedo and an increase in the land heat capacity. The rise in carbon-dioxide concentration in the atmosphere (the greenhouse effect) is a consequence of natural processes.

In our opinion, the correlation [11] between the anomalous warming of waters off the shores of Ecuador and Peru (El Niño) and the climate in the Volga basin is explained by the instability of the Earth's global climate. The moistening of the Northern hemisphere in the 1980s induced a decrease in the albedo and land heat capacity. This fact, in turn, increased the near-ground temperature of the Northern hemisphere, decreased the heat outflow from the tropics, and increased the temperature in the equatorial zone of the Pacific Ocean. The development of a vast temperature anomaly on the surface of the Pacific Ocean in its central part preceded the occurrence of El Niño and considerably enhanced it.

Indeed, prior to the occurrence of the anomalous El Niño (1982–1983), the level of the Caspian Sea had already been elevated by 86 cm (!) and the soil-moisture reserves for the European territory of Russia increased everywhere in 1972–1985 and in all the seasons at a rate of 1 to 3 cm for 10 years. Note that the correlation dependence between El Niño and the Nile run-off was noticed for the first time in [12]. It should be emphasized that the relationship between the El Niño phenomenon and the anomalies in meteorological and oceanic fields in various regions is the consequence of the instability and nonequilibrium of the global climatic system. According to the descriptive expression of I. Prigozhin, "only in a nonequilibrium state, can a system turn out to be sensitive to certain aspects of its proper reality."

4. KOLMOGOROV ESTIMATES FOR SPECTRAL DENSITIES OF TIME SERIES

Since periodic solutions are characteristic of models (1) and (5), the spectra of climatic and hydrologic series must have extrema at certain frequencies.

For the spectral densities of the series, we used the Kolmogorov estimate [13, 14]. Let the series $X(t)$ of length N be divided into T segments each of length M, which are shifted by L with respect to each other; i.e., $N = (T-1)L + M + 1$. We determine that

$$\bar{f}_N(\omega) = \frac{1}{T}\sum_{k=0}^{T-1} \left|W_M^{Lk}(\omega)\right|^2,$$

$$W_M^{Lk}(\omega) = \sum_{t=-\infty}^{\infty} a_M(t - Lk)e^{i\omega t}X(t), \quad |\omega| \le 0.5,$$

where $a_M(t)$, $t = \ldots, -1, 0, 1, \ldots$ is a certain nonnegative function ("data window") equal to zero outside the interval $[0, M]$. In the case of the Kolmogorov estimate [13, 14], this function is determined by the relation

$$a_M(t) = \mu(K, P)\left(\frac{K(P^2-1)}{12\pi}\right)^{1/4} P^{-K} C_{K,P}(t).$$

Here, $M = K(P-1)$ and $\mu(K, P)$ is the normalizing factor, the integers K and P being specified by the length

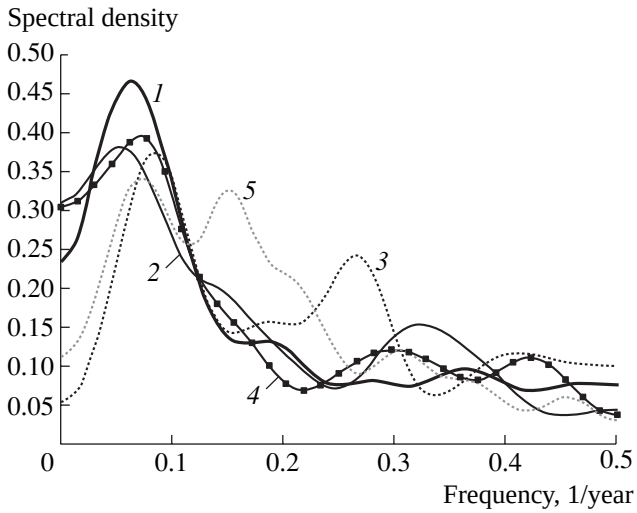

Fig. 3. Spectra of various time series characterizing the climate in the Caspian-Sea basin: (*1*) spectrum of the Volga run-off in Yaroslavl; (*2*) spectrum of the run-off into the Caspian Sea for all rivers of the Caspian basin; (*3*) spectrum of air temperature in Kazan; (*4*) spectrum of air temperature in Moscow; and (*5*) spectrum of the $\gamma^{(5)}$ sequence.

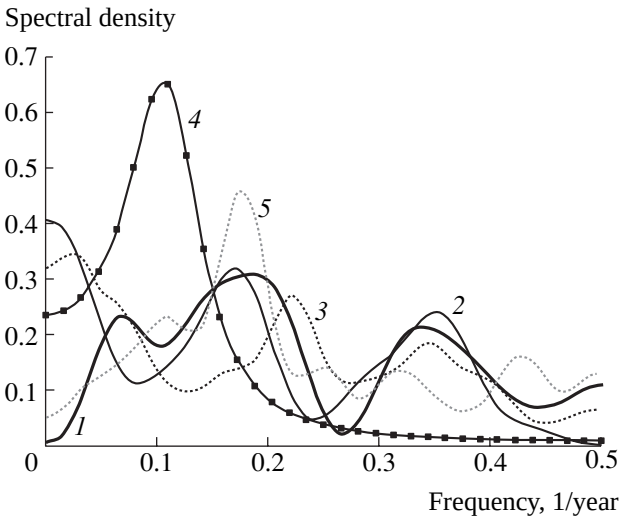

Fig. 4. Spectra of various time series: (*1*) spectrum of the Nile run-off; (*2*) spectrum of El Niño (temperature series); (*3*) spectrum of air temperature in Saint Petersburg; (*4*) spectra of the Wolf numbers; and (*5*) spectra of the Dnieper run-off.

M of a segment. The coefficients $C_{K,P}(t)$ are determined from the relationship

$$\sum_{t=0}^{K(P-1)} z^t C_{K,P}(t) = (1 + z + \ldots + z^{P-1})^K = \left(\frac{1-z^P}{1-z}\right)^K.$$

Usage of the $\bar{f}_N(\omega)$ statistic constructed on the overlapping segments makes it possible to markedly decrease the variance of the estimate and to simultaneously test the series with respect to its stationary character. The statistical properties of this estimate were thoroughly investigated in [13].

Thus, in this paper, we have constructed the spectra for the Caspian Sea and its basin, for the Volga run-off in Yaroslavl, the run-off for all the rivers into the Caspian Sea, the air temperature in Kazan and Moscow, and the sequence $\gamma^{(5)}(t)$ [see (4)] for variations in the level of the Caspian Sea (Fig. 3). Moreover, we have constructed the spectra of the Wolf numbers, the Nile run-off near the Aswan dam, the El Niño anomalous flow near the shores of Peru and Ecuador (the temperature series), the Dnieper run-off, and the air temperature in Saint Petersburg (Fig. 4).

ACKNOWLEDGMENTS

This work was supported by the Russian Foundation for Basic Research, project no. 00-01-00743.

REFERENCES

1. E. N. Lorenz, J. Atmos. Sci. **20**, 448 (1963).
2. V. M. Evstigneev, T. A. Akimenko, L. S. Evseeva, in *Problems of Hydrology and Hydroecology* (Mosk. Gos. Univ., Moscow, 1999), Vol. 1, pp. 95–140.
3. V. Ya. Sergin and S. Ya. Sergin, *Systems Analysis of Problems of Large Fluctuation in Climate and Earth Glaciation* (Gidrometeoizdat, Leningrad, 1978).
4. G. S. Golitsyn and G. N. Panin, Meteorol. Gidrol., No. 1, 57 (1989).
5. V. I. Naĭdenov and V. I. Shveĭkina, Priroda, No. 5, 19 (1997).
6. L. S. Kuchment and A. N. Gel'fan, *Dynamic and Stochastic Models of River Run-Off Formation* (Nauka, Moscow, 1993).
7. I. G. Zhurbenko and I. A. Kozhevnikova, *Stochastic Simulation of Processes* (Mosk. Gos. Univ., Moscow, 1990).
8. S. M. Pandit and S. M. Wu, Biometrika **62**, 497 (1975).
9. D. Ya. Ratkovich and M. V. Bolgov, Vodn. Resur. **21**, 389 (1994).
10. I. A. Kozhevnikova and V. I. Naĭdenov, Vodn. Resur. **24**, 601 (1998).
11. K. Arne, L. Bengtsson, G. S. Golitsyn, *et al.*, Dokl. Akad. Nauk SSSR **366**, 248 (1999).
12. Elfatih A. B. Eltahir, Water Resour. Res. **32**, 131 (1996).
13. I. G. Zhurbenko and I. A. Kozhevnikova, Probl. Peredachi Inf. **18** (1), 64 (1982).
14. A. N. Kolmogorov, in *Probability Theory and Mathematical Statistics* (Nauka, Moscow, 1986), pp. 458–467.

Translated by V. Bukhanov

Doklady Physics, Vol. 46, No. 5, 2001, pp. 346–348. Translated from Doklady Akademii Nauk, Vol. 378, No. 1, 2001, pp. 58–60.

MECHANICS

Shearing Form of Stability Loss for a Three-Layer Circular Ring under the Action of Uniform External Pressure

V. N. Paĭmushin

Presented by Academician I.F. Obraztsov October 18, 2000

Received November 3, 2000

1. The state-of-the-art in laminated-plate and shell mechanics was covered in review [1]. The current status of the stability theory for three-layer plates and shells was presented in [2]. In [2], the stages of the theory's development and lines of further inquiry were analyzed and a proposal was put forth on the classification of stability-loss forms according to Euler. In the case of three-layer plates and shells under the action of a static load, for different forms of the stressed-strained state in both supporting layers and the filler, we should distinguish the following:

(1) Skew-symmetric (equiphase) and symmetric (antiphase) stability-loss forms. These forms are realized in certain structures for equal values of subcritical forces in supporting layers and zero values of subcritical transverse tangent shear stresses in a filler.

(2) A mixed flexural stability-loss form. This is realized for unequal values of subcritical forces in supporting layers and zero values of subcritical transverse tangent shear stresses in a filler.

(3) A pure shearing stability-loss form. This is realized for zero values of subcritical forces in supporting layers and nonzero values of subcritical transverse tangent shear stresses in a filler.

(4) A flexural-shearing stability-loss form. This is realized in the case of nonzero subcritical tangential stresses in supporting layers and transverse shear stresses in a filler.

(5) A shearing stability-loss form in tangential directions. This is realized for low values of the shear modulus of a supporting-layer material in the tangential plane under conditions of pure shear.

(6) An arbitrary stability-loss form. This is a combination of the above forms for a subcritical stressed-strained state of an arbitrary form.

2. We consider a circular three-layer ring with a symmetric structure along the thickness, which is under the action of a uniform external pressure p. Let $2t$ and $2h$ be the thicknesses of the supporting layers and the filler, respectively; R be the radius of the filler middle surface; θ be the circumferential coordinate; E_3 be the filler elastic modulus in the thickness direction; and G be the filler transverse-shear modulus.

Using the results of [3, 4], we can represent the linearized equations for investigating all possible forms of the ring stability loss (ignoring variations of the metric along the filler thickness) in the following form:

$$f^2_{(k)} = \frac{dT^{(k)}}{d\theta} + N^{(k)} + \delta_{(k)}qR = 0, \quad \delta_{(1)} = -\delta_{(2)} = 1,$$
$$f^{(3)}_{(k)} = \frac{dN^{(k)}}{d\theta} - T^{(k)} + \frac{\delta_{(k)}RE_3}{2h}(w^{(2)} - w^{(1)}) = 0,$$
$$k = 1, 2, \tag{1}$$
$$v^{(1)} - v^{(2)} - (t+h)(\omega^{(1)} + \omega^{(2)})$$
$$+ \frac{2h}{G}q - \frac{2h^3}{3E_3R^2}\frac{d^2q}{d\theta^2} = 0.$$

Here, $v^{(k)}$, $w^{(k)}$ are the circumferential displacements and deflections of the middle surfaces for the upper ($k = 1$) and lower ($k = 2$) supporting layers; q are the transverse shear stresses in the filler, which are permanent along its thickness; and $T^{(k)}$, $N^{(k)}$, and $\omega^{(k)}$ are the axial thrusts, the generalized cutting forces, and the turns in the supporting layers, respectively. The latter quantities are expressed by the following formulas:

$$N^{(k)} = \frac{1}{R}\left[\frac{dM^{(k)}}{d\theta} + RT_0^{(k)}\omega^{(k)} + (t+h)Rq\right],$$
$$T^{(k)} = \frac{B}{R}\left(\frac{dv^{(k)}}{d\theta} + w^{(k)}\right), \quad \omega^{(k)} = \frac{1}{R}\left(\frac{dw^{(k)}}{d\theta} - v^{(k)}\right). \tag{2}$$

Here, B is the tension–compression stiffness of the supporting layer; and $M^{(k)}$ is the bending moment related to $v^{(k)}$ and $w^{(k)}$ by the following relation (D is the flexural stiffness of the supporting layer):

$$M^{(k)} = -\frac{D}{R}\frac{d\omega^{(k)}}{d\theta}. \tag{3}$$

Research Technological Center for Problems of Dynamics and Strength, Tupolev State Technological University, ul. Karla Marksa 10, Kazan, 420015 Tatarstan, Russia

1028-3358/01/4605-0346$21.00

The subcritical axial thrusts $T_0^{(k)}$ in the supporting layers involved in (2) can be represented in the form

$$T_0^{(k)} = T_c^0 + \delta_{(k)} T_0^a. \tag{4}$$

In particular, for p = const (uniform external pressure), it is easy to show that

$$T_0^{(1)} = -\frac{\chi}{1+2\chi} pR, \quad T_0^{(2)} = -\frac{1+\chi}{1+2\chi} pR, \tag{5}$$

$$T_c^0 = -\frac{pR}{2}, \quad T_a^0 = \frac{pR}{2(1+2\chi)}. \tag{6}$$

Here, $\chi = \dfrac{E_3 R^2}{2Bh}$ is the dimensionless defining parameter of the filler transverse squeezing.

The classical solution to the formulated problem of finding the critical external pressure p_{cr} can be found by representing the unknown functions $v^{(k)}$, $w^{(k)}$, and q in the form

$$\{w^{(k)}, v^{(k)}, q\}^{\mathrm{T}} = \{W^{(k)}, V^{(k)}, Q\}\{\sin n\theta, \cos n\theta, \cos n\theta\}^{\mathrm{T}}, \tag{7}$$

where $n = 1, 2, \ldots$ is the number of stability-loss half-waves.

Substituting (7) into (1) and using Eqs. (2), (3), and (5), we obtain a system of homogeneous equations in $V^{(k)}$, $W^{(k)}$, and Q. The critical value p_{cr} can be found from the condition that the solutions to this system are nontrivial [4]:

$$p_{cr} = \frac{D}{R^3} m_{cr}. \tag{8}$$

Here, $m_{cr} > 1$ is the dimensionless parameter of the critical load whose least value is determined by minimizing the expression for m_{cr} with respect to n.

It is worth noting that by virtue of $T_0^{(1)} \neq T_0^{(2)}$ in the case of low values of χ, we deal with a mixed flexural stability-loss form ($w^{(1)} \neq w^{(2)}$) with $n \neq 2$. When increasing χ, this form passes to the classic equiphase flexural form ($w^{(1)} \approx w^{(2)}$) with $n = 2$.

3. We now demonstrate that the above-described solution to the problem under consideration is not unique and the value of the critical pressure found from (8) need not be minimum. To this end, using Eqs. (1)–(4), we construct a homogeneous system of stability equations assuming that undulation in the coordinate θ is impossible, i.e., assuming that $\dfrac{dv^{(k)}}{d\theta} = \dfrac{dw^{(k)}}{d\theta} = \dfrac{dq}{d\theta} = 0$:

$$\begin{aligned}
f^2_{(1)} &= q + \frac{T_c^0 + T_a^0}{R}\omega^{(1)} + \frac{t+h}{R} q = 0,\\
f^2_{(2)} &= -q + \frac{T_c^0 - T_a^0}{R}\omega^{(2)} + \frac{t+h}{R} q = 0,\\
f^3_{(1)} &= \frac{B}{R^2} w^{(1)} + \frac{E_3}{2h}(w^{(1)} - w^{(2)}) = 0,\\
f^3_{(2)} &= \frac{B}{R^2} w^{(2)} - \frac{E_3}{2h}(w^{(1)} - w^{(2)}) = 0,\\
v^{(1)} - v^{(2)} &- (h+t)(\omega^{(1)} + \omega^{(2)}) + \frac{2hq}{G} = 0.
\end{aligned} \tag{9}$$

Here, we accept that $\omega^{(k)} = -\dfrac{v^{(k)}}{R}$.

In what follows, instead of the desired unknowns $v^{(k)}$ and $w^{(k)}$, it is convenient to introduce new unknowns according to the following representations:

$$\begin{aligned}
v_c &= v^{(1)} + v^{(2)}, \quad v_a = v^{(1)} - v^{(2)},\\
w_c &= w^{(1)} + w^{(2)}, \quad w_a = w^{(1)} - w^{(2)}.
\end{aligned} \tag{10}$$

After constructing the combinations

$$f_c^i = f^i_{(1)} + f^i_{(2)} = 0, \quad f_a^i = f^i_{(1)} - f^i_{(2)} = 0, \quad i = 2, 3,$$

the system of equations (9) can be rewritten in terms of the new unknowns as

$$f_c^3 = \frac{Bw_c}{R^2} = 0, \quad f_a^3 = \left(\frac{B}{R^2} + \frac{E^3}{h}\right) w_a = 0, \tag{11}$$

$$\begin{aligned}
f_c^2 &= T_c^0 \omega_c + T_a^0 \omega_a + 2(t+h)q = 0,\\
f_a^2 &= T_c^0 \omega_a + T_a^0 \omega_c + 2Rq = 0,\\
&-R\omega_a - (h+t)\omega_c + \frac{2hq}{G} = 0,
\end{aligned} \tag{12}$$

where $\omega_a = -\dfrac{v_a}{R}$, $\omega_c = -\dfrac{v_c}{R}$.

We connect subcritical forces T_c^0, T_a^0 entering into (12) by the relation

$$T_a^0 = -cT_c^0, \tag{13}$$

where, according to condition (6), the following formula holds for c:

$$c = \frac{1}{1+2\chi}. \tag{14}$$

Substituting relation (13) into Eqs. (12) and allowing for the condition of the nontrivial nature of the solutions to these equations for T_c^0, we arrive at the expression

$$T_c^0 = -\frac{[R^2 + 2cR(t+h) + (t+h)^2]G}{h(1-c^2)}. \qquad (15)$$

Furthermore, combining (15) with the first formula of (6), we can determine the critical external pressure p_{cr}, namely,

$$p_{cr} = \frac{2G[R^2 + 2cR(t+h) + (t+h)^2]}{Rh(1-c^2)}. \qquad (16)$$

The stability can be lost by the form under consideration even earlier than by the mixed flexural one if the following inequality is fulfilled:

$$\frac{2G[R^2 + 2cR(t+h) + (t+h)^2]}{Rh(1-c^2)} < \frac{D}{R^2}m_{cr}. \qquad (17)$$

When designing three-layer structures, this inequality is one of the constraints in choosing the value of the filler's transverse-shear modulus.

4. The analysis of the results obtained makes it possible to formulate the following fundamentally important conclusions.

The quantity T_c^0 is the critical load for the stability loss. As follows from formula (16), this load is physically realized only in the case of external pressure.

In accordance with the classification compiled in [1, 2], the form of stability loss under investigation in a filler is a shearing loss. It is realized without appearance of deflections in the supporting layers. This is evident from trivial solutions $w_c \equiv 0$, $w_a \equiv 0$, $w^{(1)} \equiv 0$, and $w^{(2)} \equiv 0$, which follow from (11).

The found form of shearing stability loss in the filler can occur in structures not only at nonzero values of subcritical transverse tangent shear stresses in the filler but also in the case when they are absent in the subcritical state provided that $T_c^0 > 0$. This conclusion is an extremely important addition to the results of [4], which were listed in Section 1, and significantly extends our insight into the mechanisms of stability loss for three-layer structures.

In studying the revealed form of shearing stability-loss in fillers, introduction of simplifications of the shallow-shell theory into the stability equations for three-layer structures is inadmissible.

In three-layer structures, the form of the shearing stability-loss in a filler is realized mainly through mutual tangential displacements of supporting layers without their bending.

To prevent the stability loss of three-layer structures in accordance with the forms discussed above, the corresponding conditions for the fixation of supporting layers in their contour must be provided.

ACKNOWLEDGMENTS

This study was supported by the Russian Foundation for Basic Research, project no. 00-01-00106a.

REFERENCES

1. A. K. Norr, W. S. Burton, and Ch. W. Bert, Appl. Mech. Rev. **49** (3), 155 (1996).
2. V. N. Paĭmushin, Mekh. Kompoz. Mater. **35**, 707 (1999).
3. V. N. Paĭmushin and S. N. Bobrov, Mekh. Kompoz. Mater. **36**, 95 (2000).
4. V. N. Paĭmushin, V. A. Ivanov, S. N. Bobrov, and T. V. Polyakova, Mekh. Kompoz. Mater. **36**, 317 (2000).

Translated by V. Tsarev

Doklady Physics, Vol. 46, No. 5, 2001, pp. 349–351. Translated from Doklady Akademii Nauk, Vol. 378, No. 2, 2001, pp. 187–189.

MECHANICS

Dissolution of a Drop with a High Content of a Surface-Active Substance

K. G. Kostarev and V. A. Briskman

Presented by Academician G.G. Chernyĭ December 22, 2000

Received December 22, 2000

Molecular mass–heat exchange between drops and their surrounding medium may be accompanied by macroscopic effects; these effects make this process a subject of continuum mechanics. As an example, we refer to the emergence of oscillations or the translational motion of such drops due to the instability of their equilibrium positions [1–3]. We discovered new effects pertaining to this type of phenomena in studying the dissolution of a drop of a binary mixture with a high content of a surface-active substance (SAS).

1. SPHERICAL DROP

In our experiment, a drop of a chlorobenzene–isopropyl alcohol mixture was put in a water solution of sodium chloride with a vertical density gradient. The gradient value was chosen so as to suspend the drop in the salt solution, thus decreasing the vertical motions of the drop in the process of dissolution. The initial concentration C_0 of alcohol in chlorobenzene was varied from 10 to 45%; the drop diameter, in the range 3–10 mm. Only one component of the drop, namely alcohol, was soluble in our experiment. This component served as a surface-active substance not only for the second component, chlorobenzene, but also for the surrounding liquid. All working liquids were opaque. To visualize and record the flow structure, we employed a horizontal "light knife" and a video camera. For a tracer, we used the white-colored opaque emulsions that appeared at the drop boundary due to the mutual trapping of water and chlorobenzene during alcohol dissolution.

It is convenient to subdivide the dissolution of a drop with a sufficiently high initial SAS concentration into several stages. Owing to the surface instability caused by capillary effects [4–7], the SAS dissolution initially occurred as an ejection of concentration jets of, on average, equal intensity. At each instant of time, these jets were randomly redistributed over the drop surface. As the alcohol content decreased, the number of jets diminished and their unsteady redistribution over the surface caused the drop to swing with an amplitude equal to 0.1–0.2 of the drop diameter, by analogy with the well-known effect of a "jumping drop" [1, 2]. Swinging was accompanied by the formation of an unsteady stream inside the drop in the form of two or more cells. Later on, this regime changed to the steady-state regime, and, finally, the motion of the drop, as a whole, and the visible streams in the interior of the drop ceased.

However, the achieved mechanical equilibrium was not the final stage of dissolution when the initial SAS concentration was in excess of 20%. Suddenly, a large-scale motion reappeared inside the drop and further developed in accordance with one of the two scenarios. In the first case, the convective motion inside a stagnant drop manifested itself in the symmetric rise of the liquid from the lower part of the drop along its axis in the form of a rotating torus. Such an impulsive rise of the liquid could occur repeatedly, for example, 5–6 times, when $C_0 = 35\%$.

In the second, less frequent variant, a one-cellular stream developed in the drop in the form of a rise of the liquid along one side of the drop and a sink along the other. Presumably, the type of motion changed as a result of an accidental emergence of asymmetric (e.g., thermal) conditions on the drop surface. It could be conceived that the drop was upset like a top upon completing its rotation. The upset was accompanied by the intense ejection of the SAS from the floating-up stream into the surrounding medium, which was clearly indicated by the formation of concentration "swirls." The drop itself began to perform a translation, and its displacement reached 3–5 drop diameters in a time of about 10 s.

2. CYLINDRICAL DROP

Drops of spherical shape cannot be used for precise observations and measurements. For this reason, in order to elucidate the cause of the unusual behavior of drops, we studied the dissolution of a stagnant drop in the form of a short horizontal cylinder ("tablet") with a

Institute of Mechanics of Continua, Ural Division, Russian Academy of Sciences, ul. Akademika Koroleva 1, Perm, 614061 Russia

1028-3358/01/4605-0349$21.00

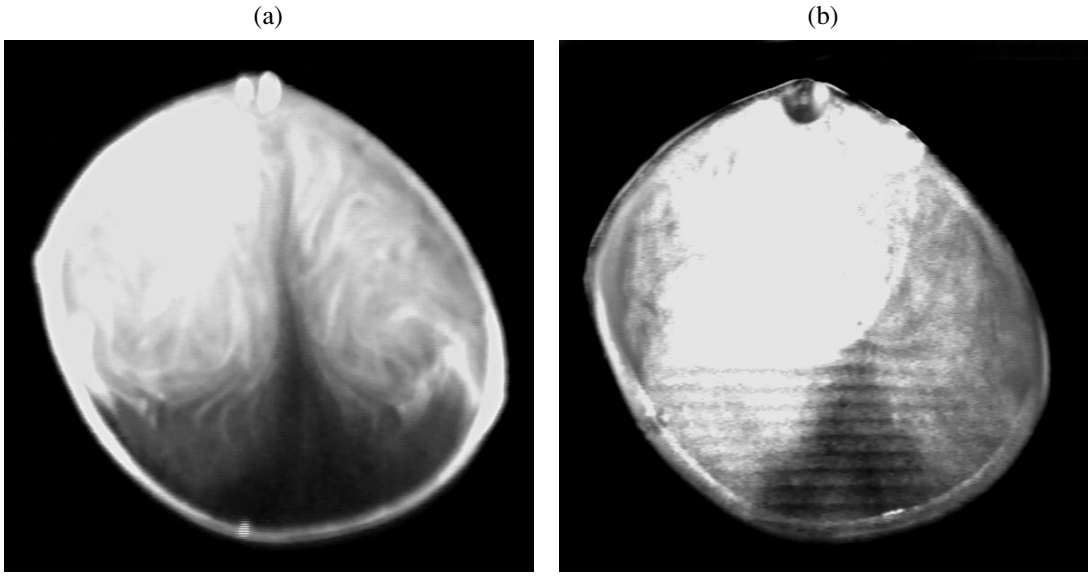

Fig. 1. The structure of the stream and concentration field in the cylindrical drop during its dissolution (D = 9 mm, C_0 = 35%). (a) Two-cellular stream visualized by a white-colored emulsion in reflected light; the time t elapsed from the onset of dissolution is 2 min; (b) field concentration in transparent monochromatic light (a transition from one interference band to the other corresponds to a change in the alcohol concentration by 0.10%); t = 4.5 min.

free side surface, the faces of which were clamped between two vertical glass plates. The gap between the plates (~1 mm), filled with distilled water, was used as a Fizeau interferometric cell, which enabled us to record, face-on, the structure of the concentration fields simultaneously with the visualization of the streams. The drop diameter was varied from 5 to 15 mm.

As the cylindrical drop dissolved we initially observed, as with the spherical drop dissolved, an intense small-scale motion near the interface. Then, a large-scale plane stream appeared inside the drop in the form of two symmetric cells. This stream was produced by the motion of the SAS-depleted mixture along the side boundaries (Fig. 1a). In parallel with the evolution of the stream, a stable, nearly linear distribution of density of the binary mixture with a downward-directed vertical (positive) gradient formed throughout the drop. As the mean alcohol concentration decreased, the intensity of the large-scale stream declined and the stream was expelled into the upper part of the drop. The stream in the lower part became slow (creeping), representing the rise of the bulk of the liquid as a whole.

As a result, two zones with different characteristic mass-transfer rates were developed inside the drop: the upper convective zone and the lower quasi-diffusive (stagnant) zone. Correspondingly, the distribution of the isopropyl alcohol concentration changed, retaining, however, its linear appearance in the stagnant zone (Fig. 1b) and becoming homogeneous in the upper part of the drop due to the convective mixing. The mean alcohol content in the convective region decreased at a higher rate, making this region heavier than the underlying zone, i.e., changing the sign of the density gradient to negative. This unstable stratification of the mixture was maintained by the creeping stream until the onset of the crisis of large-scale motion in the upper part of the drop and the breakup of this motion into isolated streams of a depleted mixture sinking through the drop body took place. When heavy streams reached the upper boundary of the stagnant zone, the negative density gradient increased, resulting in the loss of stability of the equilibrium state. The vertical distribution of alcohol concentration at this instant of time is shown in Fig. 2. (The alcohol-concentration and mixture-density gradients are directed opposite to one another; the

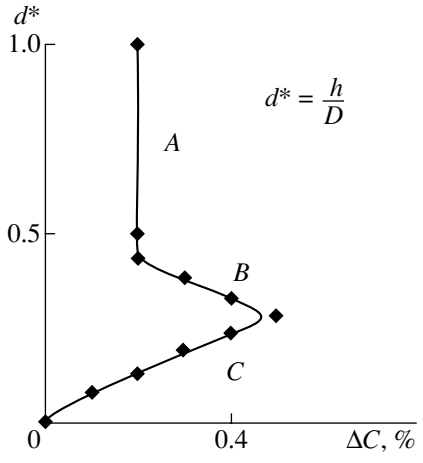

Fig. 2. Distribution of the alcohol concentration over the height of the cylindrical drop at the instant corresponding to the loss of stability and the repeated development of convective motion (D = 9 mm, C_0 = 35%, t = 5 min).

unstable stratification of density corresponds to segment "*B*.")

After the loss of stability, the light portion of the mixture began to float up along the side surface. However, the buoyant liquid lost the SAS rapidly, which led to the generation of an inverse stream and to the formation of a cell similar to the torus in the three-dimensional case. Consequently, the prerequisites arose for the repeated cycle. Note that, at the instant of the onset of repeated motion, both the concentration gradient and the mean concentration (~1%) are small compared to the initial concentration.

Thus, we experimentally studied the streams and concentration fields that are formed in the process of dissolution of spherical and cylindrical drops in an SAS-containing binary mixture due to the interaction of the concentration–capillary and gravitational convection mechanisms. We discovered and explored a new phenomenon, the reappearance of large-scale motion at the ultimate quasi-diffusive stage of dissolution. The reason for this is the loss of stability in the density distribution, which is formed by initial convective streams. Because the intensity of such flows is determined by the initial concentration of the dissolving component, the effect revealed by us has a threshold character and can be observed only at a sufficiently high SAS content.

The authors are grateful to Academician G.G. Chernyi for useful discussions.

This study was supported by the Russian Foundation for Basic Research, project no. 00-01-00614, and by the INTAS–ESA, grant no. 99-01505.

REFERENCES

1. J. B. Lewis and H. R. C. Pratt, Nature **171**, 1155 (1953).
2. Yu. K. Bratukhin and S. O. Makarov, *Interphase Convection* (Perms. Gos. Univ., Perm, 1994).
3. Yu. P. Gupalo, A. D. Polyanin, and Yu. S. Ryazantsev, *Mass Heat Exchange of Reacting Particles with Stream* (Nauka, Moscow, 1985).
4. Yu. K. Bratukhin and S. O. Makarov, Izv. Akad. Nauk, Mekh. Zhidk. Gaza, No. 4, 43 (1996).
5. Yu. K. Bratukhin and S. O. Makarov, Fluid Dyn. (USSR) **31**, 371 (1996).
6. Yu. K. Bratukhin and S. O. Makarov, Fluid Dyn. (USSR) **31**, 515 (1996).
7. Yu. K. Bratukhin and G. Z. Gershuni, Microgravity Q. **4** (3), 183 (1994).

Translated by A. Kozlenkov

Doklady Physics, Vol. 46, No. 5, 2001, pp. 352–355. Translated from Doklady Akademii Nauk, Vol. 378, No. 2, 2001, pp. 190–193.

MECHANICS

On the Existence and the Uniqueness of Solutions to Differential Equations Describing the Motion of Mechanical Systems with Dry Friction

I. V. Matrosov

Presented by Academician V.V. Rumyantsev November 24, 2000

Received November 28, 2000

The Lagrange equations of motion are written for a mechanical system consisting of kinematic dry-friction pairs. These equations are not solved for higher derivatives and constraint forces. The definition of a solution to them is given. Theorems on the uniqueness and existence of such a solution are formulated under certain sufficiently general additional assumptions. The results obtained develop and complement the mechanical theory of systems with dry friction [1–6].

1. The equations of motion are derived by the method of elimination of constraints, which is described in papers [7, 8]. According to this method, an initial system with constraints is changed for another system in which frictional constraints are replaced by reaction forces $N_1, \ldots,$ and N_m and friction forces. To describe the position of such a system, additional coordinates $q_{n+1}, \ldots, q_{n+m}$ are introduced along with the initial coordinates $q_1, \ldots, q_n$.

For the extended system under consideration, which is free of frictional constraints, an expression for kinetic energy **T** and the Lagrange equations of motion can be immediately determined. The kinetic energy **T** is assumed to be the quadratic form with respect to $\dot{q}$:

$$\mathbf{T} = \sum_{i,j=1}^{m+n} a_{ij}(q)\dot{q}_i\dot{q}_j + \sum_{i=1}^{n+m} b_i(q)\dot{q}_i + c(q);$$

its coefficients are continuously differentiable. As is shown in paper [8], the work of reaction forces, which is spent for virtual displacements along the lines of each coordinate q_i ($i = 1, \ldots, n+m$), represents a function of the form $Q_N^i(q, \dot{q}, N) = (\nu_N^i(q, \dot{q}), N)$. It is continuous with respect to q and $\dot{q}$, linear in N, and contains a vector ν_N^i, which is continuous with respect to q and $\dot{q}$. The external forces $Q_A^k(q, \dot{q})$ ($k = 1, \ldots, n+m$) are also assumed to be continuous. In this notation, the complete system of equations of motion has the form

$$\frac{d}{dt}\frac{\partial \mathbf{T}}{\partial \dot{q}_k} - \frac{\partial \mathbf{T}}{\partial q_k} = Q_A^k(q, \dot{q}) + (\nu_N^k(q, \dot{q}), N) + Q_T^k(q, \dot{q}, N), \quad k = 1, \ldots, n, \tag{1}$$

$$\frac{d}{dt}\frac{\partial \mathbf{T}}{\partial \dot{q}_l} - \frac{\partial \mathbf{T}}{\partial q_l} = Q_A^l(q, \dot{q}) + (\nu_N^l(q, \dot{q}), N) + Q_T^l(q, \dot{q}, N), \quad l = n+1, \ldots, n+m, \tag{2}$$

$$q_l = S_l(q_1, \ldots, q_n), \quad l = n+1, \ldots, n+m. \tag{3}$$

Here, the steady-state equations (3) which describe the constraints close the incomplete system of $n + m$ Lagrange equations (1), (2) in $n + m + m$ unknowns $q_1, \ldots, q_{n+m}; N_1, \ldots, N_m$.

The system presented differs from the known algebraic-differential systems in the absence of variables $N_1, \ldots, N_m$ in Eqs. (3).

According to Coulomb's law, the generalized friction forces Q_T^k are taken to be

$$Q_T^k = \sum_{i=1}^{J} f_i^k(q, \dot{q})\|N\|_i T_i^k(q, \dot{q}) + f_{J+1}^k(q, \dot{q})T_{J+1}^k(q, \dot{q}), \quad k = 1, \ldots, n+m$$

in the regions of their continuity (at nonzero velocities $\dot{q}_k$), where $f_i^k \in C(q, \dot{q})$ are the friction coefficients, $\|N\|_i = \sqrt{N_{s_i}^2 + \ldots + N_{s_i+p_i}^2}$ is the Euclidean norm of the corresponding reaction-force vector, $T_i(q, \dot{q}) \in C(U \setminus \mathcal{S})$ are piecewise continuous functions, and $\mathcal{S}$ represents the union of discontinuity surfaces of all T_i. Most widely used is the function $T_i(\dot{q}) = \dfrac{\dot{q}^*}{\|\dot{q}^*\|}$, where $\dot{q}^*$ are the components of the vector $\dot{q}$ that determine

Center of Investigation of Stability and Nonlinear Dynamics, Blagonravov Institute of Engineering Science, Russian Academy of Sciences, ul. Dmitriya Ul'yanova 5, Moscow, 117333 Russia

1028-3358/01/4605-0352$21.00 © 2001 MAIK "Nauka/Interperiodica"

velocity at a contact point. Use of other functions T_i, which can be taken, for example, from papers [1, 8, 9], is also possible.

Using (3), we eliminate the variables $q_{n+1}, \ldots, q_{n+m}$ in Eqs. (1) and (2) and obtain

$$\sum_{i=1}^{n}\left(a_{ki} + \sum_{j=n+1}^{n+m} a_{kj}\frac{\partial S_j}{\partial q_i}\right)\ddot{q}_i - (\nu_N^k(q, \dot{q}), N) - \sum_{i=1}^{J} f_i^k \|N\|_i T_i^k = F^k(q, \dot{q}), \quad k = 1, \ldots, n+m. \tag{4}$$

The left-hand sides of these equations are linear in $\ddot{q}$, while their right-hand sides are piecewise continuous with respect to their arguments and independent of $\ddot{q}$ and N.

System (4) consists of $n + m$ second-order differential equations in $n + m$ unknowns q_k ($k = 1, \ldots, n$) and N_i ($i = 1, \ldots, m$). These equations are not solved for $\ddot{q}$ and do not contain derivatives of N, while the reaction forces N themselves enter nonlinearly into them and have discontinuous coefficients.

2. We assume that $N(t)$ is a given function. By replacing $\ddot{q}$ with p in Eqs. (4) and substituting the function $N(t)$ in these equations, we construct the many-valued function

$$M_{(4)}(q, \dot{q}, N(t)) = \left\{ p \in R^n \left| \sum_{i=1}^{n}\left(a_{ki} + \sum_{j=n+1}^{n+m} a_{kj}\frac{\partial S_j}{\partial q_i}\right)p_i - (\nu_N^k(q, \dot{q}), N(t)) - \sum_{i=1}^{J} f_i^k \|N(t)\|_i T_i^k = F^k(q, \dot{q}), \quad k = 1, \ldots, n+m \right. \right\}.$$

Here, the set $M_{(4)}(q, \dot{q}, N(t))$ is formed by the values of $\ddot{q}$ satisfying system (4) at given q, $\dot{q}$, $N(t)$, and $N(t)$.

Remark 1. The set $M_{(4)}(q, \dot{q}, N(t))$ is defined by $n + m$ equations with n unknowns p_i. Therefore, this set is not empty only for certain functions $N(t)$ called admissible.

Definition 1. The pair $q(t)$: $R \longrightarrow R^n$, $N(t)$: $R \longrightarrow R^m$ is called a solution to system (4) under the following conditions:

(1) The function $\dot{q}(t)$ is absolutely continuous with respect to t and, consequently, has the measurable derivative $\ddot{q}(t)$.

(2) The many-valued function $N(t)$ is everywhere β-continuous with respect to t (has a closed graph); it is single-valued if t is such that $q(t)$ and $\dot{q}(t)$ do not belong to the discontinuity surfaces $\mathcal{S}$ of the functions $T_i^k(q, \dot{q})$.

(3) The generalized differential equation

$$\ddot{q}(t) \in \mathrm{co}\{\overline{M_{(4)}(q, \dot{q}, N(t))}\}$$

is satisfied, where, similarly to paper [10], co{·} and an over-bar mean take the convex hull and closure of a function graph in the space $\{q, \dot{q}, p\}$, respectively.

3. The unit sphere $S_1^{p_j}$ of the dimensionality p_j is considered for each reaction-force vector having the number $j = 1, \ldots, J$. It is assumed that the vector $e_j \in S_1^{p_j}$ and the vector $e = (e_1, \ldots, e_j) \in R^m$ are formed by coordinates of the vectors e_j. Outside the set $\mathcal{S}$, the norms $\|\cdot\|_j$ occurring in system (4) are replaced by the scalar products $(e_j, \cdot)$. A matrix of the derived system that is linear in $(\ddot{q}, N)$ is denoted by A_e^*.

We denote by $A_e(q, \dot{q})$ a set of matrices which are limiting matrices for $A_e^*(q^i, \dot{q}^i)$ at $q^i \longrightarrow q$, $\dot{q}^i \longrightarrow \dot{q}$ ($i \longrightarrow \infty$, $q^i \in U$). If, in addition, q and $\dot{q}$ are such that $\|A_e^{*-1}(q, \dot{q})''F(q, \dot{q})\|_{j^*} = 0$ for a certain j^*, we consider that $A_e(q, \dot{q}) = \bigcup_{e_{j^*} \in S_1^{p_{j^*}}} A_{e_1, \ldots, e_{j^*}, \ldots, e_j}$ at this point. Here, the expression $A_e^{*-1}(q, \dot{q})''$ represents the last m rows of the matrix A_e^{*-1}.

We also introduce the set of matrices that ensure the linearization of system (4) in $\ddot{q}$ and N at the point q, $\dot{q}$ for all possible vectors e of the form considered here:

$$\mathcal{A} = \{A_e: e_1 \in S_1^{p_1}, \ldots, e_J \in S_1^{p_J}\}.$$

Here, elements of the matrices $A \in \mathcal{A}$ can be discontinuous only in $\mathcal{S}$.

Theorem 1 (on the existence of the solution). *Let, at any point q, $\dot{q}$ in the region U, the following conditions be satisfied*:

(i) $\exists c > 0$ *is such that for any compact set* $K \in U$, $K \cap \mathcal{S} = \emptyset$, $\forall A_e \in \mathcal{A}$, $\forall A \in A_e$ $|\det A_e| \geq c$ *and the func-*

tion $A^{-1}(q, \dot{q})F(q, \dot{q})$ satisfies the Lipschitz condition with respect to q, $\dot{q}$ in K.

(ii) *The condition*

$$(A_*^{-1}(q, \dot{q})''(A_{**}^{-1}(q, \dot{q})'')^T e_j^0, e_j^0) > 0 \qquad (5)$$

is satisfied for $\forall A_e(q, \dot{q}) \in \mathcal{A}$ $\forall e_j^0$: $(e_j^0, e_j) = 0$, $\forall A_*$, $A_{**} \in A_e$. (By definition, in the set $\mathcal{S}$, A_e is the closure of the limiting matrix set corresponding to $q_k \longrightarrow q$ and $\dot{q}_k \longrightarrow \dot{q}$.)

Then, for $\forall t_0$, $\forall q_0$, $\dot{q}_0 \in U$, for which $\exists N_0$ is such that if $N(t_0) = N_0$, then the set $M_{(4)}(q_0, \dot{q}_0, N_0)|_{t=t_0} \neq \emptyset$, there is a solution to system (4) *in the sense of Definition* 1. *It exists in the region U and is such that $q(t_0) = q_0$, $\dot{q}(t_0) = \dot{q}_0$, and $N(t_0) = N_0$.*

For the right- and left-hand sides of the differential equation (4), condition (ii) of Theorem 1 is difficult to verify. The proposition formulated below gives the sufficient condition for item (ii) of Theorem 1, which is simple and often applicable.

Proposition 1. *Let, for any compact set $K \in U$, $\exists c > 0$: $\forall A_e \in \mathcal{A}$ and the condition $|\det A| \geq c > 0$ be satisfied for any matrix A belonging to closure of the convex hull $\mathrm{co}\{\bar{A}_e^{-1}\}$ of the set of limiting matrices.*

Then, condition (5) *of Theorem* 1 *is satisfied.*

To prove Theorem 1, the author has presented a rule making possible a construction of the approximate solution and development of the corresponding numerical algorithm.

4. We assume that there are both the initial conditions $q(0) = q_0$, $\dot{q}(0) = \dot{q}_0$ and a certain region U, which contains $(q_0, \dot{q}_0)$ and needs to be used for investigation of the properties of the solution.

The vector $N_0 \in R^m$ that describes the initial reactions at the point q_0, $\dot{q}_0$ is called admissible for system (4) if the set $M_{(4)}(q_0, \dot{q}_0, N_0) \neq \emptyset$ for this N_0.

Proposition 2. *Let the conditions of Theorem* 1 *and Proposition* 1 *be satisfied. Then, only a finite number of the admissible reaction-force vectors N_i corresponding to system* (4) *exists at each point q, $\dot{q} \in U \backslash \mathcal{S}$.*

The proposition formulated below gives the sufficient uniqueness conditions for reaction forces arising in the system.

Proposition 3. *Let the conditions of Theorem* 1 *and Proposition* 1 *be satisfied throughout the space R^{2n}. Then, the unique admissible vector N_0 exists for each q_0, $\dot{q}_0 \in R^{2n} \backslash \mathcal{S}$.*

Definition 2. The solution to system (4) is termed right-hand single-valued in the region U if any two solutions to system (4), q_1, N_1 and q_2, N_2, which have the identical initial conditions $q_1(t_0) = q_2(t_0)$, $\dot{q}_1(t_0) = \dot{q}_2(t_0)$, and $N_1(t_0) = N_2(t_0)$, coincide at $t > t_0$ belonging to a domain of their definition.

The right-hand Lipschitz condition represents the main tool for investigating the right-hand uniqueness. The vector-function G satisfies the right-hand Lipschitz condition in the region U if $\exists \mathcal{S}^*$ with $\mu(\mathcal{S}^*) = 0$: $\exists L > 0$: $\forall x, y \in U \backslash \mathcal{S}^*$:

$$(x - y, G(x) - G(y)) \leq L\|x - y\|^2, \qquad (6)$$

where $\mu(\cdot)$ is the Lebesgue measure in U.

Remark 2. Piecewise continuous functions of the form $T_* = -\dfrac{\dot{q}}{\|\dot{q}\| + |w|}\dot{q} \in R^n$ satisfy condition (6) in $\dot{q}$.

For a solution to system (4), the theorem formulated below represents the sufficient conditions of the right-hand uniqueness in the sense of Definition 2. These conditions are applicable, for example, for systems where constraint forces are independent of friction or the work of the reaction forces is equal to zero for the possible displacements along $q_1, \ldots, q_n$.

Theorem 2. *Let, along with the realization of the conditions of Theorem* 1 *and Proposition* 1 *for system* (4), *the following conditions be satisfied*:

(i) *All functions $\|N(q, \dot{q})\|_i T_i(q, \dot{q})$ and F_i satisfy the right-hand Lipschitz condition in the region U; the friction coefficients f_i are positive and satisfy the Lipschitz condition.*

(ii) *The matrix*

$$E = \left[\left(a_{ki} + \sum_{j=n+1}^{n+m} a_{kj}\frac{\partial S_j}{\partial q_i}\right)\right]_{i=1,\ldots,n;\ k=1,\ldots,n}$$

is continuously differentiable in U, self-conjugate (*symmetric*), *and positive-definite with $|\det E| \geq c > 0$.*

(iii) *Each function $((\nu_N^k(q, \dot{q}), N(q, \dot{q}))$ $(k = 1, \ldots, n)$ satisfies the Lipschitz condition with respect to the variables q, $\dot{q} \in U$ [for normal reactions $(\nu_N^k(q, \dot{q})$, $N(q, \dot{q}) = 0$].*

Then, for any initial condition q_0, $\dot{q}_0 \in U$ and each admissible reaction-force vector N_0, a solution to system (4) *that satisfies these initial conditions is right-hand single-valued in the region U in the sense of Definition 2.*

Remark 3. If $\dfrac{\partial S_j}{\partial q_i} = 0$, then E is the matrix of kinetic energy, which is assumed to be symmetric and positive-definite.

Application of the theorems discussed here is illustrated in my papers [11], where, along with other examples, those proposed by P. Painlevé concerning a body

fixed in its center of mass in a ball-and-socket joint with friction are considered.

ACKNOWLEDGMENTS

This work was supported by the Russian Foundation for Basic Research, project no. 00-01-00293.

REFERENCES

1. P. Painlevé, *Cours de mécanique professé a l'Ecole polytechnique* (Gauthier-Villars, Paris, 1970; Gostekhizdat, Moscow, 1954).
2. N. G. Chetaev, Prikl. Mat. Mekh. **24**, 35 (1960).
3. V. V. Rumyantsev, Prikl. Mat. Mekh. **25**, 969 (1961).
4. N. A. Fufaev, Izv. Akad. Nauk SSSR, Mekh. Tverd. Tela, No. 4, 48 (1991).
5. Le Xuan Anh, Prikl. Mat. Mekh. **45**, 520 (1990).
6. V. M. Matrosov and I. A. Finogenko, Dokl. Akad. Nauk **336**, 57 (1994) [Phys. Dokl. **39**, 384 (1994)].
7. P. Appell, *Traité de mécanique rationnelle* (Gauthier-Villars, Paris, 1950; Fizmatgiz, Moscow, 1960), Vols. 1, 2.
8. A. I. Lur'e, *Analytical Mechanics* (Fizmatgiz, Moscow, 1961).
9. V. F. Zhuravlev, Prikl. Mat. Mekh. **62**, 762 (1998).
10. A. F. Filippov, *Differential Equations with Discontinuous Right Part* (Nauka, Moscow, 1985).
11. I. V. Matrosov, Diff. Uravn., No. 3/4 (2001) (in press).

Translated by Yu. Verevochkin

Doklady Physics, Vol. 46, No. 5, 2001, pp. 356–358. Translated from Doklady Akademii Nauk, Vol. 378, No. 2, 2001, pp. 194–196.

MECHANICS

Uniqueness of the Solution to the Stability Problem for a Material with Nonlinear Heterogeneous Elasticity

A. I. Oleĭnikov* and E. V. Mogil'nikov**

Presented by Academician V.P. Myasnikov December 6, 2000

Received December 7, 2000

In contrast to the classical case, in the case of physically nonlinear elastic media, the uniqueness theorem usually only states uniqueness in the small. In this paper, we present the conditions of stability and uniqueness in the small and in the large for the model of a heterogeneously elastic material (with a nonuniform elastic modulus) [1–4].

This model is employed, for example, to allow for the effect of damages and microruptures on the strain characteristics of solids, when studying the stability of spatial bodies, and on the fracture mechanics. Various sufficient conditions of uniqueness in the small of a solution to the static problem for such materials and the conditions of their stability were given in [5–8]. The uniqueness theorem for a local solution to the dynamical one-dimensional problem was proved in [3].

In the geometrically linear formulation, the boundary value problem of the elasticity theory is described by the equations

$$\sigma_{ij,\,j} + F_i = 0, \quad \varepsilon_{ij} = \frac{1}{2}(u_{i,\,j} + u_{j,\,i}), \tag{1}$$

$$\sigma_{ij} = \frac{\partial W}{\partial \varepsilon_{ij}}, \tag{2}$$

$$\sigma_{ij} n_j|_{S_T} = T_i, \quad u_i|_{S_U} = U_i,$$
$$u_i l_i|_{S_{TU}} = U_l, \quad \varepsilon_{mjk}(\sigma_{js} n_s) l_k|_{S_{TU}} = T_m. \tag{3}$$

These equations admit branching of their solution. Namely, on attaining a certain stressed–strained state, two different solutions $\sigma_{ij}^{(1)}$, $\varepsilon_{ij}^{(1)}$, $u_i^{(1)}$ and $\sigma_{ij}^{(2)}$, $\varepsilon_{ij}^{(2)}$, $u_i^{(2)}$ correspond to the same problem (1)–(3). Here, $W(\varepsilon_{ij})$ is the elastic potential; $S = S_T + S_U + S_{TU}$ is the surface of the body under consideration with volume V; F_i and T_i are the specific mass loads and the given surface loads, respectively; U_i are the displacements of points on the surface S_U; U_l is the displacement component along the given unit vector l for points on the boundary S_{TU}; T_m are the surface-load components in the plane orthogonal to l; and ε_{mjk} is the absolutely antisymmetric unit tensor.

Equilibrium equations (1), the Cauchy relationships, and also the Gauss–Ostrogradskiĭ theorem lead to the equation for virtual works:

$$\int_V \sigma_{ij}\varepsilon_{ij} dV = \int_V F_i u_i dV + \int_S \sigma_{ij} n_j u_i dS. \tag{4}$$

In this case, denoting $\Delta\sigma_{ij} = \sigma_{ij}^{(1)} - \sigma_{ij}^{(2)}$, $\Delta\varepsilon_{ij} = \varepsilon_{ij}^{(1)} - \varepsilon_{ij}^{(2)}$, and $\Delta u_i = u_i^{(1)} - u_i^2$ and using (1) and (4), we obtain

$$\int_V \Delta\sigma_{ij}\Delta\varepsilon_{ij} dV = \int_S \Delta\sigma_{ij} n_j \Delta u_i dS. \tag{5}$$

The integral in the right-hand side of relationship (5) is zero because the loads are equal on S_T, ($\sigma_{ij}^{(1)} n_j = \sigma_{ij}^{(2)} n_j = T_i$); the displacements are equal on S_U, ($u_i^{(1)} = u_i^{(2)} = U_i$); and the vectors $\Delta\sigma_{ij} n_j$ and Δu_i are mutually orthogonal on S_{TU}. We now consider the left-hand side of relationship (5).

We use the expression for $W(\varepsilon)$ corresponding to the first approximation for the elastic potential of the media under consideration. This approximation was given in [4]. Similar to the classical approximation, it is the best in its class and takes the following form:

$$W(\varepsilon) = \frac{\lambda}{2} I_1^2 + \mu I_2 - \nu I_1 \sqrt{I_2},$$
$$\varepsilon = (\varepsilon_{ij}), \quad I_1 = \delta_{ij}\varepsilon_{ij}, \quad I_2 = \varepsilon_{ij}\varepsilon_{ij}. \tag{6}$$

We assume that the function $W(\varepsilon)$ is strictly convex.

1. Uniqueness in the small. In this case, the solutions are infinitely close. From (2) and (6), we find,

* *Institute of Machine Engineering and Metallurgy, Far East Division, Russian Academy of Sciences, ul. Metallurgov 1, Komsomol'sk-na-Amure, 681005 Russia*

** *Komsomol'sk-na-Amure State Technical University, pr. Lenina 27, Komsomol'sk-na-Amure, 681013 Russia*

1028-3358/01/4605-0356$21.00 © 2001 MAIK "Nauka/Interperiodica"

ignoring the values of the second and higher orders of magnitude, that

$$\Delta\sigma_{ij}\Delta\varepsilon_{ij} = \left.\frac{\partial^2 W}{\partial\varepsilon_{ij}\partial\varepsilon_{kl}}\right|_{\varepsilon_{ij}^{(1)}} \Delta\varepsilon_{ij}\Delta\varepsilon_{kl} \geq 0.$$

For $\varepsilon_{ij}^{(1)} \neq \varepsilon_{ij}^{(2)}$, integral (5) is positive.

The uniqueness in the small follows from the contradiction obtained.

For the function $W(\varepsilon)$ to be strictly convex, it is necessary and sufficient that the eigenvalues of the matrix $\left(\frac{\partial^2 W}{\partial\varepsilon_i\partial\varepsilon_j}\right)$ be positive, where ε_i are the eigenvalues of the strain tensor. According to [9], one of the eigenvalues is equal to the squared velocity of propagation of a transverse acoustoelastic wave. Using the Viète theorem for two residual eigenvalues of this matrix, we come to the desired conditions of uniqueness in the small, which take the form of three inequalities:

$$2\mu - \nu\xi > 0,$$
$$4\mu + 3\lambda - 3\nu\xi > 0, \quad (7)$$
$$6\mu\lambda + 4\mu^2 - \lambda\nu\xi^3 - 6\mu\nu\xi + 3\nu^2\xi^2 - 3\nu^2 > 0.$$

Here, $\xi = \frac{I_1}{\sqrt{I_2}}$ is the strain parameter characterizing the relation between the relative variations of volume and mean-square shears.

For $\nu = 0$, it follows from (7) that both the shear modulus and the bulk modulus are positive; this provides for the uniqueness of solutions to problems of the classical elasticity theory.

A more rigorous theorem on the uniqueness in the small can be proved for this model provided that one of the solutions is zero. In this case, the conditions of uniqueness in the small and in the large coincide.

2. Uniqueness in the large. Using the equation of a plane tangent to a convex surface and the Taylor formula, with the residual term in the Lagrange form, we have

$$\Delta\sigma_{ij}\Delta\varepsilon_{ij} = \left.\frac{\partial^2 W}{\partial\varepsilon_{ij}\partial\varepsilon_{kl}}\right|_{\varepsilon_{ij}^{(\alpha)}} \Delta\varepsilon_{ij}\Delta\varepsilon_{kl} \geq 0, \quad (8)$$

where $\varepsilon_{ij}^{(\alpha)} = \alpha\varepsilon_{ij}^{(1)} + (1+\alpha)\varepsilon_{ij}^{(2)}$ is a certain strain distribution intermediate between the solutions $\varepsilon_{ij}^{(1)}$ and $\varepsilon_{ij}^{(2)}$ with $\alpha \in (0, 1)$.

From inequality (8) and relationship (5), it follows that the necessary and sufficient condition of uniqueness is given by inequalities (7), which should be satisfied for all values of $\xi \in [-\sqrt{3}, \sqrt{3}]$.

The left-hand side of the last inequality of set (7) is a cubic polynomial and is satisfied for all given ξ if

$$\mu > 0, \quad \lambda + \frac{2}{3}\mu > 0, \quad |\nu| < \begin{cases} \frac{2}{\sqrt{3}}\mu, & \lambda \geq \frac{2}{3}\mu \\ \frac{\sqrt{3}}{2}\left(\lambda + \frac{2}{3}\mu\right), & \lambda < \frac{2}{3}\mu. \end{cases} \quad (9)$$

It is easy to verify that potential (6) is positive definite, and the first two inequalities of set (7) are also met for all ξ provided that conditions (9) are satisfied.

It is seen from (9) that the constant ν in (6), which is additional compared to the classical case, may exceed the value of the classical shear modulus, but not by more than a factor of $\frac{2}{\sqrt{3}}$; however, it is always smaller, at least by the same factor, than the bulk modulus defined by Hooke's law.

Inequalities (9) are also valid when one of the solutions is zero. In this case, the value of the parameter ξ in (7) is determined by the increments $\Delta\varepsilon_{ij}$:

$$\xi = \cos\theta + \sin\theta(\sin\varphi + \cos\varphi),$$
$$\theta = \arctan\left(\frac{\sqrt{(\Delta\varepsilon_1)^2 + (\Delta\varepsilon_2)^2}}{\Delta\varepsilon_3}\right), \quad \varphi = \arctan\left(\frac{\Delta\varepsilon_2}{\Delta\varepsilon_3}\right).$$

Then, by virtue of the necessity of considering the entire manifold $\Delta\varepsilon_{ij}$, the condition of uniqueness in the small is given by inequalities (7) for all $|\xi| \leq \sqrt{3}$, i.e., corresponds to conditions (9).

Thus, for materials described by (6) whose constants satisfy conditions (9), the distribution of stresses and strains corresponding to the boundary conditions of problem (1)–(3) is unique.

3. Stability of a material. The nonuniqueness that can arise when conditions (7) are not satisfied is caused by the instability of the material. The conditions of stability follow from the positive definiteness of the following two quadratic forms [10]:

$$\delta\sigma_{ii}\delta\varepsilon_{ii} = a_{ij}x_i x_j, \quad \delta\sigma_{mn}\delta\varepsilon_{mn} = b_{mn}\delta\varepsilon_{mn}, \quad m \neq n.$$

Here, $x_1 = \delta I_1$, $x_2 = \delta\sqrt{I_2}$, $x_3 = \delta\Psi$, Ψ is the angle of the strain-tensor form, and the coefficients are determined by the equalities

$$a_{11} = \lambda + c(\xi), \quad a_{12} = -\nu - \xi c(\xi),$$
$$a_{22} = 2\mu + \xi^2 c(\xi), \quad a_{33} = \frac{1}{3}I_2(2\mu - \nu\xi)(3 - \xi^2),$$
$$b_{mn} = 2(2\mu - \nu\xi), \quad a_{13} = a_{23} = 0, \quad c(\xi) = \frac{2\mu - \nu\xi}{3 - \xi^2}.$$

Using these relationships, we find that the necessary and sufficient conditions of stability in the small are

given by the following three inequalities:

$$2\mu - \nu\xi > 0,$$
$$2\mu - \nu\xi + \lambda(3 - \xi^2) > 0, \quad (10)$$
$$6\mu\lambda + 4\mu^2 - \lambda\nu\xi^3 - 6\mu\nu\xi + 3\nu^2\xi^2 - 3\nu^2 > 0.$$

The first and the last inequalities of sets (10) and (7), which are the most severe constraints, coincide. This fact causes sets (10) and (7) to be equivalent and the condition of stability in the small to coincide with that of uniqueness in the small.

If set (10) is satisfied, all the principal minors of the matrix $\left(\frac{\partial\sigma_i}{\partial\varepsilon_j}\right)$ are positive. From this fact and the theorem on implicit functions, it follows that, if any three (with different subscripts) of six quantities σ_i and ε_i (i = 1, 2, 3) are given, then the three remaining quantities are found unambiguously. The violation of stability condition (10) leads to ambiguous relations between strains and stresses for the given ξ. According to (7), this ambiguity is due to the nonconvexity or the weak convexity of potential (6) in its section by the cone $I_1 = \xi\sqrt{I_2}$. Thus, the nonuniqueness of the solution in the small is realized.

If inequalities (10) are satisfied for all given ξ, they also provide for stability in the large. In this case, as with deriving the uniqueness condition, we conclude that inequalities (10) are certainly satisfied if their coefficients obey constraints (9). For a material described by Eqs. (6), the condition of stability in the large coincides with the condition of uniqueness in the large for the solution to problem (1)–(3). For many actual materials, the constants λ, μ, and ν satisfy these conditions.

ACKNOWLEDGMENTS

This work was supported by the Ministry of Education of the Russian Federation, project no. 97-0-4.3-120, and the Russian Foundation for Basic Research, project no. 98-01-00478.

REFERENCES

1. A. V. Berezin, V. I. Strokov, and V. N. Barabanov, in Carbon-Based Structural Materials (Moscow, 1976), No. 11, 102.
2. E. V. Lomakin and Yu. N. Rabotnov, Izv. Akad. Nauk SSSR, Mekh. Tverd. Tela, No. 6, 29 (1978).
3. V. P. Maslov and P. P. Mosolov, *Theory of Elasticity for Different-Modulus Media* (MIÉM, Moscow, 1985).
4. V. P. Myasnikov and A. I. Oleĭnikov, Dokl. Akad. Nauk SSSR **322**, 57 (1992) [Sov. Phys. Dokl. **37**, 41 (1992)].
5. I. Yu. Tsvelodub, Din. Sploshnoĭ Sredy **32**, 123 (1977).
6. E. V. Lomakin, Izv. Akad. Nauk SSSR, Mekh. Tverd. Tela, No. 2, 33 (1979).
7. A. I. Oleĭnikov, Candidate's Dissertation in Mathematical Physics (Novosibirsk, 1987).
8. A. V. Berezin, *An Effect of Damages on Deformation and Strength Characteristics of Solids* (Nauka, Moscow, 1990).
9. A. I. Oleĭnikov, Fiz.-Tekh. Probl. Razrab. Polezn. Iskop., No. 3, 39 (1989).
10. I. Yu. Tsvelodub, *Stability Postulate and Its Application to the Creep Theory of Metal Materials* (IgiL, Novosibirsk, 1991).

Translated by V. Bukhanov

Doklady Physics, Vol. 46, No. 5, 2001, pp. 359–362. From Doklady Akademii Nauk, Vol. 378, No. 2, 2001, pp. 197–200.

MECHANICS

Stability of a Steady Front for the Water–Vapor Phase Transition in Geothermal Reservoirs[1]

G. G. Tsypkin* and A. T. Il'ichev**

Presented by Academician D.M. Klimov November 24, 2000

Received December 18, 2000

1. Investigations of natural geothermal systems show that in many reservoirs, a situation takes place wherein a water layer of a considerable thickness overlies a layer of overheated vapor [1, 2]. It is well known that the state when a heavy-liquid layer lies over a lighter liquid layer is unstable [3]. Therefore, various hypotheses of a qualitative character were formulated concerning the physical mechanisms of stability of such geothermal systems [2].

For the first time, a mathematical model explaining the linear stability of a water–vapor interface, when a water layer lies over the vapor layer, was presented in [4]. It was assumed that, in the unperturbed state, the phases are motionless and the phase transition does not occur. As a result of the numerical investigation undertaken in that paper, the critical value of permeability $k \sim 4 \times 10^{-17}$ m^2 corresponding to the boundary between the stable and unstable states for the geothermal system in question was found. When the permeability exceeds the critical value, the system turns out to be unstable. Nevertheless, the authors indicated that the critical value given is lower by approximately an order of magnitude than the characteristic permeability of geothermal systems. Therefore, the stability of the majority of systems has no explanation. The physical mechanisms of stability observed were also not clarified.

In the present study, we analyze a more complicated example of a geothermal system with allowance for the phase motion and phase transition in the unperturbed state. The solution to the bounded steady problem for the phase-transition interface is obtained under the assumption of a small convective transfer compared to the conductive one. Our analysis of the linear stability of the solution shows that, in the parameter range where this solution exists, it is always stable. Steady solutions are obtained which hold for the permeability $k \sim 4 \times 10^{-16}$ m^2 typical of geothermal systems. The criterion for the existence of the steady solution, which coincides with the criterion for the stability of a geothermal system, is presented. In this setting, the stability mechanism for the class of geothermal systems under consideration acquires a clear physical meaning that consists in the predominant conductive energy transfer compared to the convective one.

2. We consider a high-temperature geothermal reservoir consisting of two high-permeable parallel layers separated by a low-permeable layer. We assume the thermodynamic conditions to be the following. The upper highly permeable layer $x < 0$ is filled with water having a temperature T_0 and a pressure P_0. The lower layer $x > L$ has a temperature T^0 and a pressure P^0. In this case, in the low-permeable layer $0 < x < L$, there exists a surface $x = h$ of phase transitions, which separates the domain of water $0 < x < h$ and vapor $h < x < L$. Either the regime of evaporation, when the water moves downwards, or the condensation regime corresponding to upward vapor motion can take place depending on the pressure in the highly permeable layers. We examine the stability of the interface with respect to small perturbations.

Processes of heat and mass transfer under the condition of equilibrium phase transitions are described by equations of mass and energy conservation, the Darcy rule for water and vapor, equations of state, and thermodynamic relations [5]. Following [3, 4], we assume, for simplicity, that water and vapor are incompressible. Then, the system of defining equations for the both domains has the form

$$\operatorname{div} v_j = 0, \quad v_j = -\frac{k}{\mu_j}(\operatorname{grad} P - \rho_j g),$$

$$(\rho C)_{1,2}\frac{\partial T}{\partial t} + \rho_j C_j v_j \operatorname{grad} T = \operatorname{div}(\lambda_{1,2}\operatorname{grad} T), \quad (1)$$

[1] The article was submitted by the authors in English.

* *Institute for Problems in Mechanics, Russian Academy of Sciences, pr. Vernadskogo 101, Moscow, 117526 Russia*

** *Steklov Mathematical Institute, Russian Academy of Sciences, ul. Gubkina 8, Moscow, 117333 Russia*

1028-3358/01/4605-0359$21.00

$$\lambda_{1,2} = m\lambda_j + (1-m)\lambda_s,$$
$$(\rho C)_{1,2} = m\rho_j C_j + (1-m)\rho_s C_s, \quad j = v, w.$$

Here, v is the filtration rate, m is porosity, k is permeability, μ is viscosity, P is pressure, g is the acceleration of gravity, ρ is density, C is specific heat, T is temperature, and λ is heat conductivity. The subscripts w, v, s correspond to the properties of water, vapor, and the porous-medium skeleton, respectively. The domains *1* and *2* correspond to vapor and water.

The conditions on the interface are formulated as those for a thermodynamically equilibrium jump of the water-saturation function [6]. These conditions are of the form

$$T_+ = T_- = T_*, \quad P_+ = P_- = P_*,$$
$$\ln\frac{P_*}{P_a} = A + \frac{B}{T_*},$$
$$A = 12.512, \quad B = -4611.73, \quad P_a = 10^5 \text{ Pa},$$
$$m\left(1 - \frac{\rho_v}{\rho_w}\right)V_n = \frac{k}{\mu_v}\frac{\rho_v}{\rho_w}(\text{grad}P)_{n+} - \frac{k}{\mu_w}(\text{grad}P)_{n-} + \frac{k}{\mu_w}\rho_w g\left(1 - \frac{\mu_w}{\mu_v}\frac{\rho_v^2}{\rho_w^2}\right), \quad (2)$$
$$mq\rho_w V_n = \lambda_-(\text{grad}T)_{n-} - \lambda_+(\text{grad}T)_{n+} - \frac{kq\rho_w}{\mu_w}((\text{grad}P)_{n-} - \rho_w g).$$

Here, V is the velocity of the interface and q is the evaporation heat per unit mass. The subscripts n, plus, minus, and * correspond to the normal vector, domains of water and vapor, and values on the interface, respectively.

Hereafter, we consider a particular case where the convective heat transfer in Eq. (1) may be ignored. The ratio of the convective to the conductive term in the energy equation entering into Eq. (1) is determined for the water domain by the dimensionless parameter

$$\frac{\rho_w C_w}{\mu_w \lambda_1} k(\delta P - \rho_w g l).$$

In this parameter, the permeability and pressure variations can considerably change, while the other physical parameters vary insignificantly. Therefore, after substituting characteristic values of the parameters, the condition of smallness for the convective transfer may be written out in the form

$$\frac{\rho_w C_w}{\mu_w \lambda_1} k|\delta P - \rho_w g l| \sim 10^{10}\text{N}^{-1} k|\delta P - \rho_w g l| \ll 1$$
$$\text{or } k|\delta P - \rho_w g l| \ll 10^{-10}\text{N},$$

where l is the characteristic length.

Performing similar estimates for the vapor domain, we can show that the condition of a small convective transfer is weaker than that for the water domain. In the vapor domain, this condition is fulfilled automatically in the case of a weak convective transfer in the water domain. Then, the energy equations are reduced to the usual equations of heat conduction for both domains.

3. We now consider the one-dimensional problem of the phase transfer. If the pressure and temperature in both highly permeable layers are constant (which is provided by the heat inflow from the surrounding rocks and high permeability, respectively), then the boiling front occupies a certain equilibrium position and the problem has a steady solution. The position of the interface $x = h$ is unknown and can be determined in the process of solving the problem. The equations for the desired pressure and temperature in both the water domain and the vapor domain now take the form

$$P''(x) = 0, \quad T''(x) = 0.$$

The conservation laws for the mass and energy on the interface are given by

$$\frac{\mu_w}{\mu_v}\frac{\rho_v}{\rho_w}P'_+ - P'_- + \rho_w g\left(1 - \frac{\mu_w}{\mu_v}\frac{\rho_v^2}{\rho_w^2}\right) = 0,$$
$$\lambda_+ T'_+ - \lambda_- T'_- + \frac{kq\rho_w}{\mu_w}(P'_- - \rho_w g) = 0,$$

where prime denotes the derivative with respect to x. These equations, along with the conditions of thermodynamic equilibrium at the interface, constitute the complete system of relations.

The solutions in the domains of water and vapor have the respective forms

$$P = P_0 + \frac{P_* - P_0}{h}x, \quad T = T_0 + \frac{T_* - T_0}{h}x,$$
$$P = \frac{P^0 - P_*}{L-h}x + \frac{LP_* - hP^0}{L-h}, \quad (3)$$
$$T = \frac{T^0 - T_*}{L-h}x + \frac{LT_* - hT^0}{L-h}.$$

Substituting solution (3) into the conditions (2) on the interface, we arrive at the system of equations for the unknown quantities T_*, P_*, and h:

$$\frac{\mu_w}{\mu_v}\frac{\rho_v}{\rho_w}\frac{P^0 - P_*}{L-h} - \frac{P_* - P_0}{h} + \rho_w g\left[1 - \frac{\mu_w}{\mu_v}\frac{\rho_v^2}{\rho_w^2}\right] = 0,$$
$$\lambda_+\frac{T^0 - T_*}{L-h} - \lambda_-\frac{T_* - T_0}{h} + \frac{kq\rho_w}{\mu_w}\left[\frac{P_* - P_0}{h} - \rho_w g\right] = 0,$$
$$P_* = f(T_*) = P_a \exp\left(A + \frac{B}{T_*}\right).$$

We now consider, as an example, the solution corresponding to the following values of the parameters and initial and boundary conditions: $\mu_w = 1.48 \times 10^{-4}$ Pa s; $\mu_v = 1.59 \times 10^{-5}$ Pa s; $\rho_w = 888.66$ kg m^{-3}; $\rho_v = 4.82$ kg m^{-3}; $q = 2 \times 10^6$ J kg^{-1}; $L = 10$ m; $T_0 = 450$ K; $T^0 = 460$ K; and $P_0 = P^0 = 10^6$ Pa. The values of the permeability are taken to be $k \times 10^{16} = 2$, 1, and 0.5 m^2. The pressures in the highly permeable layers are chosen to be equal in order to provide minimum pressure variation. This makes it possible to strongly increase the value of permeability and, at the same time, satisfy the criterion of small convective energy transfer. Physically, this flow regime corresponds to the downward motion of water under the action of gravity forces and its further evaporation in lower layers of higher temperatures.

The solution to the system of equations on the interface yields the following values of the desired quantities: $h = 4.6$, 3.2, 2.94 m; $T_* = 453.39$, 452.9, 452.81 K; and $P_* = 1.038 \times 10^6$, 1.027×10^6, 1.025×10^6 Pa.

It is worth mentioning that in the cases under consideration, the maximum value of the parameter $k\delta P$ is 0.76×10^{-11}, which is by more than an order of magnitude lower than the critical value. Therefore, the assumption on the smallness of the energy convective transfer is valid. For $k = 4 \times 10^{-16}$ m^2, we have $P_* = 1.046 \times 10^6$ Pa and $k|\delta P - \rho_w g l| = 1.5 \times 10^{-11}$ N; i.e., the conductive term in the energy equation is seven times higher than the convective one. Further increase in the permeability enhances the role of the convective transfer and, in turn, violates the above criterion.

4. Systems of defining equations linearized with respect to the steady solution under the condition of the small convective energy transfer in both domains have the form

$$\Delta P = 0, \quad \frac{\partial T}{\partial t} = a_{1,2}\Delta T, \quad a_{1,2} = \frac{\lambda_{1,2}}{(\rho C)_{1,2}}, \quad 0 < x < h, \quad h < x < L. \tag{4}$$

Hereafter, we assume for simplicity that the specific heats and heat conductivities in both domains are determined by the corresponding parameters $a = a_1 = a_2$ for the skeleton of the porous medium.

The boundary conditions for perturbations are given by the relations

$$P = 0, \quad T = 0 \text{ at } x = 0, L,$$

$$P_- = P_+ + \Gamma_1\eta, \quad \Gamma_1 = \left(\frac{P_0}{h} + \frac{P^0 h - P_* L}{h(L-h)}\right) \text{ at } x = h,$$

$$T_- = T_+ + \Gamma_2\eta, \quad \Gamma_2 = \left(\frac{T_0}{h} + \frac{T^0 h - T_* L}{h(L-h)}\right) \text{ at } x = h,$$

$$P_- = \left(\frac{\partial f(T)}{\partial T}\right)_{T=T_*} T_- + \left[\left(\frac{\partial f(T)}{\partial T}\right)_{T=T_*}\left(\frac{\partial T}{\partial x}\right)_- - \left(\frac{\partial P}{\partial x}\right)_-\right]\eta = -\Gamma T_- - \Gamma_0\eta, \tag{5}$$

$$\Gamma = \frac{P_* B}{T_*^2}, \quad \Gamma_0 = \frac{P_* B}{T_*^2}\frac{T_* - T_0}{h} + \frac{P_* - P_0}{h} \text{ at } x = h,$$

$$m(1-R)\frac{\partial \eta}{\partial t} = \frac{k}{\mu_v}R\left(\frac{\partial P}{\partial x}\right)_+ - \frac{k}{\mu_w}\left(\frac{\partial P}{\partial x}\right)_-, \quad R = \frac{\rho_v}{\rho_w} \text{ at } x = h,$$

$$mq\rho_w\frac{\partial \eta}{\partial t} = \lambda_-\left(\frac{\partial T}{\partial x}\right)_- - \lambda_+\left(\frac{\partial T}{\partial x}\right)_+ - \frac{kq\rho_w}{\mu_w}\left(\frac{\partial P}{\partial x}\right)_- \text{ at } x = h.$$

Here, $x = h + \eta(t, y)$ is the equation for the interface. We assume furthermore that the temperature and the pressure have the form $g(x)\exp(\sigma t + i\kappa y)$. Then, from the condition of the existence of the nontrivial solution to the problem (4), (5), we obtain the dispersion relation

$$\begin{aligned} F(\sigma, \kappa) \equiv{}& \alpha\coth[\alpha(L-h)]\left[\Gamma_3\kappa\frac{k}{\mu_w}\coth(\kappa h) + \Gamma_4 R\kappa\frac{k}{\mu_v}\coth[\kappa(L-h)] - m(1-R)\sigma\right] \\ &+ \alpha\coth(\alpha h)\left[\Gamma_5 R\kappa\frac{k}{\mu_v}\coth[\kappa(L-h)] + \Gamma_0\kappa\frac{k}{\mu_w}\coth(\kappa h) - m(1-R)\sigma\right] + \frac{\Gamma q\rho_w k R\kappa}{\lambda} \\ &\times\left[\sigma\frac{m}{\mu_v}\coth[\kappa(L-h)] + \sigma\frac{m}{\mu_w}\coth(\kappa h) + \Gamma_1\kappa\frac{k}{\mu_v\mu_w}\coth(\kappa h)\coth[\kappa(L-h)]\right] = 0, \end{aligned} \tag{6}$$

where

$$\Gamma_3 = \Gamma\frac{T^0 - T_*}{L-h} + \frac{P_* - P_0}{h},$$

$$\Gamma_4 = \Gamma\frac{T^0 - T_*}{L-h} + \frac{P^0 - P_*}{L-h},$$

$$\Gamma_5 = \Gamma\frac{T_* - T_0}{h} + \frac{P^0 - P_*}{L-h},$$

$$\alpha = \sqrt{\kappa^2 + \frac{\sigma}{a}}.$$

The function $F(\sigma)$ is analytical everywhere in the complex plane of σ except for the negative part of the real axis, where it has a finite set of isolated poles separated from zero.

If for the fixed real κ there exist complex roots σ of Eq. (6) with a positive real part, then the corresponding perturbations exponentially grow with time and the basic steady solution (3) is unstable.

We now consider the left side of the dispersion relation obtained as a function of the complex variable $F(\sigma)$. Zeroes of this function correspond to the roots of Eq. (6). The absence of zeroes with a positive real part that would provide exponential growth of small perturbations implies the stability of the solution. To investigate the stability, we use the argument principle [7], which implies that the difference between the number of zeroes and poles of the function $F(\sigma)$ inside a certain contour C lying in the $(\mathrm{Re}(\sigma), \mathrm{Im}(\sigma))$ plane is equal to the number of rotations for the radius-vector in the complex $(\mathrm{Re}F(\sigma), \mathrm{Im}F(\sigma))$ plane while going around the contour C_1, which is the image of C while mapping $F(\sigma)$.

In the plane of σ, we choose a contour consisting of an imaginary axis and a semicircle lying in the right half-plane. By virtue of the analytical properties of the function $F(\sigma)$, as was mentioned before, it has no singularities in the right half-plane. If $F(\sigma)$ has zeroes there, then, increasing the radius of the contour, we can make all zeroes and poles lie inside the contour C. The F-images of C, i.e., the contours C_1, were constructed for a large variety of parameters. All these contours have a shape similar to that for the contours presented in the figure. In this figure, the comparative shape of C_1 is presented for the three regimes mentioned in Section 3. In this case, the fact of principal importance, which underlies the absence of zeroes for $F(\sigma)$ independently of the radius of C, is the negative value of the coordinate for the point A.

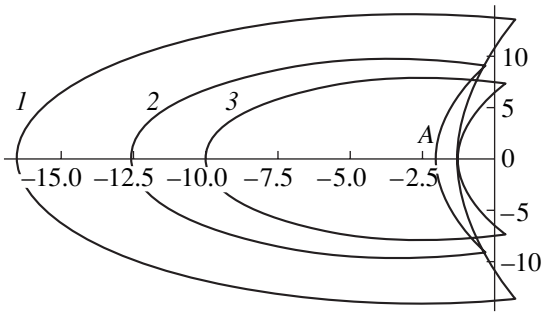

Characteristic shape of the function $F(\sigma) = 0$ in the complex plane $(\mathrm{Re}F(\sigma), \mathrm{Im}F(\sigma))$ for $\kappa = 3$ and three different permeability values (*1*) $k = 2 \times 10^{-16}$; (*2*) 1×10^{-16}; and (*3*) 0.5×10^{-16} m^2.

We note here that the investigation carried out in [4] is based on the assumption of the absence of complex roots for the increment σ, which, generally speaking, requires substantiation.

The analysis performed of the linear stability shows that the solution is always stable in the case under consideration. This corresponds to the stability of the physical configuration when the water layer lies over the vapor layer. Hence, the smallness of the convective heat transfer can serve as a stability criterion. This fact makes it possible to understand the physical mechanism of the stability. Such a mechanism implies that perturbations of the interface and penetration of the so-called water fingers into the vapor domain are prevented by the dominating conductive heat flow leading to the evaporation of the liquid phase. As computations show, stable solutions can exist corresponding to the permeability values $k \sim 4 \times 10^{-16}$ m^2, which exceed the critical value given in [4] by an order of magnitude. For higher values of the permeability, the role of the convective heat transfer increases and the basic solution becomes invalid. However, it is natural to assume that growth in the permeability does not immediately lead to the rise of instability. In other words, in actual conditions, the water layer can also exist over the vapor layer in the case of a higher permeability so that our analysis allows us to assume the existence of stable regimes up to $k \sim 10^{-15}$ m^2.

ACKNOWLEDGMENTS

The authors are grateful to A.G. Kulikovskiĭ for fruitful discussions.

This work was fulfilled under the financial support of the Russian Foundation for Basic Research, project no. 99-01-0277.

REFERENCES

1. D. E. White, L. J. P. Muffler, and A. H. Truesdell, Econ. Geol. **66**, 75 (1971).
2. M. A. Grant, Geothermics **12**, 251 (1983).
3. S. Chandrasekhar, *Hydrodynamic and Hydromagnetic Stability* (Oxford Univ. Press, New York, 1967).
4. G. Schubert and J. M. Straus, J. Geophys. Res. B **85**, 6505 (1980).
5. M. J. O'Sullivan, Int. J. Energy Res. **9**, 319 (1985).
6. G. G. Tsypkin, Dokl. Akad. Nauk **337**, 748 (1994) [Phys. Dokl. **39**, 594 (1994)].
7. B. V. Shabat, *Introduction to the Complex Analysis* (Nauka, Moscow, 1985), Part 1.

Translated by G. Tsypkin

Doklady Physics, Vol. 46, No. 5, 2001, pp. 363–365. Translated from Doklady Akademii Nauk, Vol. 378, No. 3, 2001, pp. 333–335.

MECHANICS

On the Similarity of the Initial Stage of Failure of Solids and Liquids under Impulse Loading

A. S. Besov*, V. K. Kedrinskiĭ*, Academician N. F. Morozov, Yu. V. Petrov**, and A. A. Utkin****

Received January 9, 2001

Cavitation is the disturbance of continuity of a liquid (the initial stage of failure) in the field of tensile stresses; it is accompanied by the growth of vapor-gas bubbles on the cavitation nuclei that are always present in liquid media as microbubbles of a free gas, or microparticles, or both [1, 2]. One of the parameters that characterize the cavitation strength of water is the cavitation threshold, which is understood as a negative pressure, the excess above which causes an intense growth of cavitation nuclei and, as a consequence, a steep change in the dynamics of the free surface of the liquid [3], in the intensity of light scattering [1, 3], etc. Depending on the measuring technique and quality of water purification, the cavitation threshold varies from units [2, 3–6] to several hundred atmospheres [4–6], and its statistical dispersion, based on standard measuring procedures, reaches 50–100% [5, 6] and is determined by the size dispersion of cavitation nuclei, fluctuations in the nucleus distribution, nonlinear dynamics of microbubbles, and by the measuring technique.

Statistical scatter of experimental values of the cavitation threshold can be considerably lowered by using the capacitance technique [3, 7] for recording this threshold through the observation of the dynamics of the free surface of the liquid at the reflection of a shock wave from this liquid. Such a wave is created in a shock tube by the pressure of a pulsed magnetic field on the conducting membrane that translates the pressure pulse to the liquid. As a result of the wave reflection, the downward propagating rarefaction pulsed wave is formed near the surface, initiating the growth of cavitation nuclei and the formation of a cavitation cluster. The dynamics of the latter at different degrees of cavitation is reflected by the free surface of water (Fig. 1) [7]. Curve *1* in Fig. 1 corresponds to the dynamics of the free surface of a specimen of distilled water that is 25 mm in height, which is observed at the reflection of the compression wave from this surface before the manifestation of cavitation phenomena (prethreshold mode). Curve *2* demonstrates the displacement of the free surface at the threshold amplitude of loading. It is readily seen that a minor change in the amplitude of the shock wave gives rise to a considerable change in the free surface dynamics. Curve *3* corresponds to the intense development of cavitation at which the displacement of the free surface due to the growth of the cavitation cluster is comparable to its displacement at the instant of reflection of the shock wave. The slope U_i of curves *1*, *2* and *3* to the right of the bound *AA* (Fig. 1), which corresponds to the completion of the shock wave reflection from the free surface, is linked to the specific volume φ of the formed bubbles (gas content) by the simple relationship $\varphi_i = \frac{U_i}{c}$, where U_i is the velocity of the free surface and *c* is the speed of sound

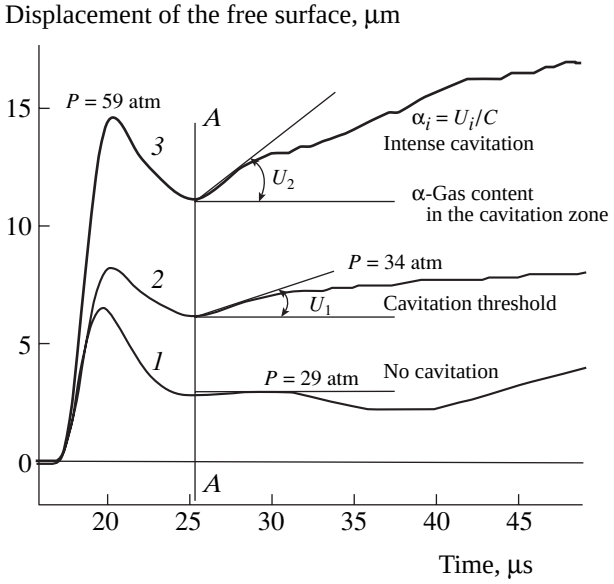

Fig. 1. Dynamics of the free surface of specimen of distilled water 25 mm in height observed at the reflection of the rarefaction wave from this surface.

* *Lavrent'ev Institute of Hydrodynamics, Siberian Division, Russian Academy of Sciences, pr. Akademika Lavrent'eva 15, Novosibirsk, 630090 Russia*

** *St. Petersburg State University, Universitetskaya nab. 7/9, St. Petersburg, 199164 Russia*

1028-3358/01/4605-0363$21.00 © 2001 MAIK "Nauka/Interperiodica"

Dependence of the cavitation threshold amplitude on the length of the positive phase of the pressure pulse

Pulse length, μs	Pressure, atm
2.9	65
3.2	52.5
4	34
4.5	31
4.8	27
6	18

in water [2]. In practice, for threshold loading, the φ value falls in the range from 10^{-4} to 10^{-3}.

The data in Table 1 illustrate the dependence of the amplitude of the cavitation threshold, which is detected as a sharp increase in the slope of the U_i-curves of the free surface, on the length of the positive phase T of the pressure pulse. The pressure profile of the incident shock wave was reconstructed from the dynamics of the free water surface in the precavitation reflection mode.

It is commonly accepted in acoustics that a liquid in a field of an acoustic emitter is destroyed immediately after the appearance of the first oscillating bubble, which begins to disintegrate, resulting in the formation of a cavitation region. In our case (Fig. 1, curve *3*), we can consider that the cavitation zone (cluster) forms near the free surface, which continues to move by inertia, as in the case of the split-off occurring in a solid body.

A similar phenomenon—an increase in the strength with decreasing the sounding time—is observed in the failure of solids. The situation closest to the onset of cavitation appears in solids in the case of a split-off failure. In this case, the material strength rises as the sounding time decreases, while in the case of threshold pulses, a weak dependence of failure time on the amplitude of the starting loading pulse is established. This effect was termed the dynamical branch phenomenon.

The structure–time failure criterion proposed in [8, 9] enables one to calculate the increase in strength observed in split-off experiments. This criterion provides a reasonable explanation for the phenomena observed in split-off experiments with brittle materials [8]. A similar criterion, enabling an effective prediction of the behavior of the dynamic yield strength [10], is used for plastic materials:

$$\frac{1}{\tau}\int_{t-\tau}^{t}\left(\frac{\sigma(t)}{\sigma_c}\right)^{\alpha}dt < 1. \qquad (1)$$

Here, α_c is the static yield strength and τ is the incubation period pertaining to the dynamics of the dislocation process. The parameter α characterizes the sensitivity of the material to the level of stresses that cause an irreversible deformation. Its value for solids is higher than or equal to unity. For some materials, α attains several tens; e.g., α = 10–30 for steels and alloys. It should be noted that the condition for the irreversible growth of cavitation bubbles under critical loading, which leads to the failure of a liquid specimen, is also used for liquids [11].

In order to analyze the initial stage of cavitation failure, we will use criterion (1), taking into account that the tensile stresses are positive in the mechanics of deformable solids, while the tensile pressures in liquids are negative. In addition, it is necessary to make allowance for the contribution of compression. As a result, relationship (1) takes the form

$$\frac{1}{\tau}\int_{t-\tau}^{t}\operatorname{sgn}(\sigma(t'))\left(\operatorname{abs}\left(\frac{\sigma(t')}{\sigma_c}\right)\right)^{\alpha}dt' < 1. \qquad (2)$$

For distilled water, we take $\sigma_c \approx 1$ atm, because an intense growth of cavitation nuclei under the action of tensile stresses begins after neutralization of surface tension forces, i.e. when $\sigma_c = \dfrac{2\sigma_w}{r}$, where σ_w is the surface tension for water and $r \approx 1.5$ μm is the radius of cavitation nuclei [1]. The values of τ and α were chosen using experimental points. The load realized in the experiments is approximated by the formula

$$\sigma(t) = -P_A\sin\left(\frac{\pi t}{T}\right)e^{-t/T_1}, \qquad (3)$$

where P_A is the pulse amplitude and T is the pulse length. The parameter T_1 characterizes the degree of damping. The highest absolute value of the pulse amplitude P_m is attained at the time $t = \dfrac{T}{\pi}\arctan\left(\dfrac{\pi T_1}{T}\right)$:

$$P_m = \frac{\pi T_1}{\sqrt{T^2 + \pi^2 T_1^2}}\exp\left(\frac{T}{\pi T_1}\arctan\left(\frac{\pi T_1}{T}\right)\right).$$

The applied loading tension $\sigma(t)$ induces a pressure wave which moves toward the surface. If we take the surface coordinate as zero and count off the time from the instant of the wave arrival to the surface, the wave can be written in the form $\sigma\left(t + \dfrac{x}{c}\right)H\left(t + \dfrac{x}{c}\right)$. Upon reflecting from the surface, the wave takes the form $-\sigma\left(t - \dfrac{x}{c}\right)H\left(t - \dfrac{x}{c}\right)$ and the pressure will be determined by the sum of these waves. Here, $H(t)$ is the Heaviside function and c is the speed of the wave in the liquid (c = 1500 m/s). Computations show that experimental loading curves are well described by formula (3) at $T_1 = 2.85 \times 10^{-6}$ s.

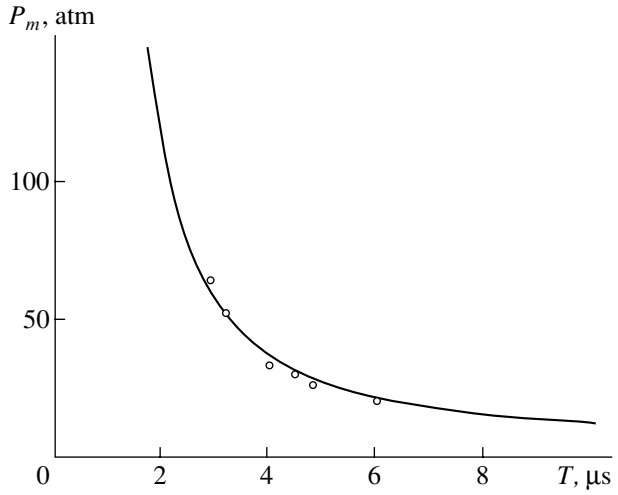

Fig. 2. Experimental and calculated, according to criterion (2), strengths as a function of the pulse length T for $\alpha = 0.5$ and $\tau = 19$ μs.

The critical strength is calculated as follows. We substitute the normalized pressure values at all points of the liquid at all instants of time corresponding to nonzero pressure into integral (2). Then, the instant and the coordinate are determined for which this integral reaches a maximum. The P_m value for which criterion (2) becomes an equality at the instant of time and for the coordinate corresponding to the maximum value of the integral represents the required amplitude. Calculations show that the best coincidence with experimental values is observed for α values in the range from 0.4 to 0.5.

The dependence of the strength on the pulse length T for $\alpha = 0.5$ and $\tau = 19$ μs calculated from criterion (2) is plotted in Fig. 2. The open circles are the experimental points.

CONCLUSIONS

It is shown experimentally that the cavitation strength of water rises with a decrease in the pulse length and that the corresponding dependence is nonlinear.

The use of the structure–time criterion makes it possible to calculate the increase in the cavitation threshold with a decrease in the pulse length, which is observed experimentally.

The data obtained testify to the fundamental importance of the structure–time approach, which provides an adequate description of both the dynamics of failure of solids and the initial stage of destruction of liquids.

REFERENCES

1. A. S. Besov, V. K. Kedrinskiĭ, Y. Matsumoto, *et al.*, Din. Sploshnoĭ Sredy, No. 104, 16 (1992).
2. M. Kornfeld, *Elasticity and Plasticity of Liquids* (Inostrannaya Literatura, Moscow, 1951).
3. A. S. Besov, V. K. Kedrinskiĭ, and E. I. Pal'chikov, Pis'ma Zh. Tekh. Fiz. **15** (16), 23 (1989) [Sov. Tech. Phys. Lett. **15**, 630 (1989)].
4. L. Y. Briggs, J. Appl. Phys. **26**, 1001 (1955); **21**, 721 (1950).
5. R. T. Knapp, J. W. Daily, and F. G. Hammitt, *Cavitation* (McGraw-Hill, New York, 1970; Mir, Moscow, 1974).
6. A. D. Pernik, *Problems of Cavitation* (Sudostroenie, Leningrad, 1966).
7. A. Besov and V. Kedrinskiĭ, in *Proceedings of the International Symposium on Bubble Dynamics and Interface Phenomena, Birmingham*, 1994, p. 93.
8. N. F. Morozov, Yu. V. Petrov, and A. A. Utkin, Dokl. Akad. Nauk SSSR **313**, 276 (1990) [Sov. Phys. Dokl. **35**, 646 (1990)].
9. N. F. Morozov and Yu. V. Petrov, *Problems of Dynamics of Failure of Solid Bodies* (Sankt-Peterb. Gos. Univ., St. Petersburg, 1997).
10. A. A. Gruzdkov and Yu. V. Petrov, Dokl. Akad. Nauk **364**, 766 (1999) [Dokl. Phys. **44**, 114 (1999)].
11. V. K. Kedrinskiĭ, Prikl. Mekh. Tekh. Fiz., No. 3, 74 (1993).

Translated by A. Kozlenkov

Doklady Physics, Vol. 46, No. 5, 2001, pp. 366–368. Translated from Doklady Akademii Nauk, Vol. 378, No. 3, 2001, pp. 336–338.

MECHANICS

Poisson's Ratios for Interfacial Layers of Polymer Matrix Composites

Academician I. F. Obraztsov, Yu. G. Yanovskiĭ, A. N. Vlasov, and V. É. Zgaevskiĭ

Received December 21, 2000

In most cases, extensively used polymeric materials represent heterogeneous media with phase interfaces of large relative areas. Polymer macromolecules situated on the interface between a highly elastic matrix and the rigid particles of a filler interact with the filler surface. This effect leads to the formation of an interfacial polymer layer whose mechanical characteristics differ from those for the matrix [1, 2]. The specific character of the interaction of the macromolecules with the surface imposes restrictions on the elastic properties of the interfacial layer. In particular, the ranges of the Poisson's ratios for the interfacial layer are noteworthy and attract interest (see [3, 4]).

The filler surface is assumed to be flat and to contain uniformly distributed active centers; in each of these centers, one end of a macromolecule is rigidly fixed. We assume furthermore that the macromolecules are surrounded by a certain medium (a solution) and the forces of adhesive interaction between segments of the macromolecules and the surface are negligible as compared to the forces caused by chemical bonds. The filler surface is impermeable to the segments of the macromolecules. Both the impermeability of the surface and the steric restrictions leading to interaction of the macromolecules cause a specific variation of their conformation.

Let the other macromolecule ends, which are not fixed on the surface, be bonded with nodes of a three-dimensional polymer mesh (a polymer matrix) having known mechanical characteristics and assumed to be incompressible. Figure shows a scheme of the near-surface layer. The X_2- and X_3-axes of coordinates are parallel to the plane of the near-surface layer, while the X_1-axis is perpendicular to it. Dots on the surface show the positions to which the macromolecule ends are attached. In addition, the dots label those nodes of the polymer mesh that are bonded with the other ends of the macromolecules forming the interfacial layer. Naturally, the presented scheme of the interfacial layer describes the actual physical picture only approximately because there can exist different types of macromolecule bonding with the surface. Moreover, it is difficult, in fact, to distinguish between the near-surface layer and the polymer matrix itself. Nevertheless, the scheme proposed turns out to be useful for analyzing features of the micromechanical characteristics of the interfacial layer.

Further, the effect of the surface is replaced by a certain force, which is applied to each restrained macromolecule and causes its deformation, with the conformation of a free macromolecule considered as its unperturbed state. This concept makes it possible to use the classical stress–strain relation of the geometric-nonlinear elasticity theory.

Within the scope of the above-proposed approach, the stress tensor σ_{ls} of the interfacial layer can be written as [5]

$$\sigma_{ls} = 2C\lambda_{ln}\lambda_{sn}\alpha_{(n)}^2 - p\delta_{ls} - \sigma_{ls}^0. \quad (1)$$

Here, C is the constant characterizing the material of the matrix; $\lambda_{ln} = \dfrac{\partial x_l'}{\partial x_n}$, where x_n and x_l' are the coordinates of a point belonging to the interfacial layer before and after deformation, respectively; $\alpha_{(n)}$ is the surface-caused relative variation of the coordinates of a point in the interfacial layer, with $\alpha_2 = \alpha_3 = \alpha_1^{-1/2}$; p is the hydrostatic pressure; δ_{ls} is the Kronecker delta; and σ_{ls}^0 are the components of the initial stress field arising in the interfacial layer under the effect of the surface. Here, the summation is performed over each pair of identical subscripts, while the subscript in parentheses excludes the summation.

In the coordinate system shown in the figure, the components of the stress tensor σ_{ls}^0 are expressed as

$$\sigma_{11}^0 = 2C(\alpha_1^2 - \alpha_2^2), \quad \sigma_{22}^0 = \sigma_{33}^0 = 0,$$
$$\sigma_{ik}^0 = 0 \text{ if } i \neq k. \quad (2)$$

Considering the small strains of the interfacial layer,

Institute of Applied Mechanics,
Russian Academy of Sciences,
Leninskiĭ pr. 32a, Moscow, 117334 Russia

1028-3358/01/4605-0366$21.00

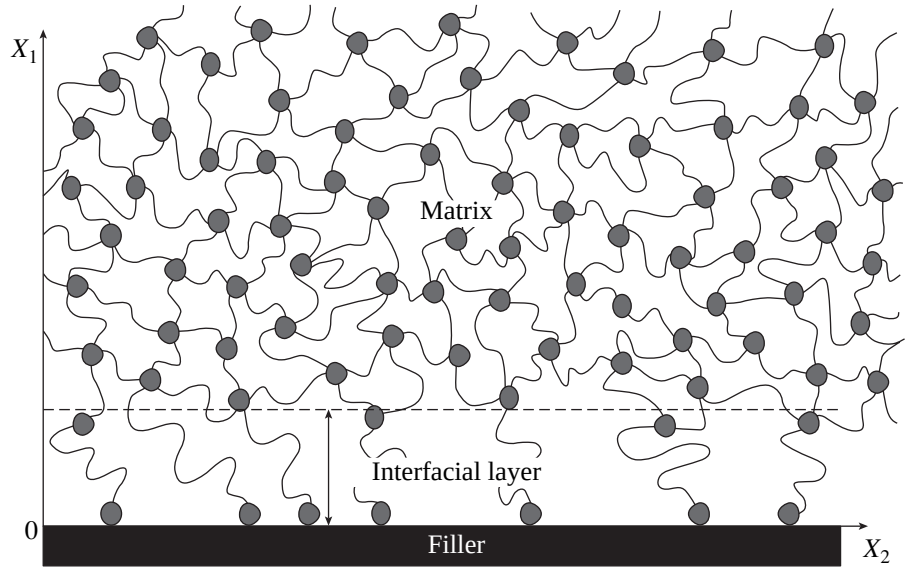

Schematic drawing of the near-surface layer.

we can write out λ_{ik} in the form

$$\lambda_{ik} = \delta_{ik} + \frac{\partial u_i}{\partial x_k} = \delta_{ik} + u_{i,k}. \quad (3)$$

Then, we represent $u_{i,k}$ as a sum of the symmetric (ε_{ik}) and the skew-symmetric (ω_{ik}) parts; i.e., $u_{i,k} = \varepsilon_{ik} + \omega_{ik}$, where $\varepsilon_{ik} = \frac{1}{2}(u_{i,k} + u_{k,i})$ and $\omega_{ik} = \frac{1}{2}(u_{i,k} - u_{k,i})$. Since the resultant moment of the forces acting on an elementary volume of the interfacial layer must be equal to zero, the condition $\omega_{ik} = 0$ is satisfied. Consequently, relation (3) takes the form

$$\lambda_{ik} = \delta_{ik} + \varepsilon_{ik}, \quad (4)$$

where ε_{ik} are components of the small-strain tensor.

Substituting (4) into (1) and ignoring the terms of the second order of smallness in strain, we have

$$\sigma_{is} = 2C(\delta_{in}\delta_{sn}\alpha_{(n)}^2 + \delta_{sn}\alpha_{(n)}^2\varepsilon_{in} + \delta_{in}\alpha_{(n)}^2\varepsilon_{sn}) - p\delta_{is} - \sigma_{is}^0. \quad (5)$$

Now, we consider the uniaxial tension along the X_1-axis of coordinates. Then, according to (5),

$$\sigma_{11} = 2C(\alpha_1^2 + 2\alpha_1^2\varepsilon_{11}) - p - \sigma_{11}^0. \quad (6)$$

In this case, $\sigma_{22} = \sigma_{33} = 0$. This allows us to find the quantity p from the relationship

$$C(\alpha_2^2 + \alpha_3^2 + 2\alpha_2^2\varepsilon_{22} + 2\alpha_3^2\varepsilon_{33}) - p = 0. \quad (7)$$

Substituting into (6) expressions for σ_{11}^0 and p from (2) and (7), respectively, and using both the incompressibility condition $\varepsilon_{11} + \varepsilon_{22} + \varepsilon_{33} = 0$ for the interfacial layer and the equality $\alpha_3 = \alpha_2$, we have

$$\sigma_{11} = 2C(2\alpha_1^2 + \alpha_2^2)\varepsilon_{11}. \quad (8)$$

Using (8), we now derive the following formula for the elastic modulus of the interfacial layer in the direction normal to the filler surface:

$$E_1 = 2C(2\alpha_1^2 + \alpha_2^2). \quad (9)$$

Here and below, the notation for elastic characteristics corresponds to that in [6].

It also follows from the condition $\sigma_{22} = \sigma_{33} = 0$ that

$$p = 2C(\alpha_2^2 + 2\alpha_2^2\varepsilon_{22}) = 2C(\alpha_3^2 + 2\alpha_3^2\varepsilon_{33}). \quad (10)$$

Based on formula (10) and the incompressibility condition, we relate the longitudinal (along the elongation axis) and transverse strains as

$$\varepsilon_{11} = -2\varepsilon_{22} = -2\varepsilon_{33}. \quad (11)$$

As a result, the corresponding Poisson's ratios are

$$\nu_{12} = \nu_{13} = 0.5. \quad (12)$$

A similar consideration of tensions along the X_2- and X_3-axes of coordinates leads to the following expressions for the corresponding elastic moduli and Poisson's ratios:

$$E_2 = 4C\frac{\alpha_2^2(2\alpha_1^2 + \alpha_2^2)}{\alpha_1^2 + \alpha_2^2}, \quad E_3 = 4C\frac{\alpha_2^2(2\alpha_1^2 + \alpha_2^2)}{\alpha_1^2 + \alpha_2^2}; \quad (13)$$

$$\nu_{21} = \frac{\alpha_2^2}{\alpha_1^2 + \alpha_2^2}, \quad \nu_{23} = \frac{\alpha_1^2}{\alpha_1^2 + \alpha_2^2},$$
$$\nu_{31} = \frac{\alpha_2^2}{\alpha_1^2 + \alpha_2^2}, \quad \nu_{32} = \frac{\alpha_1^2}{\alpha_1^2 + \alpha_2^2}. \tag{14}$$

Formula (1), the pure-shear conditions, and the equality of the quantities α_2 and α_3 lead to the following relationships:

$$\sigma_{12} = 2C(\alpha_1^2 + \alpha_2^2)\varepsilon_{12}, \quad \sigma_{13} = 2C(\alpha_1^2 + \alpha_2^2)\varepsilon_{13},$$
$$\sigma_{23} = 4C\alpha_2^2\varepsilon_{23}. \tag{15}$$

Consequently, the shear moduli of the interfacial layer are given by

$$G_{12} = G_{13} = C(\alpha_1^2 + \alpha_2^2), \quad G_{23} = 2C\alpha_2^2. \tag{16}$$

In the absence of the disturbing effect of the surface, $\alpha_1 = \alpha_2 = \alpha_3 = 1$ and Eq. (1) turns into an equation of rubberlike elasticity of an isotropic body. In this case, according to relations (9), (13), (14), and (16), the elastic moduli for the matrix are

$$E = 6C, \quad G = 2C, \quad \nu = 0.5. \tag{17}$$

Denoting α_1 by α and using both (17) and the relation between α_2 and α_1, we rewrite formulas (9), (13), (14), and (16) in the following form:

$$E_1 = \frac{1}{3}\left(2\alpha^2 + \frac{1}{\alpha}\right)E, \quad E_2 = E_3 = \frac{2}{3}\frac{1 + 2\alpha^3}{\alpha(1 + \alpha^3)}E,$$
$$G_{23} = \frac{1}{\alpha}G, \quad G_{12} = \frac{1}{2}\left(\alpha^2 + \frac{1}{\alpha}\right)G,$$
$$\nu_{12} = \nu_{13} = 0.5, \quad \nu_{21} = \nu_{31} = \frac{1}{1 + \alpha^3}, \tag{18}$$
$$\nu_{23} = \nu_{32} = \frac{\alpha^3}{1 + \alpha^3}.$$

The derived expressions for the elastic characteristics of the interfacial layer lead to the relations

$$\frac{\nu_{12}}{E_1} = \frac{\nu_{21}}{E_2}, \quad \frac{\nu_{13}}{E_1} = \frac{\nu_{31}}{E_3}, \quad \frac{\nu_{23}}{E_2} = \frac{\nu_{32}}{E_3},$$
$$G_{23} = \frac{E_2}{2(1 + \nu_{23})} = \frac{E_3}{2(1 + \nu_{23})}, \quad \nu_{12} + \nu_{23} + \nu_{31} = \frac{3}{2}. \tag{19}$$

Thus, within the framework of the model under consideration, the elastic properties of the interfacial layer are adequately defined by both the elastic characteristics of the matrix and the parameter α, with the interfacial layer representing an incompressible transverse-isotropic medium.

The values obtained for the Poisson's ratios are of certain interest. For example, according to (18), an increase in α ($\alpha \geq 1$) causes a decrease in the Poisson's ratios $\nu_{21} = \nu_{31}$ in the half-interval [0, 0.5] and a growth of the Poisson's ratios $\nu_{23} = \nu_{32}$, corresponding to the isotropy plane, in the half-interval [0.5, 1). Thus, the restrictions imposed on the Poisson's ratios for the interfacial layers arising in polymer matrix composites are more severe than the general restrictions imposed on the Poisson's ratios for transverse-isotropic media [4].

We note also that, according to (18),

$$k^2 = \frac{E_1}{E_2} = \frac{E_1}{E_3} = \frac{G_{12}}{G_{23}} = \frac{1}{2}(1 + \alpha^3) \geq 1;$$

i.e., the anisotropy factors corresponding to the Young's and shear moduli are equal to each other and increase with α.

The results of this paper allow us to make the following basic conclusion. An interfacial layer of a polymer matrix composite whose matrix represents an incompressible isotropic medium is transverse-isotropic. The anisotropy of this layer is caused by the effect of the surface on the macromolecule conformation, and its Poisson's ratios satisfy the conditions $0 < \nu_{21} = \nu_{31} \leq 0.5$, $0.5 < \nu_{23} = \nu_{32} \leq 1$.

ACKNOWLEDGMENTS

This work was supported by the Russian Foundation for Basic Research, project no. 99–01–01250.

REFERENCES

1. J. B. Donnet, in *Proceedings of the IRC'94, Moscow, 1994*, Vol. 1, p. 129.
2. *Structure and Properties of Polymer Surface Layers*, Ed. by Yu. S. Lipatov (Naukova Dumka, Kiev, 1971).
3. Ph. Boulanger and M. Hayes, J. Elast. **50**, 87 (1998).
4. D. J. Pickering, Geotechnique **20**, 271 (1970).
5. V. É. Zgaevskiĭ and Yu. G. Yanovskiĭ, Mekh. Kompoz. Mater. Konstr. **3** (1), 105 (1997).
6. S. G. Lekhnitskiĭ, *Theory of Elasticity of Anisotropic Solids* (Gostekhteorizdat, Moscow, 1950).

Translated by Yu. Verevochkin

Doklady Physics, Vol. 46, No. 5, 2001, pp. 369–372. Translated from Doklady Akademii Nauk, Vol. 378, No. 3, 2001, pp. 339–342.

MECHANICS

The Laws of Defect-Size Distribution in the Failure of Materials

T. B. Petersen

Presented by Academician N.P. Lyakishev November 28, 2000

Received November 11, 2000

The evolution of a stochastic system consisting of a set of elements whose initiation times are randomly distributed, the initial size obeys the normal distribution, and the growth dynamics is determined by the equation $\frac{da}{dt} = f(a)$, where $f(a)$ is a power-law function, is analyzed. The aim of this study is to describe the behavior of such a system at different stages of its evolution, to estimate the basic probabilistic characteristics of the system, and to analyze the self-simulation conditions for the system.

For the sake of clarity, we consider a particular example of a physical system of this type related to material failure. This enables us to estimate quantitatively, without loss of generality, the system parameters.

1. The basic elements of the failure process are defects (micro- and macrocracks) whose growth, at different loading modes, is described in the general form by the equation

$$\frac{da}{dt} = Ca^m. \tag{1}$$

Here, a is the crack length, $\frac{da}{dt}$ is the crack growth rate, C is the parameter that depends on the properties of the material and on the level of the nominal stress γ, and m is the exponent ($m \geq 1$).

Let us consider the interval of time $[0, t]$ on which the cracks originate at random instants of time t_i (i is the crack index) and grow over the periods $\tau_i = t - t_i$. Integration of Eq. (1) from $t = t_i$ to t yields an exponential ($m = 1$) or a power-law ($m > 1$) dependence of the crack size on the time of its growth:

$$a_i(\tau_i) = a_{0i}\exp(C\tau_i), \tag{2a}$$

$$a_i(\tau_i) = (a_{0i}^{1-m} + C\tau_i(1-m))^{\frac{1}{1-m}}. \tag{2b}$$

Russian Research Centre, Kurchatov Institute, pl. Kurchatova 1, Moscow, 123182 Russia

Here, a_{0i} is the initial size of the ith crack. The variable parameters in these equations are a_{0i}, $\tau_i(t, t_i)$, while C and m are the constant parameters.

To estimate the shape of the function (density) of the size distribution of cracks and the numerical characteristics of the system, we will assume that, at the initial stage of the process, cracks develop independently and originate at a constant rate μ depending on the level of the applied load [1]. This implies that the process of crack initiation can be conceived as a steady-state Poisson flow which is characterized by a uniform distribution of instants of crack initiation and, therefore, by a uniform distribution of time intervals of crack growth, $P(\tau) = \frac{l}{t}$, where τ is the random quantity (RQ) that characterizes the period of crack growth [2]. We will assume initially that a_0 = const. Using standard relationships of the probability theory [see Appendix (A.1)] and formulas for the crack growth (2a) and (2b), we can deduce the law of the size distribution of cracks assuming that the crack size is a function of just one RQ, τ:

$$p(a; t, a_0, a_t) = \begin{cases} 0 \text{ for } a \leq a_0 \\ \frac{a^{-m}}{Ct} \text{ for } a_0 < a \leq a_t \\ 0 \text{ for } a > a_t. \end{cases} \tag{3}$$

Here, a_t is the maximum value of the parameter a, which is determined from (2) at $\tau = t$.

The obtained distribution is a truncated power-law distribution whose form does not undergo change after similarity transformation (the β-fold change in the length and time scales, $a' = \beta a$, $t' = \beta t$):

$$p(a'; t', a_0, a_{t'}) = \beta^{-m-1}(a; t, a_0, a_t). \tag{4}$$

This relationship shows that the process is invariant in the sense of distribution; i.e., it is statistically self-similar [3]. Note that the processes whose distributions on the middle segment of the curve have a power-law form are widespread in nature. The mechanisms of formation of such distributions and the reasons for the manifestation and violation of their self-similarity have

1028-3358/01/4605-0369$21.00

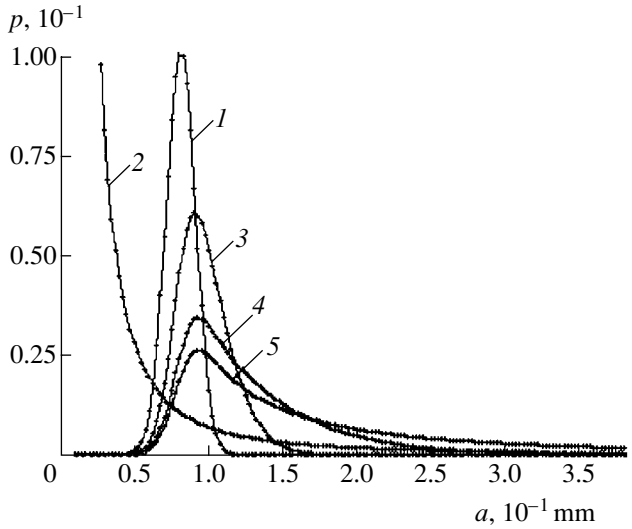

Fig. 1. Distributions of the density of fatigue microcracks over size. Curve *1* is the normal distribution of incipient cracks $p(a_0)$: $a_m = 0.08$ mm, $\sigma = 0.009$ mm; curve *2* is the distribution of cracks $p(a)$: $a_0 = 0.025$ mm, $t = 190000$ cycles; and curves *3–5* represent the distributions of cracks $p(a)$ corresponding to the normal size distribution of initial cracks: $C = C_1\Delta\gamma^m$; $m = 2$, $C_1 = 1.9 \times 10^{-10}$, $\Delta\gamma = 30$ kgf/mm^2, $t_3 = 25000$ cycles (curve *3*), $t_4 = 50000$ cycles (curve *4*), $t_5 = 190000$ cycles (curve *5*).

long been a matter of discussions [3–6], and we analyze them in this work.

The expressions for the mean size of cracks in terms of time period t can be obtained by substituting formulas (2a) and (2b) into the formula for the estimation of average (A2):

$$\langle a\rangle = \frac{1}{t}\int_0^t a(t)d\tau = \frac{a_0(\exp Ct - 1)}{Ct}, \quad m = 1,$$
$$\langle a\rangle = a_0 + \frac{a_0^m Ct}{2}, \quad m > 1. \tag{5}$$

The second expression is obtained by expanding (2b) in a power series, keeping only the linear term in this expansion.

In various physical applications, not only the density function but also the cumulative distribution function, expressed in the log–log scale, are often analyzed. The distribution function for $m > 1$ has the form

$$F(a) = P\{a < \alpha\} = \int_a^\infty p(\alpha)d\alpha$$
$$= \int_a^{a_t}\frac{\alpha^{-m}}{Ct}d\alpha = \frac{1}{Ct(1-m)}(a_t^{1-m} - a^{1-m}). \tag{6}$$

We take a logarithm of this expression and analyze the dependence of the function $\log F$ on the argument $\log a$. To do this, we estimate the derivative of the function

$$\log F = \log\left(\frac{1}{Ct(1-m)}\right) + \log(a_t^{1-m} - a^{1-m}), \tag{7}$$

$$\log F'_{\log a} = \frac{(1-m)a^{1-m}}{a^{1-m} - a_t^{1-m}}. \tag{8}$$

From (8) it follows that in the region of low and moderate values of the parameter ($a \ll a_t$), we can ignore the term a_t^{1-m}; in this case, the derivative takes the value $1 - m$. This means that in the given region, the function of the cumulative distribution, plotted in the log–log scale, has a linear form. In the region of large parameter values, where $a \longrightarrow a_t$, this function tends to zero in a nonlinear manner.

2. Consider now the case when the initial crack size is a random quantity. This means, physically, that the cracks arise on the structural inhomogeneities of the material whose distribution determines the distribution of incipient cracks. Assuming that the characteristic size of the structure (e.g., the grain size) is distributed according to the normal law with mean a_m and variance σ and considering that the growth interval τ and the initial crack size a_0 are independent RQs, we find, using (A.3), the density of the length distribution of cracks as a random function of two RQs with the known distributions

$$p(a; t, a_m, \sigma) = \frac{a^{-m}}{Ct}\left\{\Phi_0\left(\frac{a - a_m}{\sigma}\right) - \Phi_0\left(\frac{a' - a_m}{\sigma}\right)\right\}, \tag{9}$$

where Φ_0 is the Gauss probability integral and a' is determined by the formulas

$$a' = a\exp(-Ct), \quad m = 1,$$
$$a' = \{a^{1-m} + Ct(m-1)\}^{\frac{1}{1-m}}, \quad m > 1. \tag{10}$$

An analysis of function (9) shows that it reaches a maximum in the segment of small parameter values. In this region, the density $p(a)$ is determined largely by the product of the first factor (the distribution at the constant a_0 value) and the size distribution of the original cracks. In the region of moderate and large parameters, the shape of the curve is determined mainly by the first factor and has an appearance similar to that considered above. To illustrate the results obtained, the size distributions of fatigue microcracks, calculated with the aid of (9), are plotted in Fig. 1. We show the variation of the distribution profile with the observation time [when $t \longrightarrow 0$, the function $p(a) \longrightarrow p(a_0)$]. In these calculations, we used real values of the characteristics of fatigue failure [1].

It should be noted that at sufficiently large observation times, which are usually realized in practice, we have $a' \ll a_m$; if, in addition, $a_m > 3\sigma$, the second term in braces in formula (9) can be ignored. In this case, the expression for the function of the density distribution is reduced to a simple form, which allows the observed experimental distributions to be interpreted from the standpoint of the size distribution of initial cracks and the dynamics of their growth:

$$p(a; t, a_m, \sigma) = \frac{a^{-m}}{Ct}\Phi_0\left(\frac{a - a_m}{\sigma}\right). \quad (11)$$

[In this example, formula (11) gives an exact description of the density distribution when the number of cycles $t > 20000$.]

The mean size of cracks for distribution (9) is determined with the use of formula (A.2) as

$$\langle a\rangle = \frac{1}{\sqrt{2\pi\sigma t}}\int_{-\infty}^{+\infty}\int_{0}^{t} a_0 e^{C\tau} \quad (12a)$$

$$\times \exp\left(-\frac{(a_0 - a_m)^2}{2\sigma^2}\right)da_0 d\tau = \frac{a_m \exp(Ct - 1)}{Ct},$$

$$m = 1,$$

$$\langle a\rangle = a_m + \frac{Ct}{2}(a_m^2 + \sigma^2), \quad m = 2. \quad (12b)$$

For other values of the exponent m, the formula for the average can be obtained in a similar way.

It is easy to verify that distributions (9) and (11) are self-similar, because they are obtained by multiplication of the self-similar distribution (3) by the self-similar Gauss function. The self-similarity of the resulting distributions follows from the fact that we analyze the stage of independent growth and accumulation of cracks occurring as a result of a single mechanism according to the Poisson distribution law. However, an increase in the crack concentration with time leads to the interaction and fusion of cracks, which results in an increase in the share of large-sized cracks and promotes the localization and acceleration of the failure process. In this case, the distribution function changes its shape and the self-similar evolution of the system breaks down. Figure 2 shows the cumulative distribution function that demonstrates the effect of crack fusion. The bend on the curve in the region of large parameter values corresponds to the initiation of cracks of size $k\langle a\rangle$. In this region, the mean size of cracks is calculated from formula (12); the number of intersecting cracks $k = 2, \ldots, \infty$ and the probability of intersection of k cracks is estimated from the binomial distribution [7].

Along with size distributions of cracks [8] and pores [9], a shape similar to those plotted in Figs. 1 and 2 is typical of the distributions of drainage areas of river basins [10], amplitudes of acoustic emission signals, magnitudes of seismic events [4–6], etc. The identical form of such distributions testifies to the analogy in the dynamics and statistics of the processes responsible for their formation, which allows these processes to be considered within the framework of the proposed model.

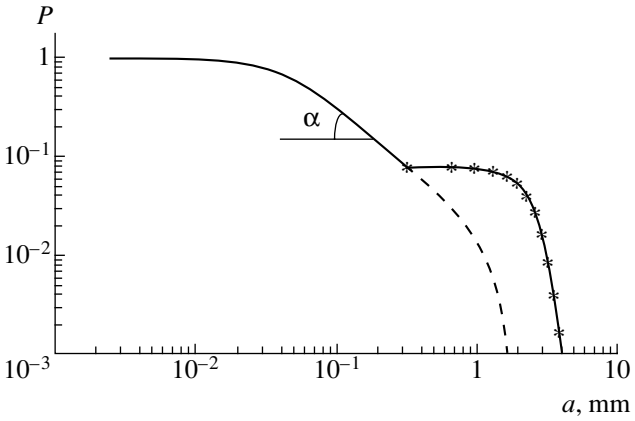

Fig. 2. The cumulative function of crack-size distribution obtained with allowance for crack fusion. The dotted line shows the part of the curve where crack fusion is disregarded: $m = 2$, $\tan\alpha \approx 1$, $a_m = 0.04$ mm, $\sigma = 0.03$ mm, $\mu = 0.00008$ cracks per cycle, $C_1 = 2 \times 10^{-10}$, $\Delta\gamma = 30$ kgf/mm^2, $t = 350000$ cycles, $\langle a\rangle = 0.12$ mm.

This study was supported by the INTAS grant no. 93-809 and by the Russian Foundation for Basic Research, project no. 97-05-65952. The author is grateful to L.R. Botvina for her valuable collaboration and discussion of the results obtained.

APPENDIX

1. The distribution of the function $Y = \varphi(X)$ of random quantity X is determined by the relationship

$$p(y) = f(\varphi^{-1}(y))\left|\frac{d\varphi^{-1}(y)}{dy}\right|, \quad (A.1)$$

provided the distribution of parameter $f(x)$ is known.

2. The mathematical expectation (the mean) of the function $Y = \varphi(X_1, X_2)$ of random quantities X_1 and X_2 is calculated from the formula

$$M[\varphi(X_1, X_2)] = \int_{-\infty}^{+\infty}\int_{-\infty}^{+\infty}[\varphi(x_1, x_2)]f(x_1, x_2)dx_1 dx_2, \quad (A.2)$$

if the joint distribution $f(x_1, x_2)$ is known.

3. The distribution of the function $Y = \varphi(X_1, X_2)$ of two random quantities X_1 and X_2 is determined by the relation

$$f_y(y) = \int_{-\infty}^{+\infty} f_x(\Psi, x_2)\left|\frac{\partial\Psi}{\partial y}\right| dx_2, \qquad \text{(A.3)}$$

if we know the joint distribution $f(x_1, x_2)$ of these quantities, where $x_1 = \Psi(y, x_2)$.

REFERENCES

1. K. J. Miller, Fatigue Fract. Eng. Mater. Struct. **10** (1), 75 (1987).
2. T. B. Petersen, Pis'ma Zh. Tekh. Fiz. **21** (2), 74 (1995) [Tech. Phys. Lett. **21**, 76 (1995)].
3. B. B. Mandelbrot, *The Fractal Geometry of Nature* (Freeman, San Francisco, 1982).
4. P. Bak and C. Tang, J. Geophys. Res. **94** (B11), 15635 (1989).
5. S. J. Steacy, J. McCloskey, *et al.*, Geophys. Res. Lett. **23**, 383 (1996).
6. Y. Y. Kagan, Physica D (Amsterdam) **77** (16a), 192 (1994).
7. T. B. Petersen, Preprint IAÉ-5936/15 (Kurchatov Institute of Atomic Energy, Moscow, 1995).
8. L. R. Botvina, *Kinetics of Destruction of Structural Materials* (Nauka, Moscow, 1989).
9. D. N. Dewhurst and A. C. Aplin, J. Geophys. Res. **103** (B1), 651 (1998).
10. A. Gave and P. Dave, Tectonophysics **269**, 91 (1997).

Translated by A. Kozlenkov

Doklady Physics, Vol. 46, No. 5, 2001, pp. 373–375. Translated from Doklady Akademii Nauk, Vol. 378, No. 3, 2001, pp. 343–346.

MECHANICS

Noncommutative Plastic Deformation and the Essence of the Ul'yushin's Isotropy Postulate

Chin' Van Khoa

Presented by Academician A.R. Khokhlov October 2, 2000

Received October 3, 2000

1. We consider a model of a nonuniform continuous medium. When being subjected to ultimate stress, the medium is known to make a transition into the plastic state. Many plasticity models with different defining relations have been previously developed. One of the phenomenological approaches to these models consists in allowing for only predominant microstructural mechanisms and subsequently correcting the defining relations on the basis of experimental data. However, all the plasticity experiments show that in the plastic state, the strain–stress field exhibits strong fluctuations. In addition, the stress–strain diagram $\sigma = f(e)$ turns out to be similar to the pressure–volume diagram $P = f(V)$ for a liquid. Moreover, phase transition has even been observed in the vicinity of a crack edge [2–4]. Hence, we can consider the plastic-deformation process as a critical (phase) transition in which a certain structure is spontaneously formed [5]. The probability density for a transition to the plastic state is governed by the Fokker–Planck equation. Taking the potential character of the deformation process into account, we may use the Schrödinger equation rather than the Fokker–Planck equation. This implies that the plastic-deformation process can be treated as a process possessing supersymmetric properties. Below, we consider the strain tensor as an order parameter. In [6], Il'yushin introduced the notion of strain trajectories in E_5 space. This space is actually a fiber in fiber-bundle strain space [5]. This implies that the strain field can be considered a gauge field in which the generalized Il'yushin's strain trajectory is a section of the fiber bundle. Identifying the generalized strain trajectory with nodes, we analyzed (in [6]) the topological features of the deformation process, which are related to the Witten invariant. In this way, we obtained the probability density for a transition to the plastic state:

$$Z = \int \exp[-kS_{\mathrm{CS}}(e)]de.$$

Here, k is the elasticity coefficient and S_{CS} is the Chern–Simons action:

$$S_{\mathrm{CS}} = \int \Gamma_{\mathrm{CS}},$$

where Γ_{CS} is the Chern–Simons form for the strain manifold.

2. From the most general standpoint, the strain space $P = \{E_n(x, t)\}$ is a noncommutative space. In [7], Connes developed a noncommutative geometry in which the properties of a function ring rather than the character of a point space are considered. Within the framework of this geometry, we construct a model for the plastic deformation, i.e., a noncommutative fiber bundle of the strain field [8]. The associative algebra A and the universal algebra $\Omega(A)$ of forms over A are two basic objects in the Connes' geometry. We consider the strain space $P = \{E_n(x, t)\}$ as an associative algebra. We should then choose the Connes' universal algebra. According to [8], each form of such an algebra is associated with a certain differential calculus. Hence, we choose the Hopf algebra as $\Omega(P)$, thus using differential calculus of the Voronovich type. The strain space $P = \{E_n\}$ is known to be an associative algebra in which both the derivative form and the differential form can be defined. Therefore, we choose the Connes' universal algebra $\Omega(P)$ as an algebra of differential forms over the strain space P. Thus, the differential calculus on $\Omega_D(P)$ is of a type similar to that considered in [9]. According to this paper, the least differential algebra for the algebra of the cocycles $C(\mathrm{Der}(P), P)$, which contains the space P, is the $\Omega_D(P)$ algebra, i.e., an algebra of $C(\mathrm{Der}(P), P)$, where $\mathrm{Der}(P)$ is an algebra of derivatives on P. We define the basis $\{1, E_1, E_2, \ldots, E_{n^2-1}, n = 1, \ldots, 9\}$ in the space $P = \{E_n\}$ and assume that P is a Hermitian space with the following commutative rules:

$$E_k E_l = \delta_{kl} + C^m_{kl} - \frac{i}{2} C^m_{kl} E_l,$$

$$[E_k, E_l] = -2iC^m_{kl} E_m.$$

Moscow State University,
Vorob'evy gory, Moscow, 119899 Russia

1028-3358/01/4605-0373$21.00

Here, $\delta_{kl} = \frac{1}{2}\mathrm{Tr}(E_k E_l)$, $S^m_{kl} = S^m_{lk}$, $C^m_{kl} = -C^m_{lk}$, C^m_{kl} is the structure constant, and S^m_{kl} is the invariant of the group $sl(n)$ [10]. In the space $\Omega^1_D(P)$, the basis θ^k, $k \in \{1, 2, \ldots, n^2 - 1\}$ is defined with its properties: $\theta^k(\partial_l) = \delta^k_l 1$, $\theta^k\theta^l = -\theta^l\theta^k$, and $E_k\theta^l = \theta^l E_k$. Therefore, the differential in $\Omega^1_D(P)$ is an ordinary exterior differential:

$$dE_k = -C^m_{kl}E_m\theta^l, \quad d\theta^k = -\frac{1}{2}C^k_{lm}\theta^l\theta^m,$$

$$d(\theta^k\theta^j) = d\theta^k\theta^j - \theta^k d\theta^j, \text{ and } d^2 = 0.$$

The above-mentioned fiber bundle yields a section that is either a strain field or an Il'yushin's generalized strain trajectory [5]. According to Connes' noncommutative geometry, the vector fiber bundle of the noncommutative strain space P is either a left or a right modulus, with the trivial fiber bundle of the strain field being a free modulus and the nontrivial fiber bundle being a factorization of the free modulus over the space P. As a matter of fact, this is the cotangent bundle $\Omega^1_D(P)$.

We now construct the action for the process of noncommutative plastic deformation. In accordance with Connes' method, we first choose a Hermitian modulus H over the strain space P. This implies that on the Hermitian P-modulus H, there exists a Hermitian structure h such that $h(\alpha, \beta) \in P$ for all $\alpha, \beta \in H$, and the equality $h(\alpha A \text{ and } \beta B) = A^* h(\alpha, \beta)B$ holds for all $A, B \in P$. We should then choose a connectivity ∇, i.e., a mapping of H onto $H \otimes \Omega^1_D$ for which the following conditions are satisfied for all $\phi, \psi \in H$ and $A \in P$:

$$\nabla(\phi A) = (\nabla\phi)A + \phi \otimes dA,$$

$$dh(\phi, \psi) = h(\nabla\phi, \psi) + h(\phi, \nabla\psi).$$

The connectivity ∇ is expanded up to the linear mapping D_∇ of the first rank (D_∇: $H \otimes \Omega^1_D \longrightarrow H \otimes \Omega^1_D$) so that $D_\nabla(\phi \otimes \alpha) = (\nabla\phi)\alpha + \phi \otimes d\alpha$ for all $\phi \in H$ and $\alpha \in \Omega^1_D$. Thus, in terms of ∇, the curvature is defined as the mapping ∇^2: $H \longrightarrow H \otimes \Omega^2_D$; i.e.,

$$\nabla^2(\phi B) = (\nabla^2\phi)B$$

for all $\phi \in H$ and $B \in P$.

The action for the process of noncommutative plastic deformation is expressed in terms of ∇ as

$$S = \|\nabla^2\|^2 = \langle\varphi|\varphi\rangle,$$

where φ is the connectivity component for the gauge with scalar product

$$\langle\varphi|\varphi\rangle = -\int\varphi(*\varphi) = \mathrm{Tr}[\varphi(*\varphi)].$$

Thus, we obtain the probability distribution for the transition to the plastic state:

$$Z = \int\exp(-kS),$$

where k is the elasticity coefficient. The distribution Z depends on the connectivity ∇ defined for a certain gauge. In order to derive an explicit form of Z, we now consider the following example. We choose a gauge e that is unity in the Hermitian space H and, then, a connectivity in the form $\nabla e = e \otimes \alpha$, where $\alpha \in \Omega^1_D$ with $\alpha = -\bar{\alpha}$ and $\bar{\alpha}$ conjugate to α. The form α is a complex-valued matrix in the Muskhelishvili sense. However, within the framework of the symplectic geometry for the three-dimensional case, this form has a complex-valued structure. Hence, each element $\phi \in H$ takes the form $\phi = eB$, where $B \in P$ so that we obtain, by definition, that $\nabla\phi = (\nabla e)B + e \otimes dB$. In differential geometry, B and α are referred to as elements ϕ and ∇, respectively, for the gauge e. If the component φ of the curvature ∇^2 for the gauge e is chosen as $\varphi = d\alpha + (\alpha)^2$, we arrive at $\nabla^2 = e \otimes \varphi$. Furthermore, we write out α in the conventional complex-valued form $\alpha = B_k\theta^k + iE_l\theta^l$ ($B, E \in P$), subject α to the action of the operator d, evaluate α^2, and substitute the results into the expression for φ. Finally, we arrive at

$$\varphi = \frac{1}{2}([B_k, B_l] - C^m_{lk}B_m)\theta^k\theta^l.$$

Thus, the action takes the form

$$S = -\frac{1}{8}\sum_{k,l}\mathrm{Tr}\{([B_k, B_l] - C^m_{lk}B_m)^2\}.$$

It should be noted that the above integral and the Hermitian modulus H is the Connes' K-cycle. However, since Connes did not define the notion of "secondary calculus," we here evaluate the integral Z in a regular manner.

3. In [6], Il'yushin suggested that, within the range of fairly small strains, the defining relations for continuous initially isotropic media are consistent with the isotropy postulate; namely, they would be invariant with respect to orthogonal transformations in the space E_5. In the case of finite strains, the defining relation was described in [14, 15]. Within the framework of the noncommutative plastic-deformation model when using strain-potential formalism, this postulate would become a theorem which could be proved. Indeed, in each cotangent fiber bundle, there always exists a symplectic structure [8, 13]. As was shown above, the spaces cotangent to the spaces $P = \{E_n(x, t)\}$ and P are spaces $\mathrm{Der}(P)$ and $\Omega^1_D(P)$, respectively. The symplectic form is a 2-form $\omega^2 \in \Omega^2_D(P)$ such that, for all $A \in P$ and $X \in \mathrm{Der}(P)$, the equation $\omega^2(X, H(A)) = XA$ has the unique solution $H(A) \in \mathrm{Der}(P)$, where $H(A)$ is the

Hamiltonian vector field at the point $A \in P$. If I is an isomorphism, i.e., $\Omega^1_D(P) \longrightarrow \mathrm{Der}(P)$, then the Hamiltonian vector field takes the form IdH, with H being the Hamiltonian function and the symplectic 2-form taking the form $\omega^2 = dH$. For each vector field $H(A)$, there exists a one-parameter diffeomorphism group g^t: $M^{2N^2} \longrightarrow M^{2n^2}$, which is called the Hamiltonian phase flow:

$$\left.\frac{d}{dt}\right|_{t=0} g^t A = IdH(A).$$

Here, the symplectic manifold is denoted by (M^{2n^2}, ω^2). It should be noted that the orthogonal mapping is a special case of diffeomorphisms. Hence, the isotropy postulate can be formulated in terms of the strain-potential formalism: the defining relation is invariant with respect to the Hamiltonian flow, in particular, to orthogonal transformations.

Within the framework of the commutative geometry, Arnold proved that the Hamiltonian phase flow conserves the symplectic structure $(g^t)^*\omega^2 = \omega^2$ [13]. In the case of noncommutative geometry, the Arnold's method can also be employed, the only difference being that the dimension of the symplectic space over P is $2n^2$ and the space points are matrices. However, if, in addition, the space P satisfies the axioms of the Hopf algebra, the above method cannot be employed because of the unconventional properties of the Voronovich-type differential calculus. By definition, $\omega^2 = dH = \sum \frac{\partial H}{\partial e_i} de_i$; this form is invariant with respect to the flow g^t. Under the additivity condition, this implies that the quantity $\frac{\partial H}{\partial e_i}$ is also invariant with respect to the mapping g^t.

In the singular model [11], the defining relation was presented in the form

$$d\sigma_i = \frac{\partial f_a}{\partial e_i} dk_a,$$

where f_a is the current ultimate surface. The components dk_a are nonzero if disturbances take place on the corresponding surfaces f_a, i.e., if $\frac{\partial f_a}{\partial e_i} d\sigma \geq 0$. Introducing the potential H (free energy) [6, 12], we arrive at the relation

$$\sigma_i = \frac{\partial H}{\partial e_i}.$$

In the model under consideration, the plastic deformation is a stochastic process for which the free energy serves as the system Hamiltonian function [5]. Indeed, the defining relation in the potential formalism is invariant with respect to the orthogonal transformations.

4. Thus, the general model of plastic deformation is the following. Let Il'yushin's deformation process be given. To construct the general model, we have, first of all, to reject the conventional notions of the elasticity theory, which are adequate only for static processes described by commutative variables. We should treat the strain space as a noncommutative space. Under the action of forces, this space turns into a cotangent fiber bundle. When the stress attains the ultimate value, the strain state becomes subjected to strong fluctuations. As a result, we can describe this state by the probability density of the transition to the plastic state. Because of the noncommutativity, we arrive at a symplectic space. This symplectic space over the noncommutative strain space is larger than the conventional space of classical theory. The essence of Il'yushin's postulate on isotropy can be understood only in this case. All the results of classical theory (e.g., the Coiter's sectors) could seemingly be treated as special cases of this general model.

REFERENCES

1. M. Ausloos, Solid State Commun. **59**, 401 (1986).
2. V. G. Gargin, Sverkhtverd. Mater., No. 2, 17 (1982).
3. V. A. Pesin, N. N. Pachenko, and L. I. Fal'dchuk, Éksp. Prikl. Fiz. Khim. **53**, 2794 (1979).
4. Li-Shing Li and R. J. Pabst, Mater. Sci. **15**, 2861 (1980).
5. Chin' Van Khoa, Dokl. Akad. Nauk **372**, 473 (2000) [Dokl. Phys. **45**, 245 (2000)].
6. A. A. Il'yushin, *Mechanics of Continua* (Mos. Gos. Univ., Moscow, 1990).
7. A. Connes, Publ. I.H.E.S. **62**, 257 (1986).
8. A. T. Fomenko, *Symplectic Geometry* (Mos. Gos. Univ., Moscow, 1989; Gordon and Breach, New York, 1988).
9. M. Dubois-Violette, R. Kerner, and J. Madore, J. Math. Phys. **31**, 316 (1990).
10. A. J. Madarlan, Commun. Math. Phys. **11**, 77 (1986).
11. V. D. Klyushnikov, *Physicomathematical Fundamentals of Strength and Plasticity* (Mos. Gos. Univ., Moscow, 1994).
12. Yu. N. Rabotnov, *Mechanics of Deformable Solids* (Nauka, Moscow, 1988).
13. V. I. Arnol'd, *Mathematical Methods of Classical Mechanics* (Nauka, Moscow, 1989).
14. Ch. Tsakmakis, Arch. Mech. **49**, 677 (1997).
15. Yu. N. Shevchenko, Prikl. Mekh. **35**, 14 (1999).

Translated by V. Chechin